Activation and functionalisation of carbon dioxide by *bis*-tris(pyrazolyl)borate-supported divalent samarium and trivalent lanthanide silylamide complexes

Tajrian Chowdhury, Claire Wilson, and Joy H. Farnaby.*

School of Chemistry, Joseph Black Building, University of Glasgow, Glasgow, G12 8QQ, UK.

Corresponding author(s): * joy.farnaby@glasgow.ac.uk.

Supporting Information

Contents

A. Spectroscopic Data for Complexes

A1 Nuclear magnetic resonance (NMR) data

A1.1 $[Sm(Tp)_2(THF)_2]$ 1-Sm(THF)

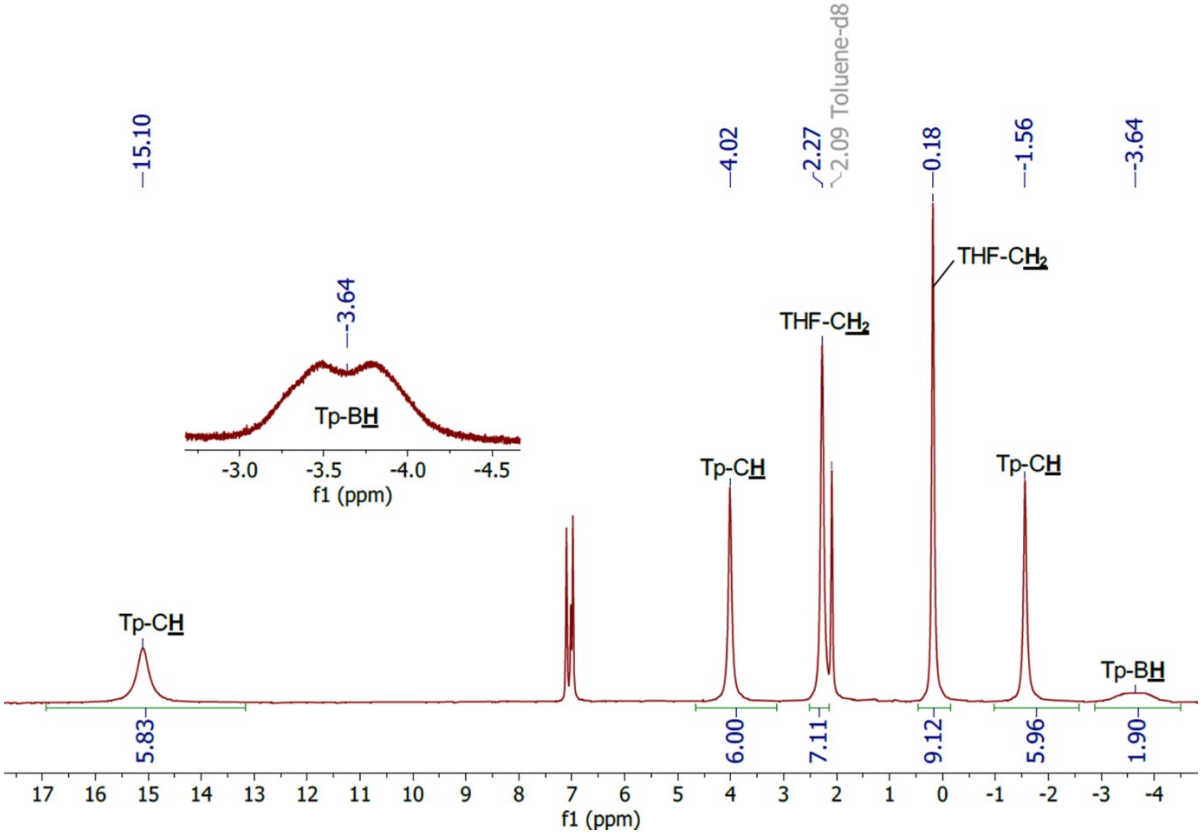

Figure S 1. ^{1}H NMR spectrum of $[Sm(Tp)_2(THF)_2]$ **1-Sm(THF)**, recorded in d_8-toluene.

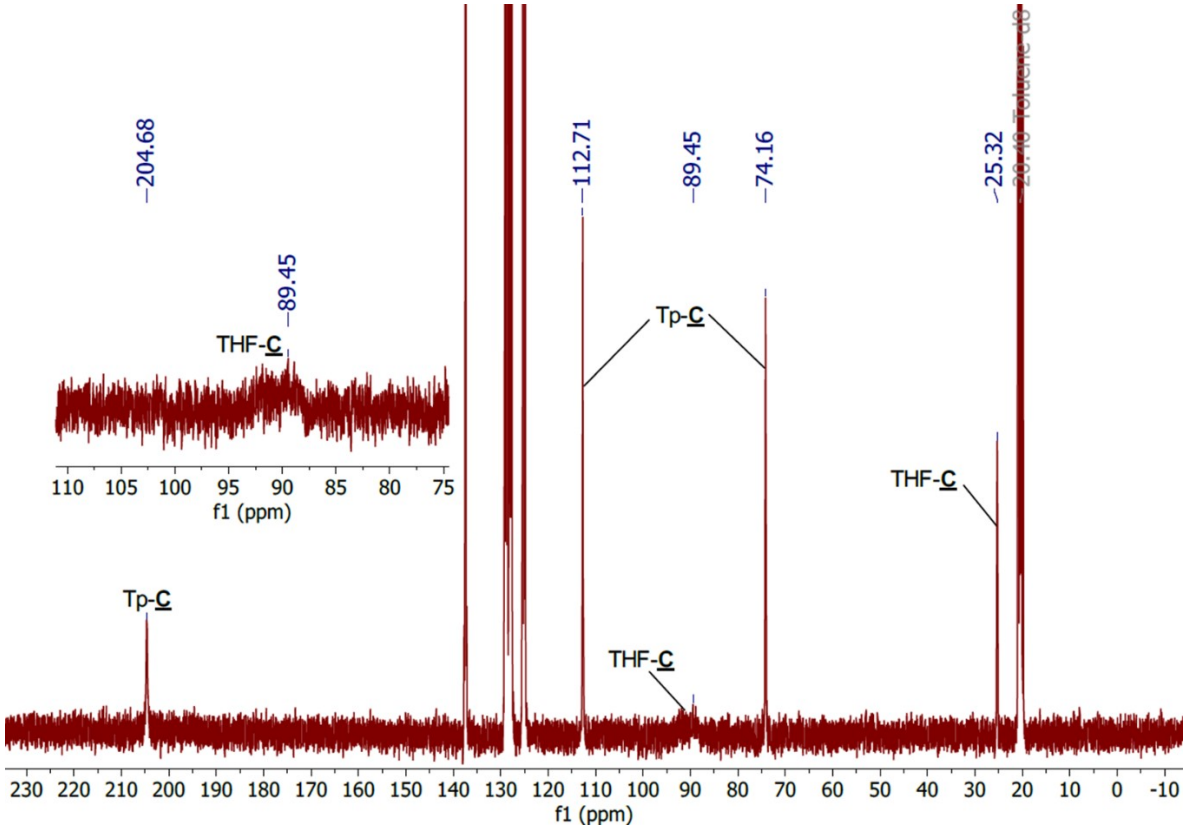

Figure S 2. $^{13}C\{^{1}H\}$ NMR spectrum of $[Sm(Tp)_2(THF)_2]$ **1-Sm(THF)**, recorded in d_8-toluene.

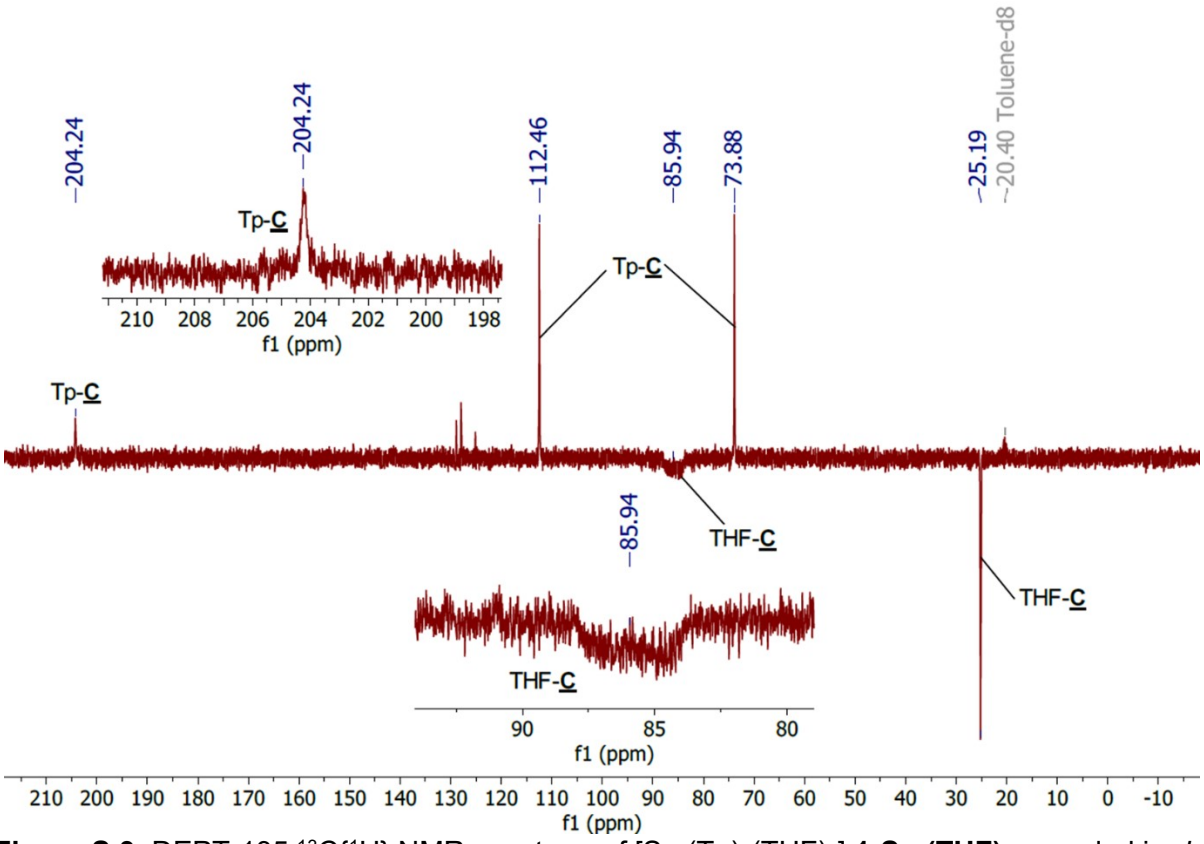

Figure S 3. DEPT-135 $^{13}C\{^{1}H\}$ NMR spectrum of $[Sm(Tp)_2(THF)_2]$ **1-Sm(THF)**, recorded in d_8-toluene.

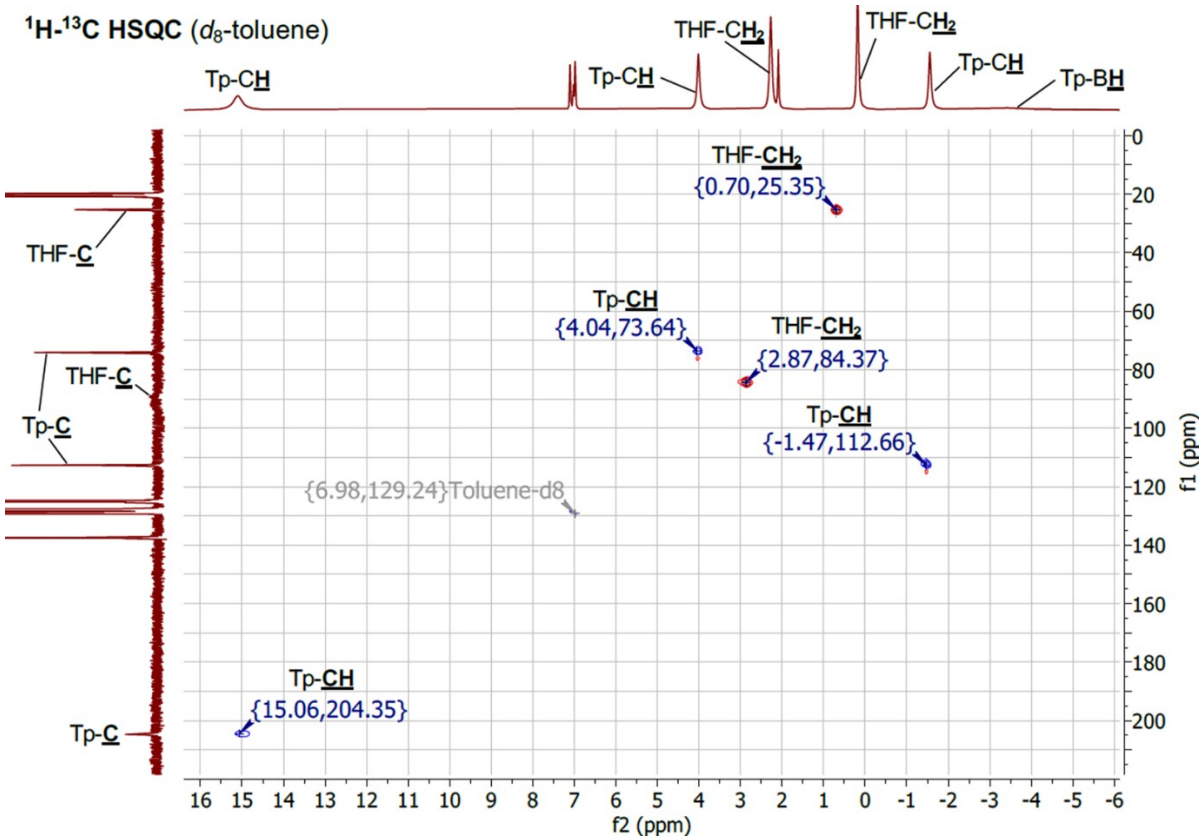

Figure S 4. ^{1}H-^{13}C HSQC NMR spectrum of $[Sm(Tp)_2(THF)_2]$ **1-Sm(THF)**, recorded in d_8-toluene.

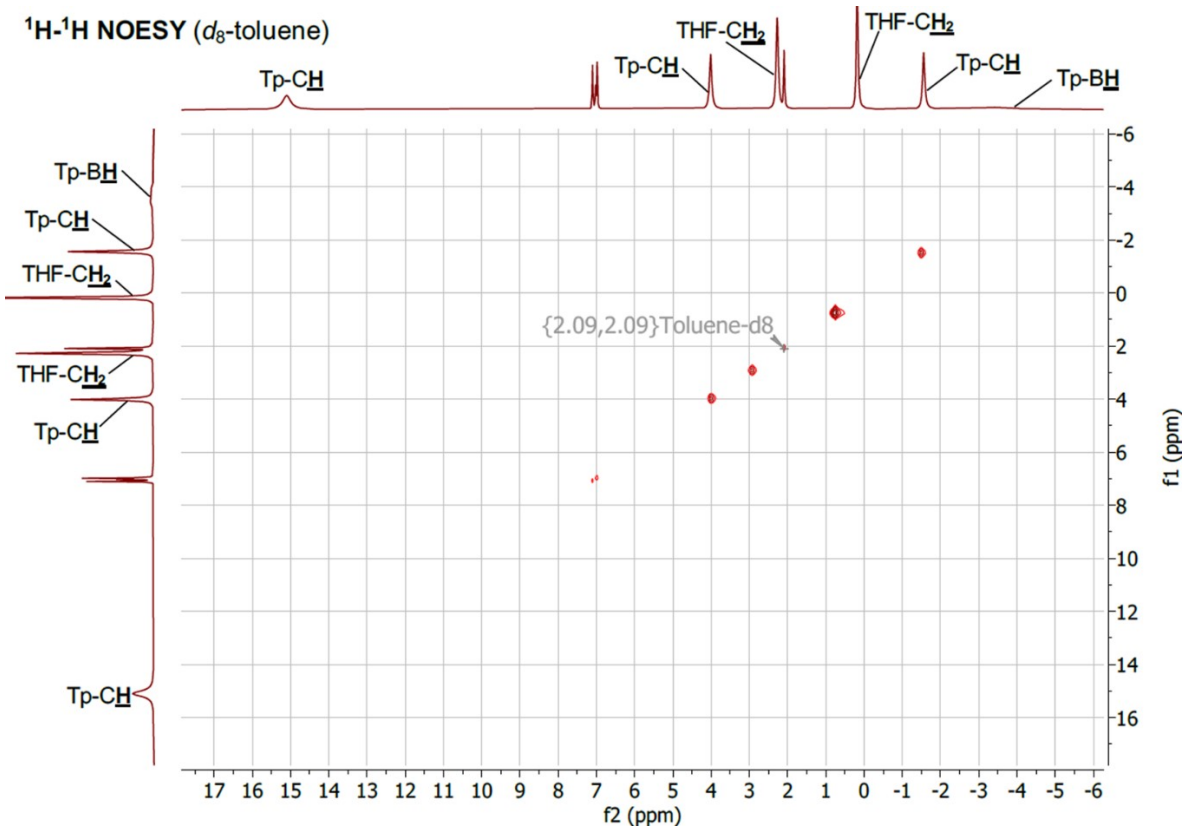

Figure S 5. ^{1}H-^{1}H NOESY NMR spectrum of $[Sm(Tp)_2(THF)_2]$ **1-Sm(THF)**, recorded in d_8-toluene.

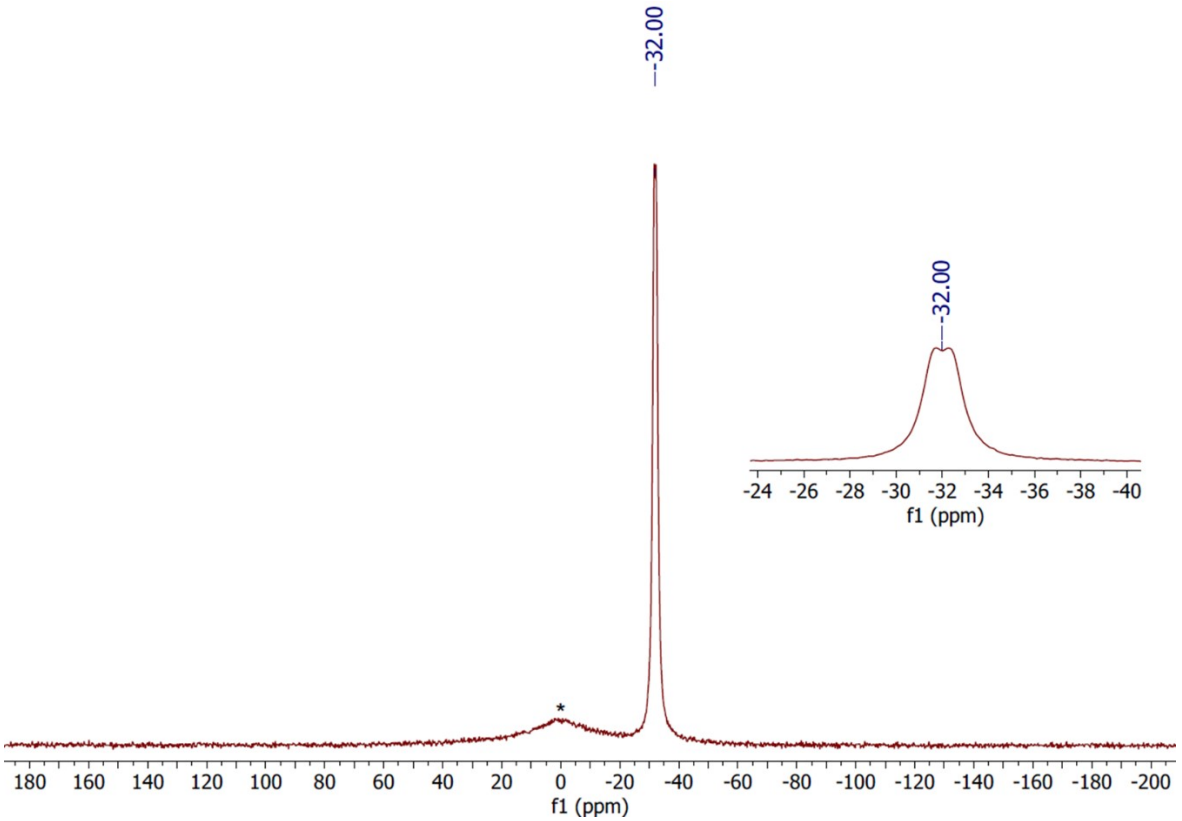

Figure S 6. ^{11}B NMR spectrum of $[Sm(Tp)_2(THF)_2]$ **1-Sm(THF)**, recorded in d_8-toluene. Borosilicate glass is denoted with *.

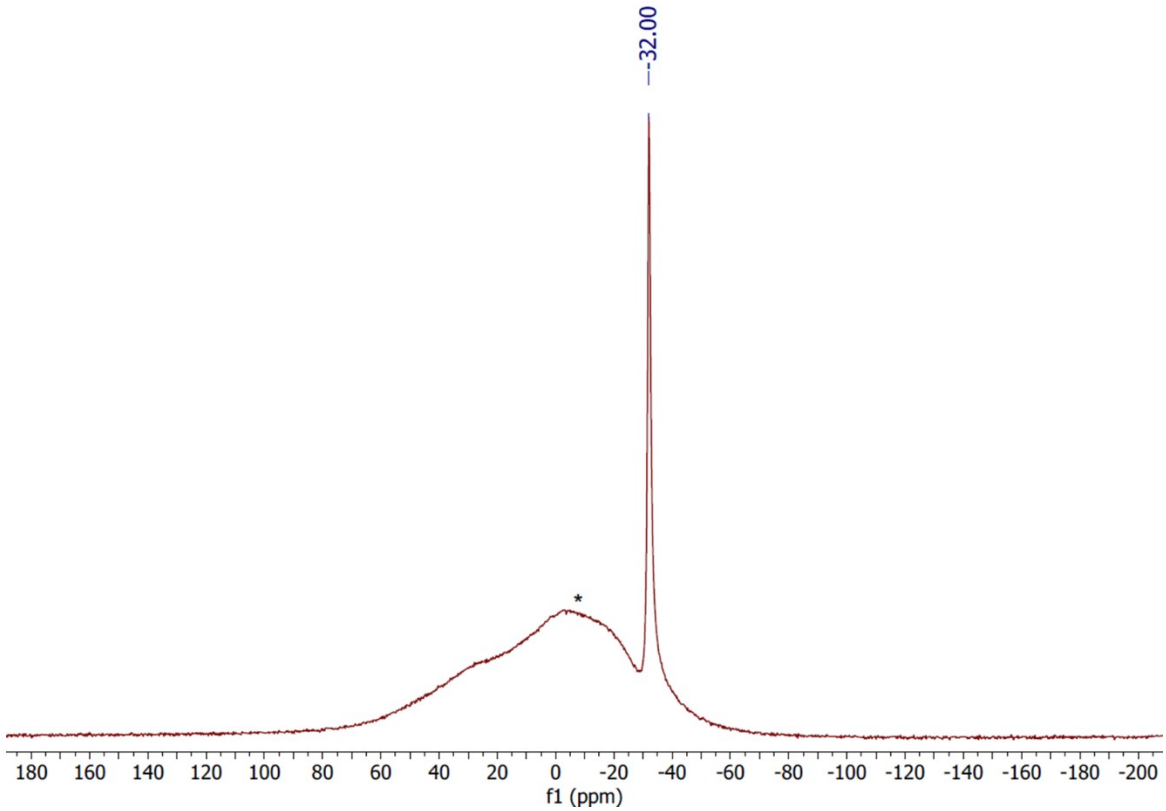

Figure S 7. $^{11}B\{^{1}H\}$ NMR spectrum of $[Sm(Tp)_2(THF)_2]$ **1-Sm(THF)**, recorded in d_8-toluene. Borosilicate glass is denoted with *.

A1.2 [Sm(Tp)$_2$(DME)] 1-Sm(DME)

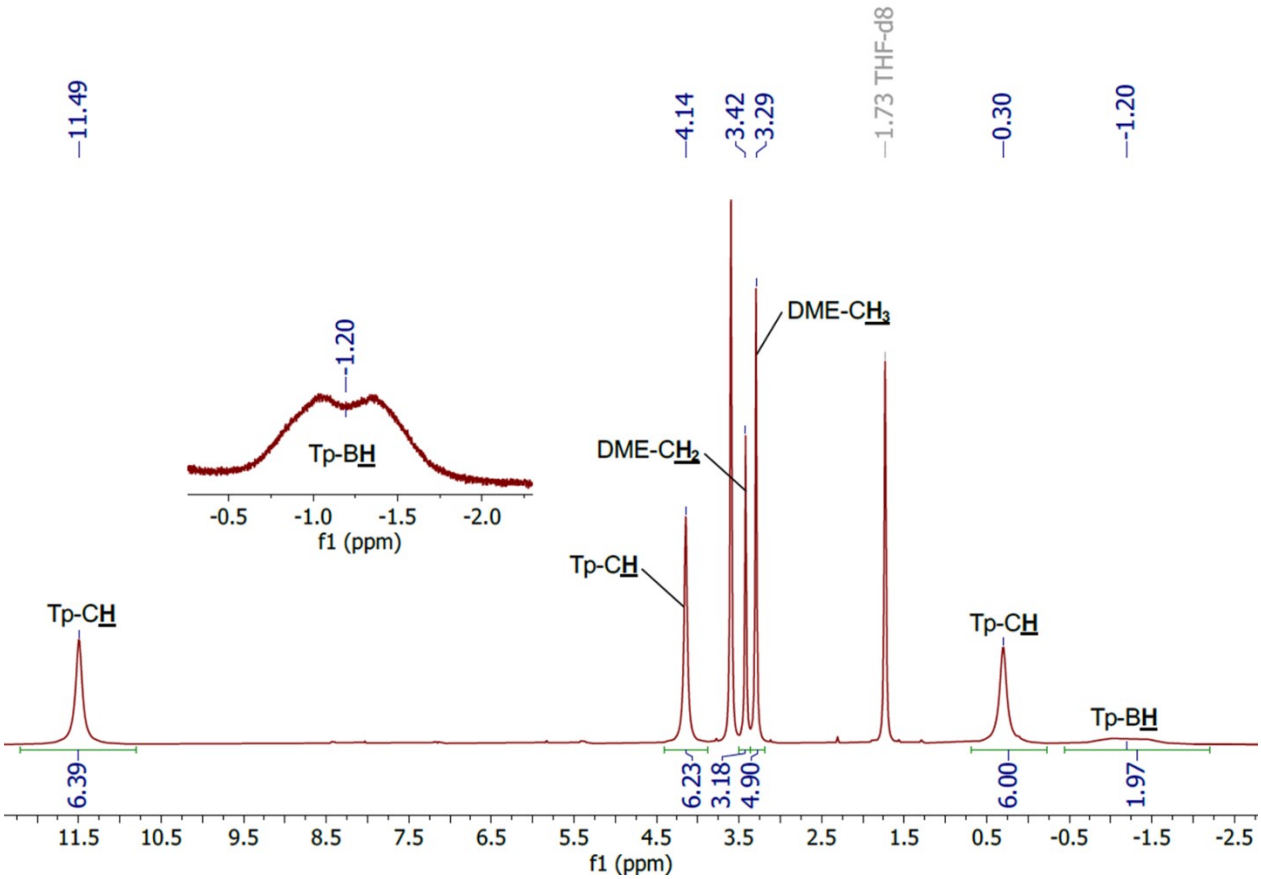

Figure S 8. ^{1}H NMR spectrum of $[Sm(Tp)_2(DME)]$ **1-Sm(DME)**, recorded in d_8-THF.

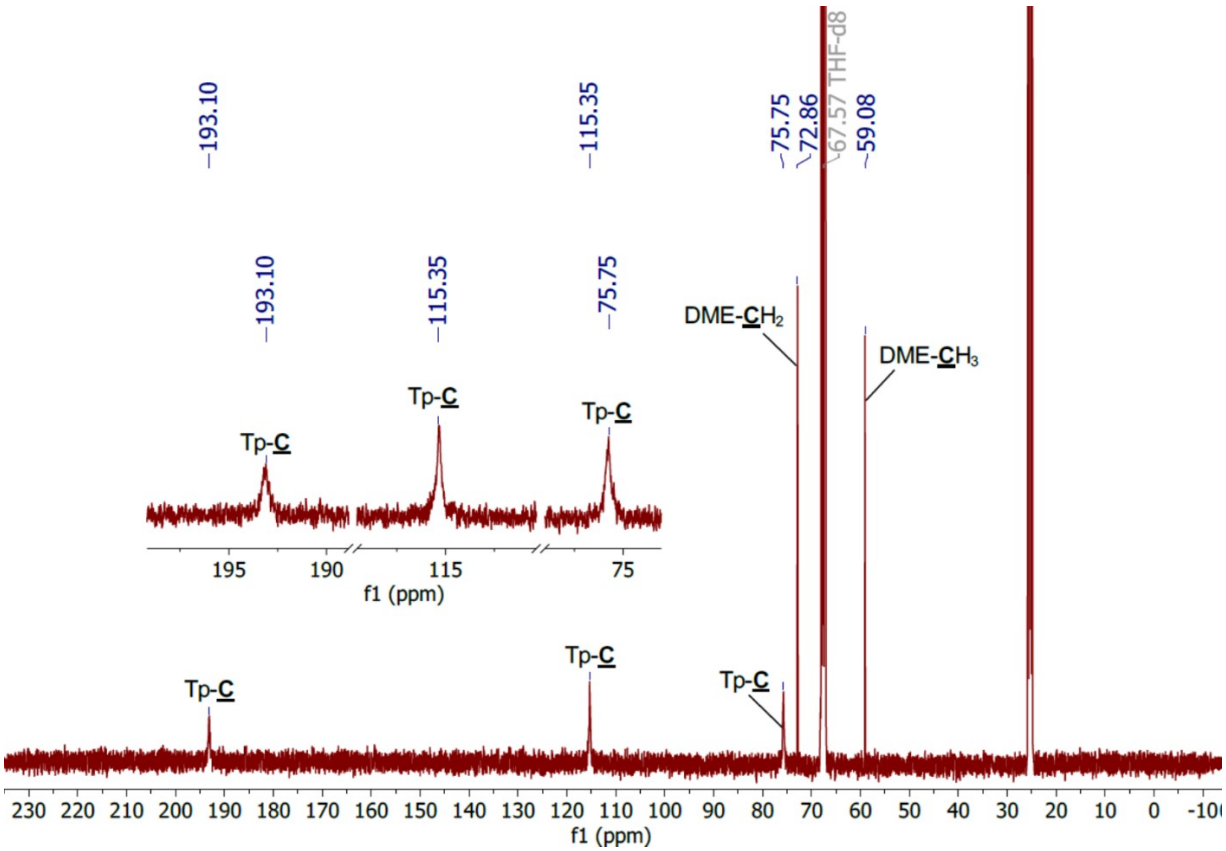

Figure S 9. $^{13}C\{^{1}H\}$ NMR spectrum of $[Sm(Tp)_2(DME)]$ **1-Sm(DME)**, recorded in d_8-THF.

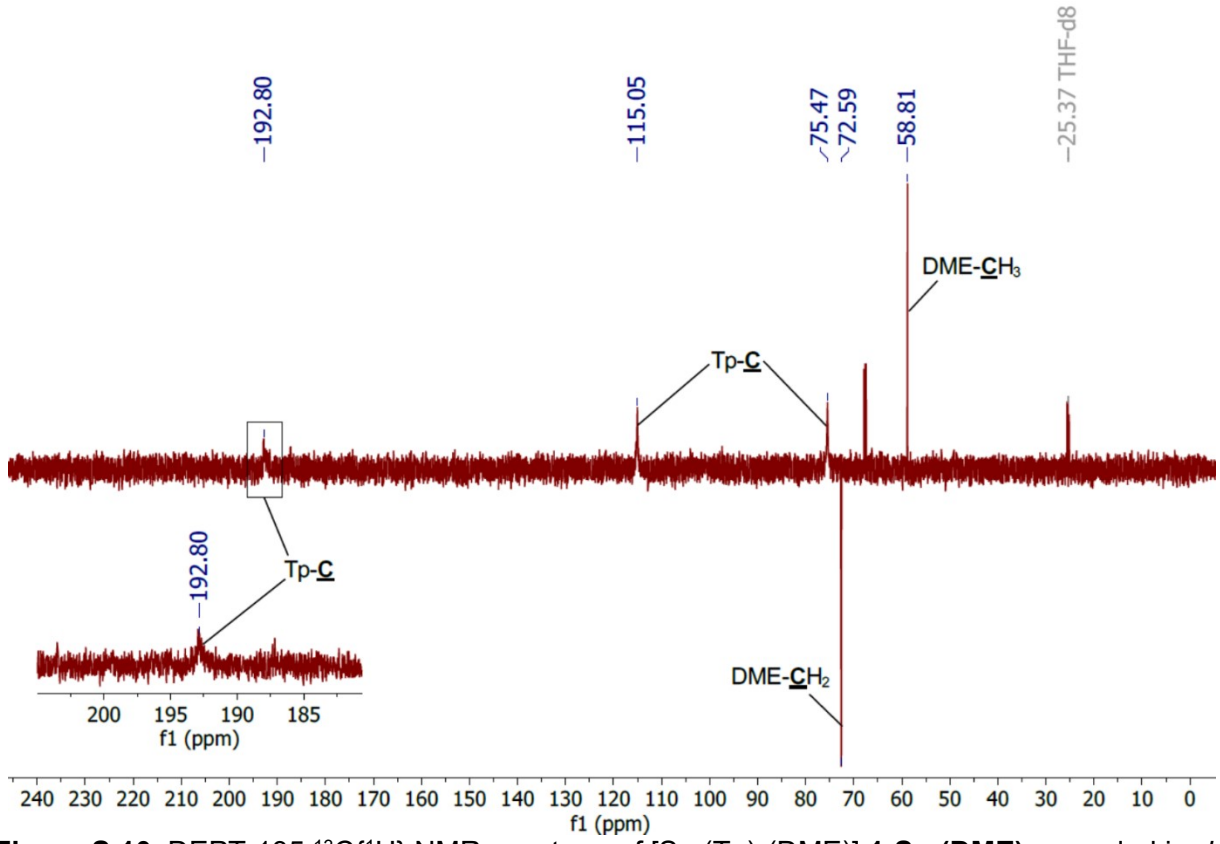

Figure S 10. DEPT-135 $^{13}C\{^{1}H\}$ NMR spectrum of $[Sm(Tp)_2(DME)]$ **1-Sm(DME)**, recorded in d_8-THF.

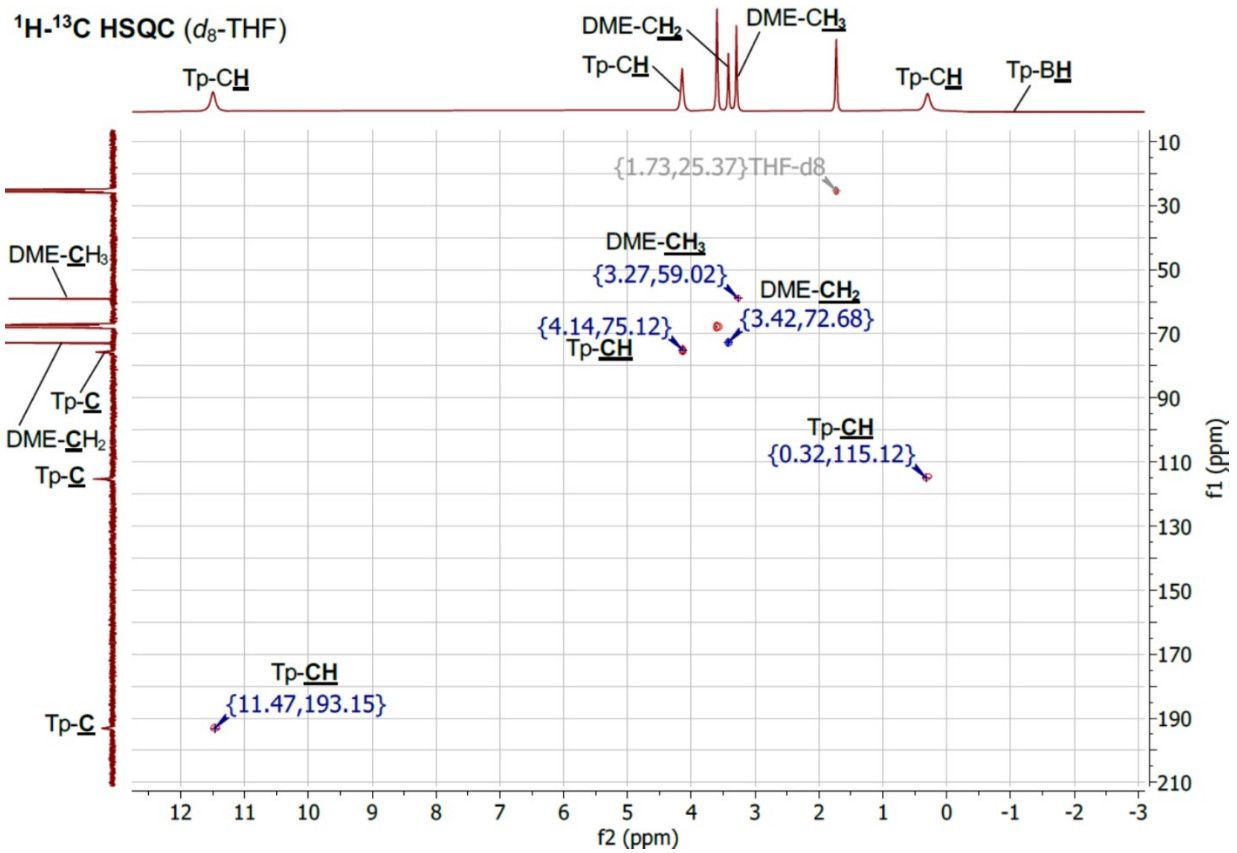

Figure S 11. ^{1}H-^{13}C HSQC NMR spectrum of [Sm(Tp)$_2$(DME)] **1-Sm(DME)**, recorded in d_8-THF.

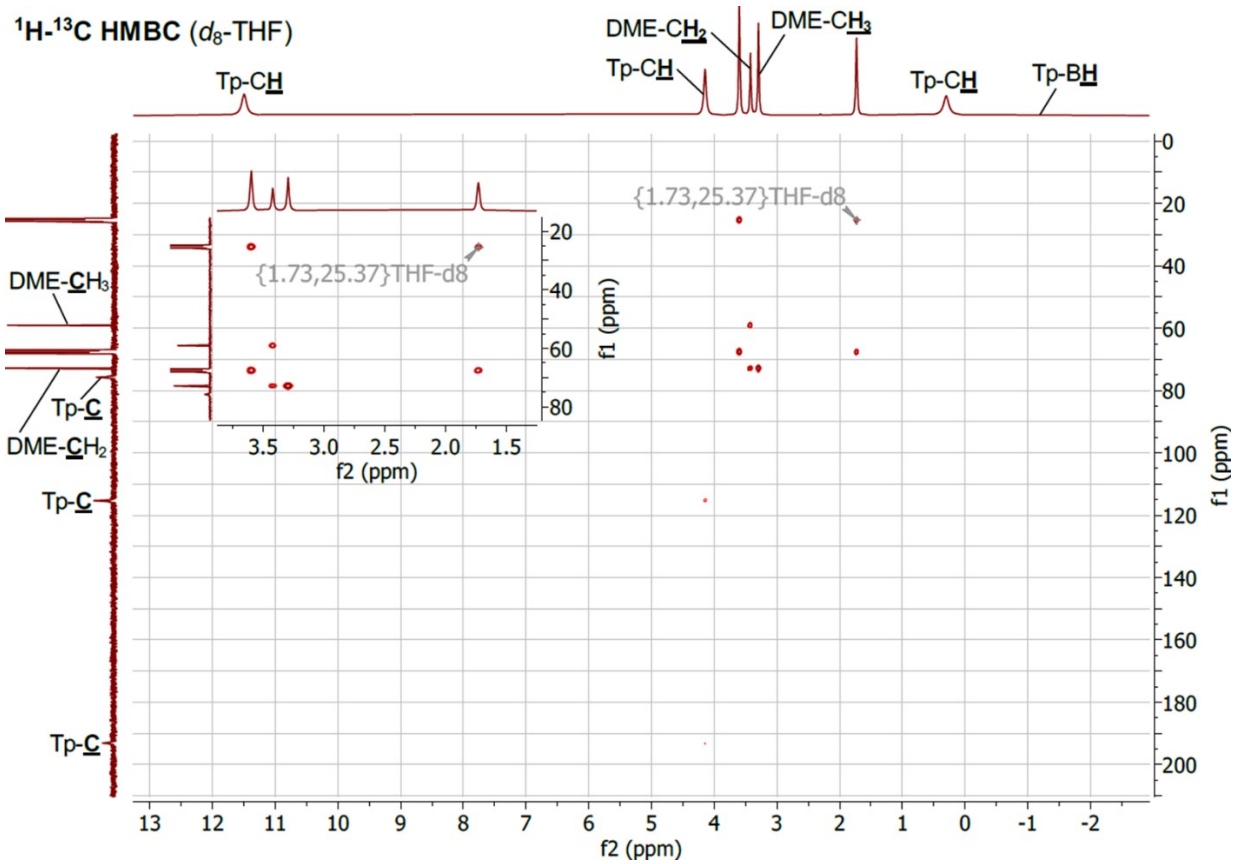

Figure S 12. ^{1}H-^{13}C HMBC NMR spectrum of [Sm(Tp)$_2$(DME)] **1-Sm(DME)**, recorded in d_8-THF.

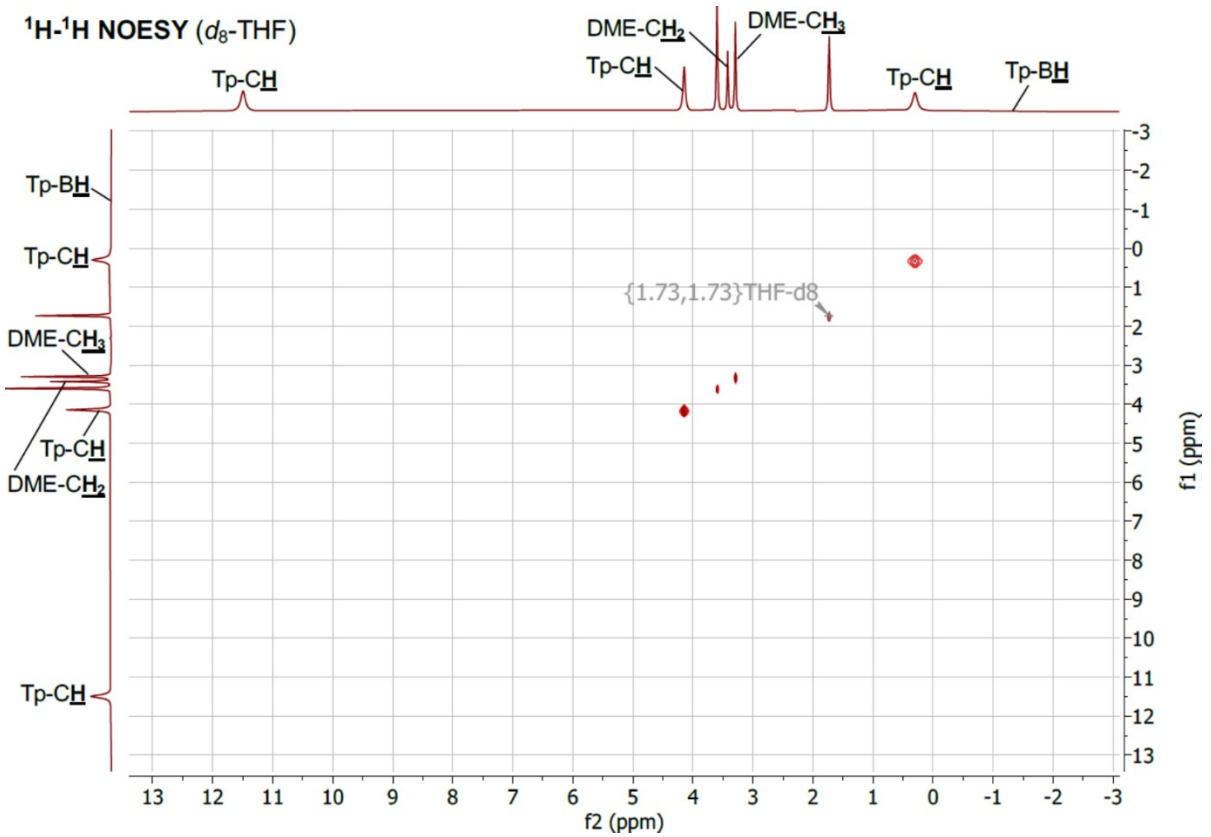

Figure S 13. ^{1}H-^{1}H NOESY NMR spectrum of [Sm(Tp)$_2$(DME)] **1-Sm(DME)**, recorded in d_8-THF.

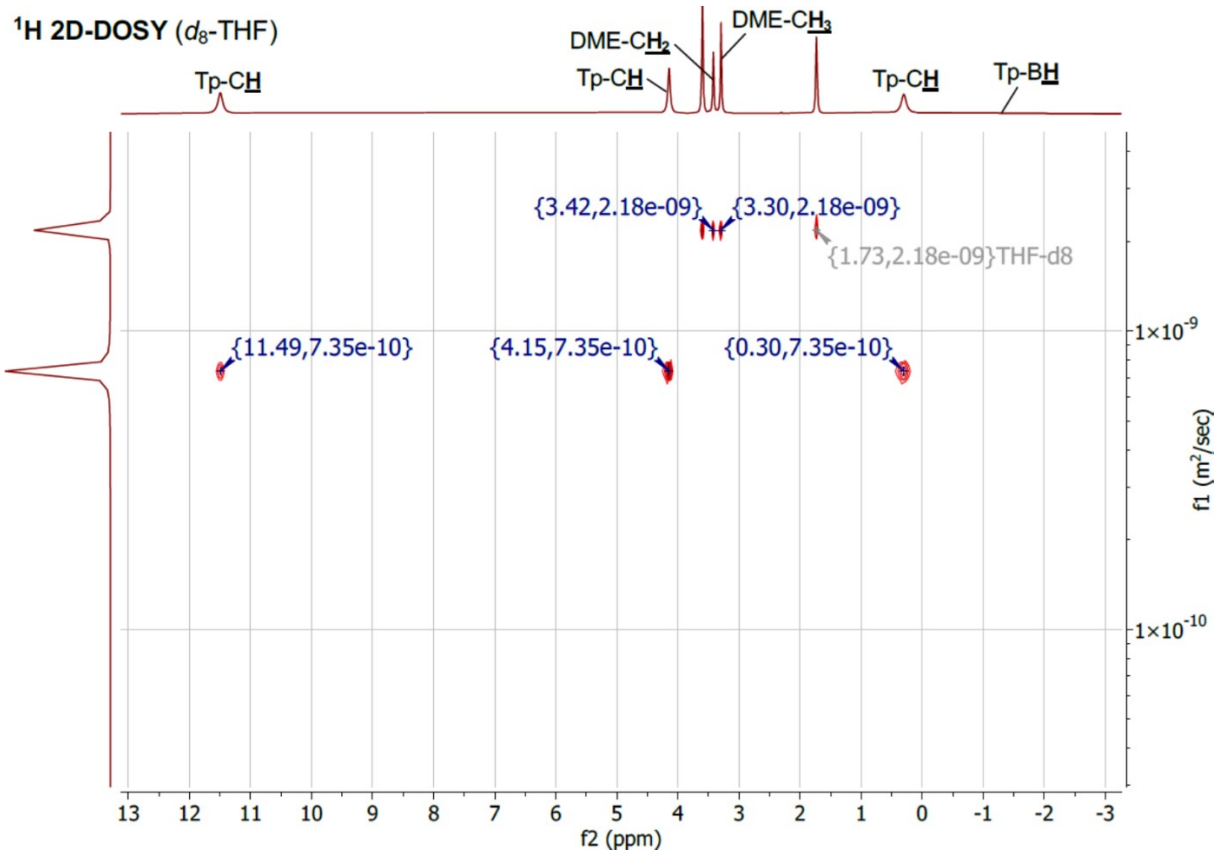

Figure S 14. ^{1}H 2D-DOSY NMR spectrum of [Sm(Tp)$_2$(DME)] **1-Sm(DME)**, recorded in d_8-THF. The horizontal scale shows ^{1}H chemical shifts (ppm) of **1-Sm(DME)**. The vertical dimension shows the diffusion scale (m^2s^{-1}) with diffusion cross-peaks for the Tp pyrazolyl protons of the equilibrium complex [Sm(Tp)$_2$(DME)$_n$] (DME; 0<n<1) centred at 7.35 × 10^{-10} m^2s^{-1} and the equilibrium position of 1-n equivalents of DME protons centred at 2.18 × 10^{-9} m^2s^{-1}.

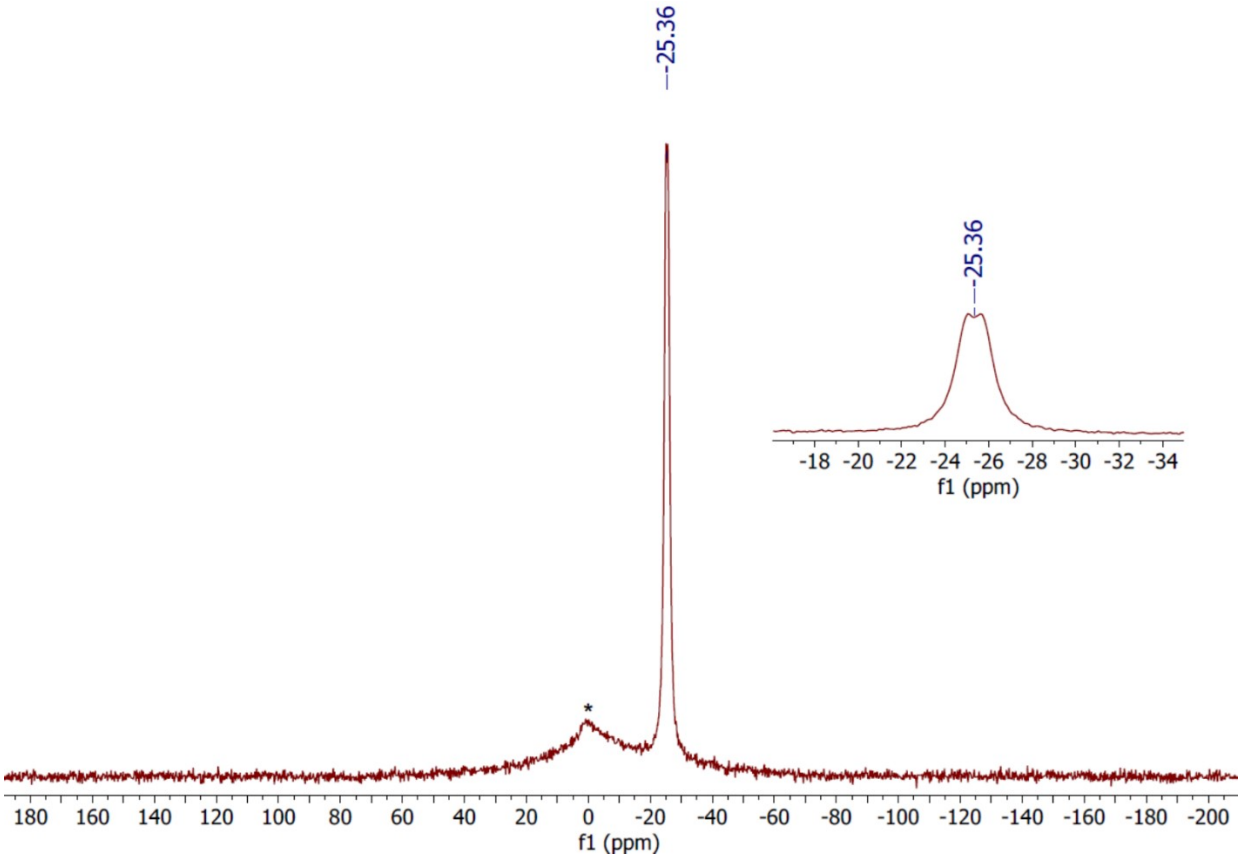

Figure S 15. ^{11}B NMR spectrum of [Sm(Tp)$_2$(DME)] **1-Sm(DME)**, recorded in d_8-THF. Borosilicate glass is denoted with *.

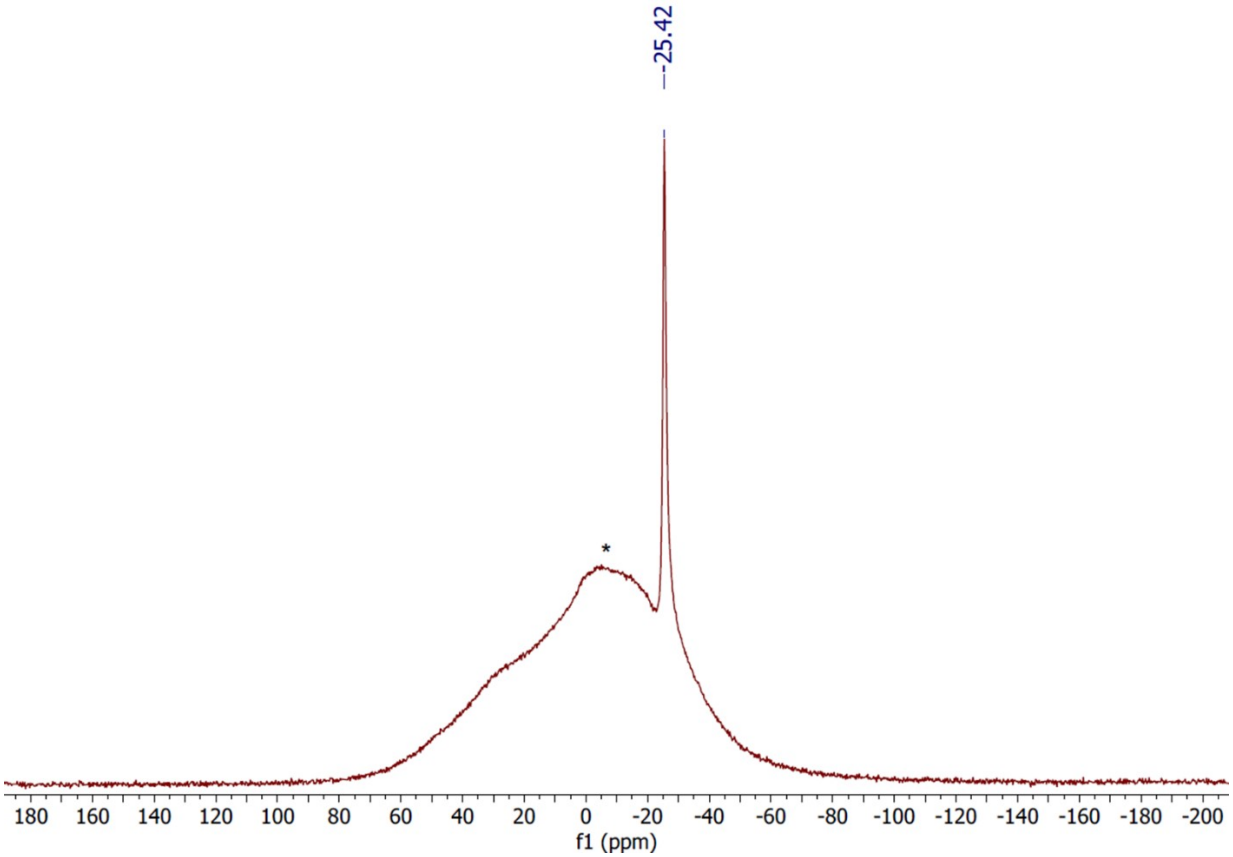

Figure S 16. ^{11}B{^{1}H} NMR spectrum of [Sm(Tp)$_2$(DME)] **1-Sm(DME)**, recorded in d_8-THF. Borosilicate glass is denoted with *.

A1.3 [Y(Tp)$_2$(κ^2-pz)] (pz = pyrazolyl)

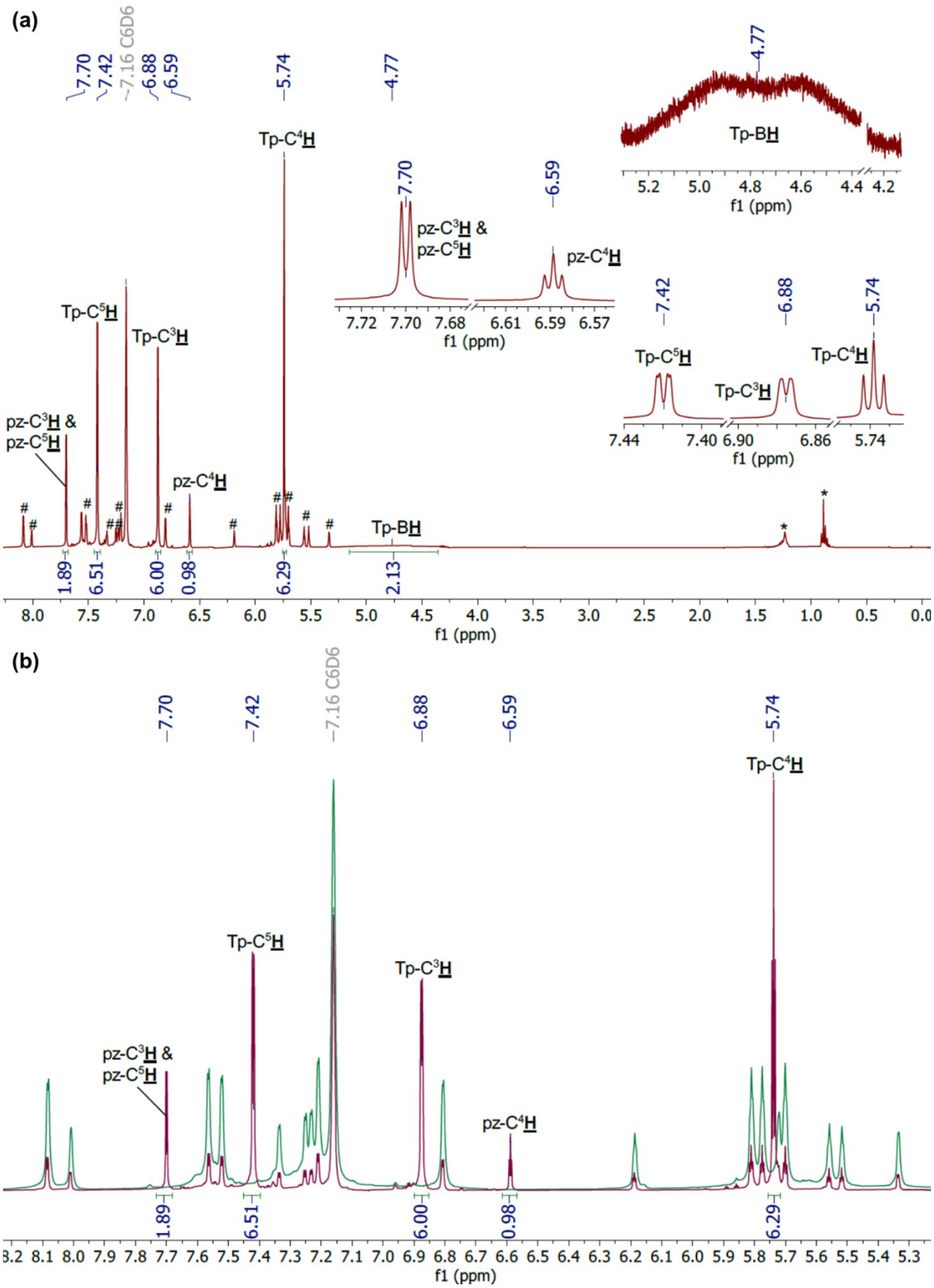

Figure S 17. (a) ^{1}H NMR spectrum of [Y(Tp)$_2$(κ^2-pz)], recorded in d_6-benzene. Residual hexane is denoted with * and minor [Y(Tp)$_3$] impurity is denoted with #. (b) Overlay of the ^{1}H NMR spectra of [Y(Tp)$_2$(κ^2-pz)] (maroon trace) and [Y(Tp)$_3$] (green trace).[1]

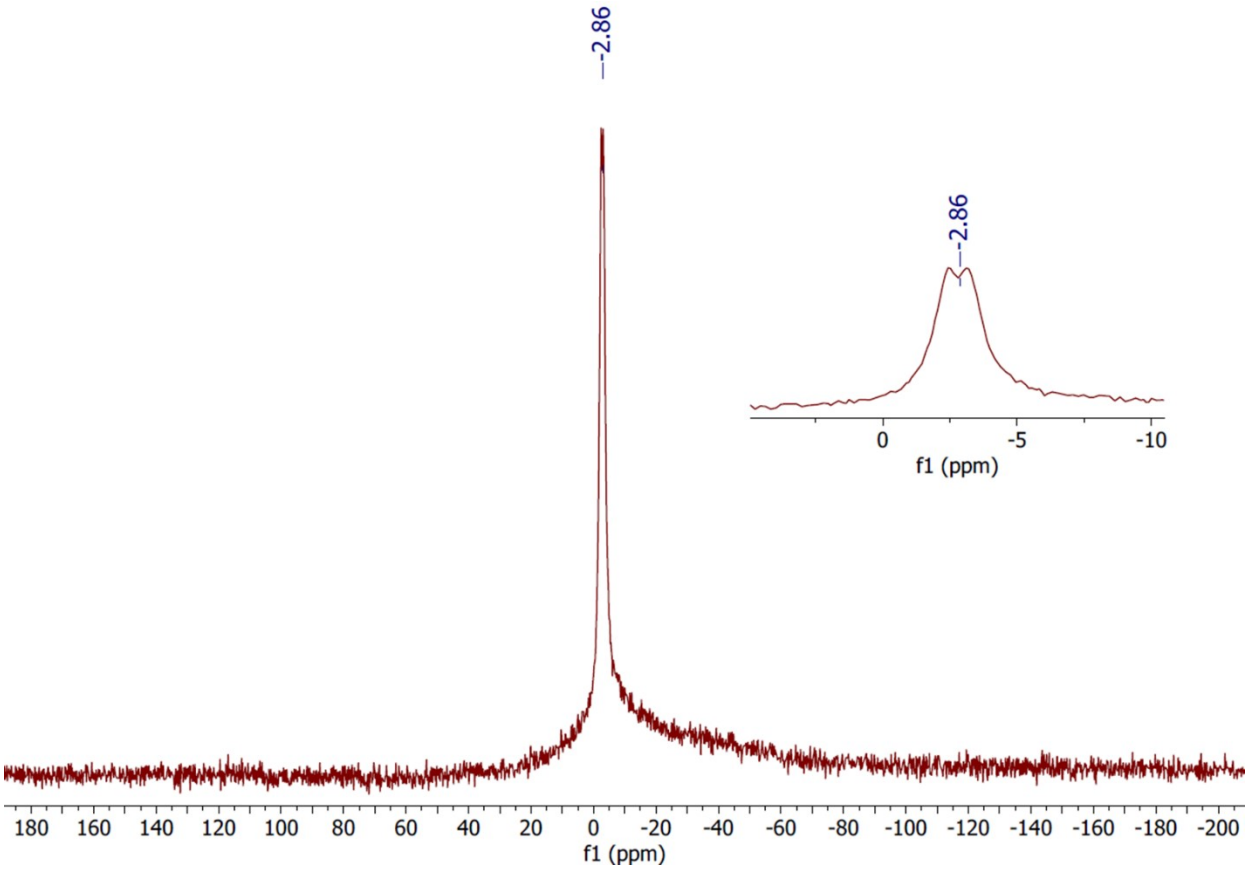

Figure S 18. ^{11}B NMR spectrum of [Y(Tp)$_2$(κ^2-pz)], recorded in d_6-benzene.

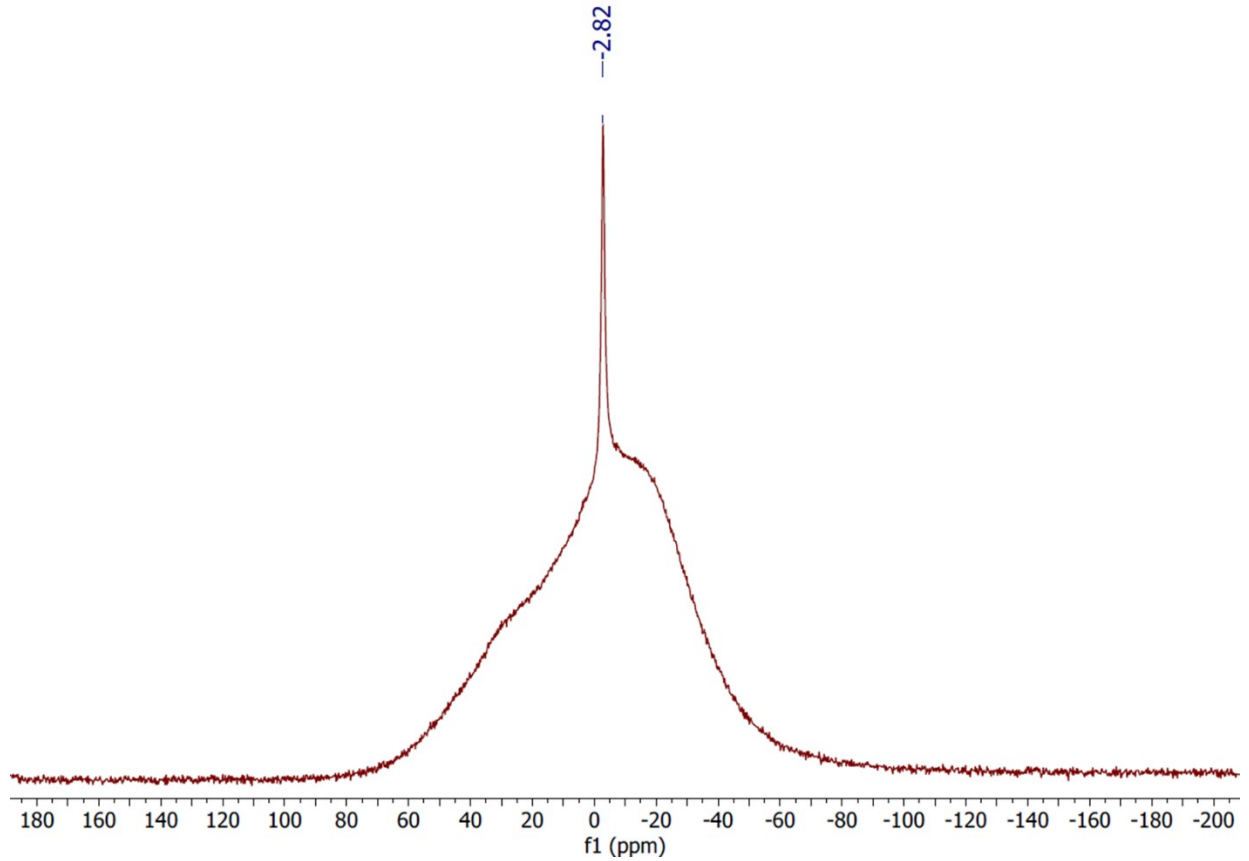

Figure S 19. ^{11}B{^{1}H} NMR spectrum of [Y(Tp)$_2$(κ^2-pz)], recorded in d_6-benzene.

A1.4 [Y(Tp)$_2$(OSiMe$_3$)] 3-Y

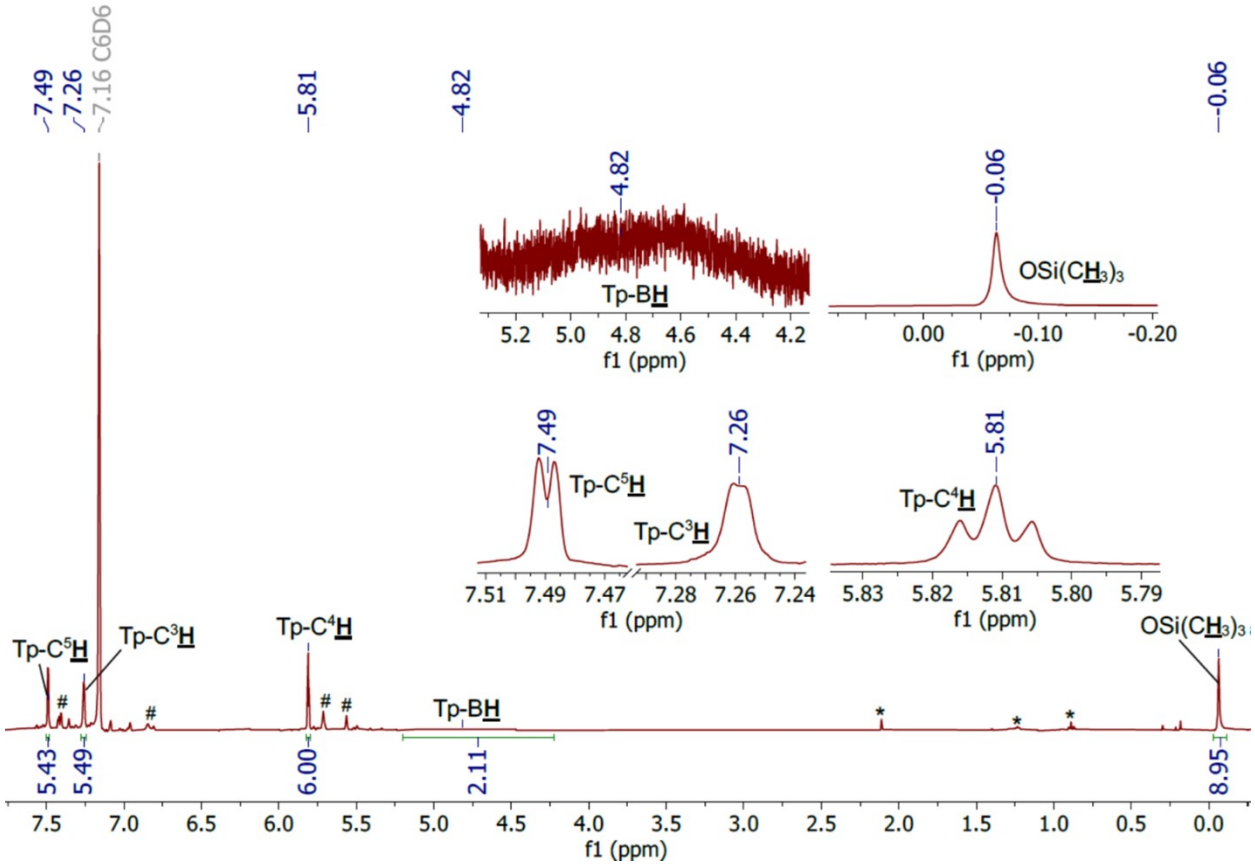

Figure S 20. ^{1}H NMR spectrum of [Y(Tp)$_2$(OSiMe$_3$)] **3-Y**, recorded in d_6-benzene. Residual hexane and toluene are denoted with * and minor byproducts are denoted with #.

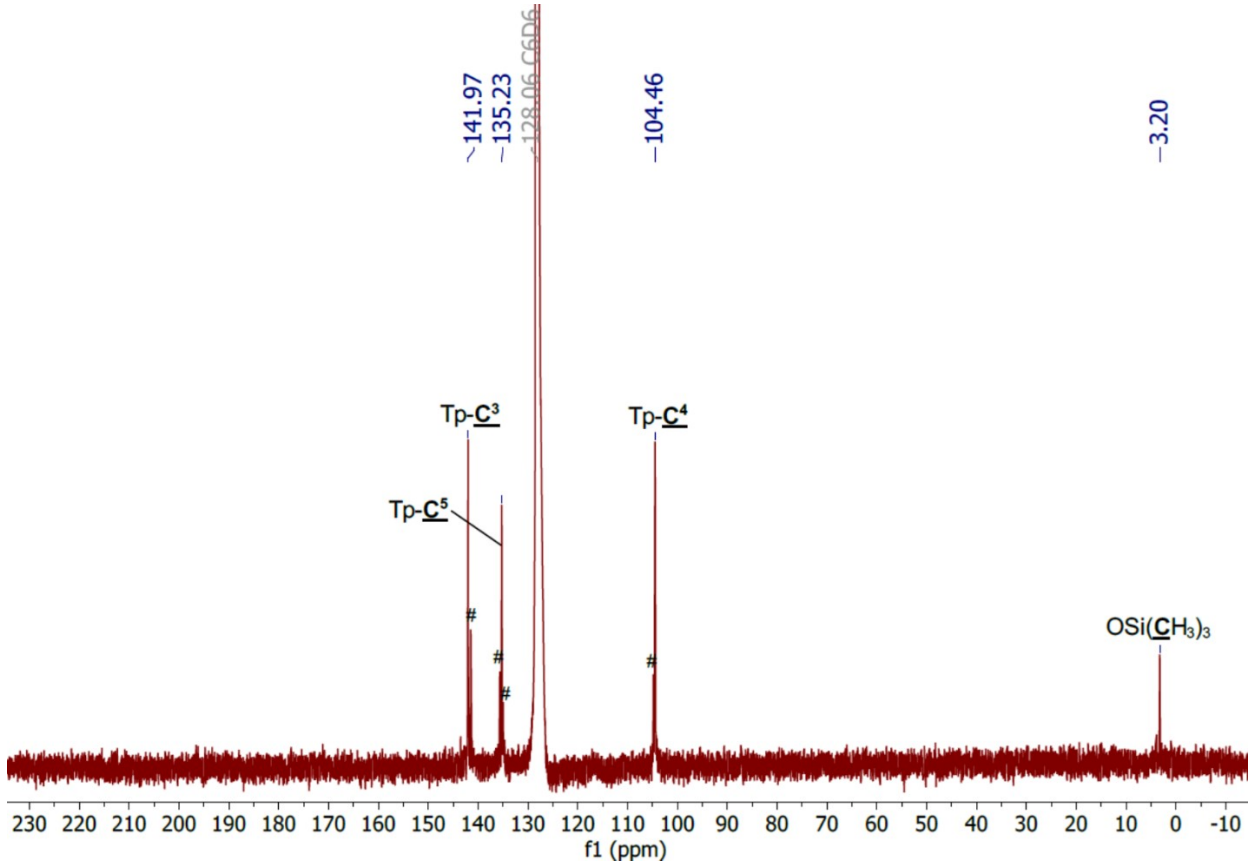

Figure S 21. ^{13}C{^{1}H} NMR spectrum of [Y(Tp)$_2$(OSiMe$_3$)] **3-Y**, recorded in d_6-benzene. Residual hexane and toluene are denoted with * and minor byproducts are denoted with #.

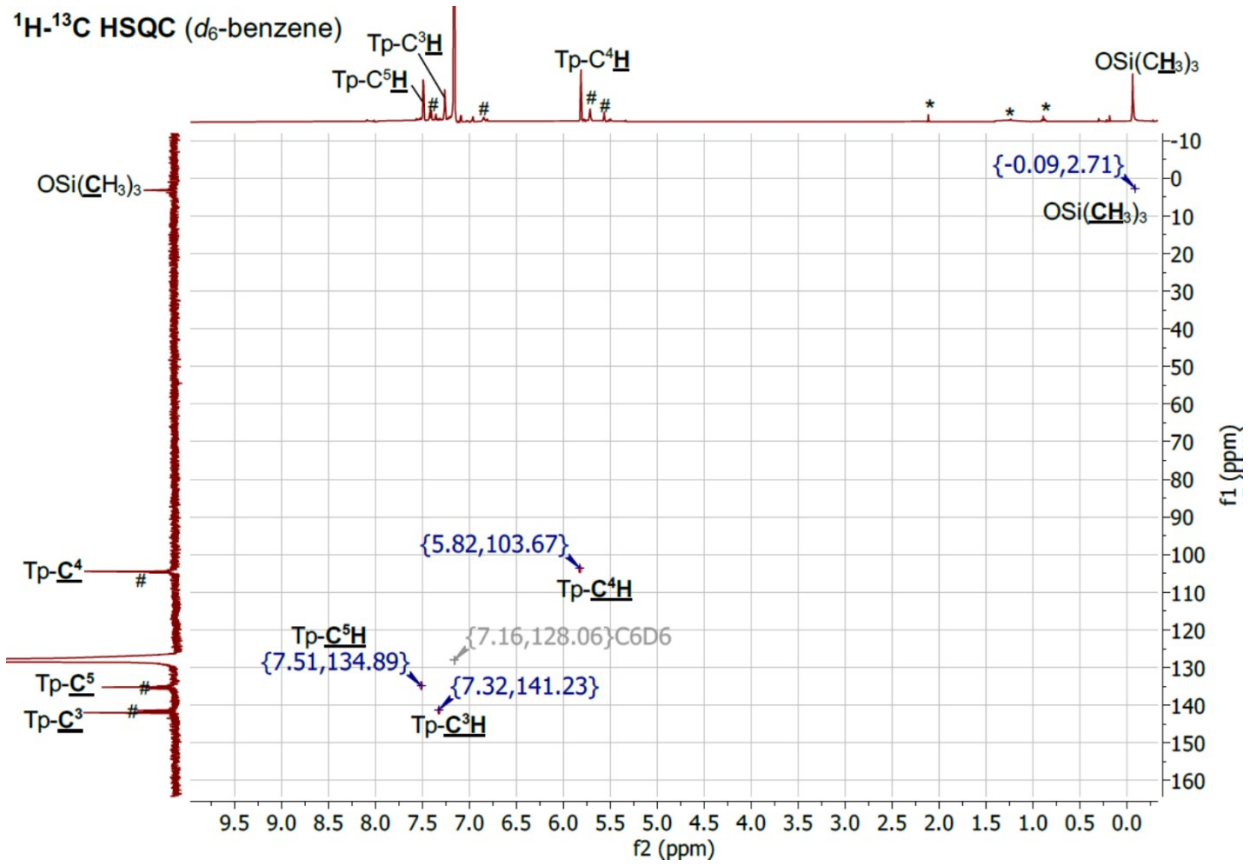

Figure S 22. ^{1}H-^{13}C HSQC NMR spectrum of $[Y(Tp)_2(OSiMe_3)]$ **3-Y**, recorded in d_6-benzene. Residual hexane and toluene are denoted with * and minor byproducts are denoted with #.

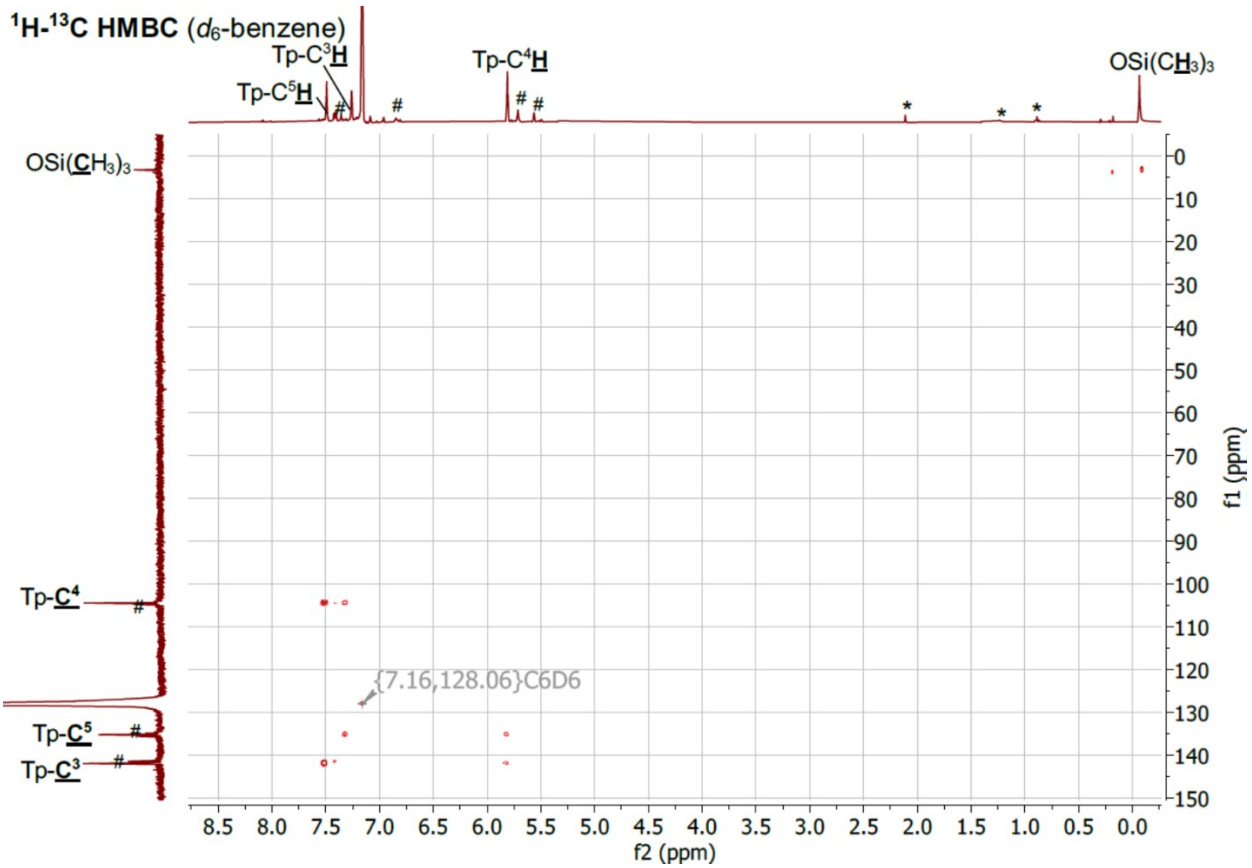

Figure S 23. ^{1}H-^{13}C HMBC NMR spectrum of $[Y(Tp)_2(OSiMe_3)]$ **3-Y**, recorded in d_6-benzene. Residual hexane and toluene are denoted with * and minor byproducts are denoted with #.

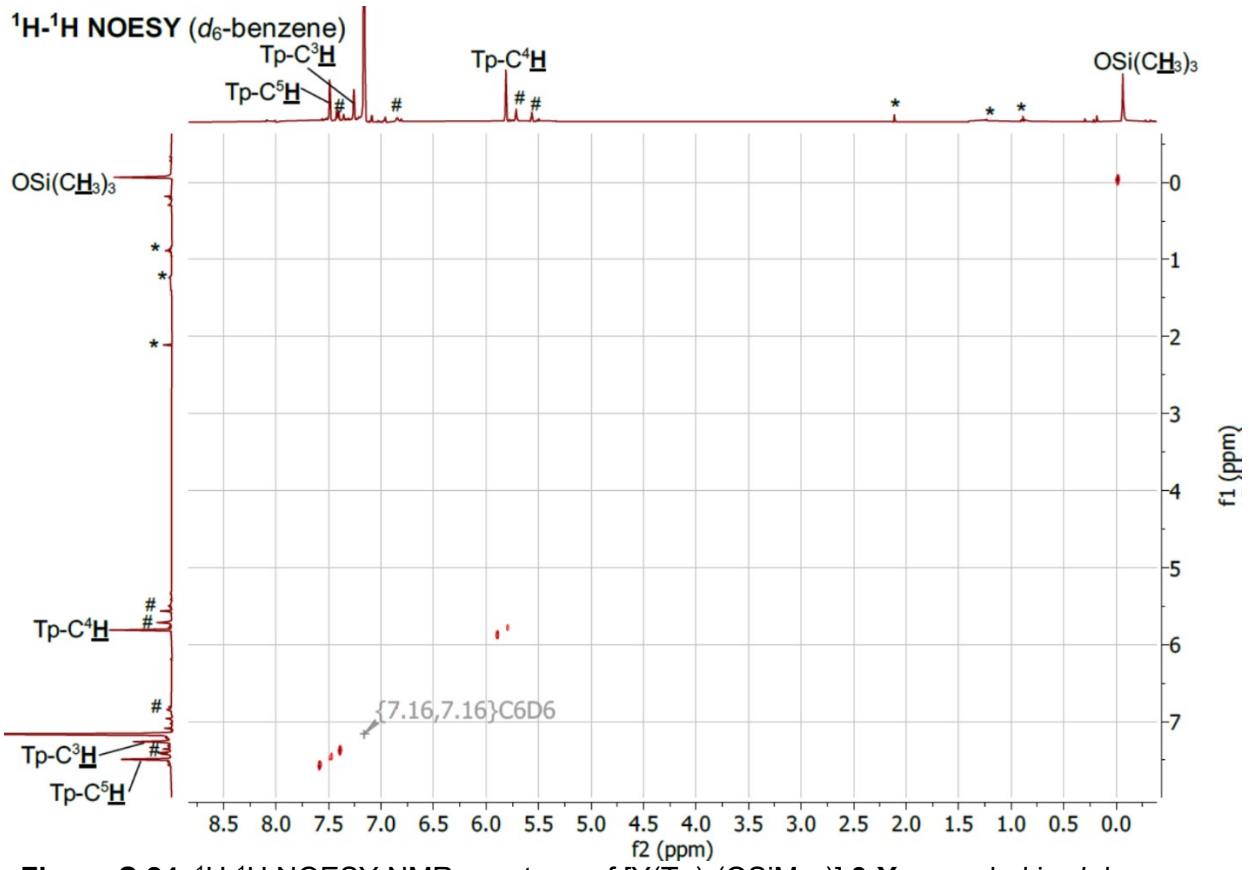

Figure S 24. ^{1}H-^{1}H NOESY NMR spectrum of [Y(Tp)$_2$(OSiMe$_3$)] **3-Y**, recorded in d_6-benzene. Residual hexane and toluene are denoted with * and minor byproducts are denoted with #.

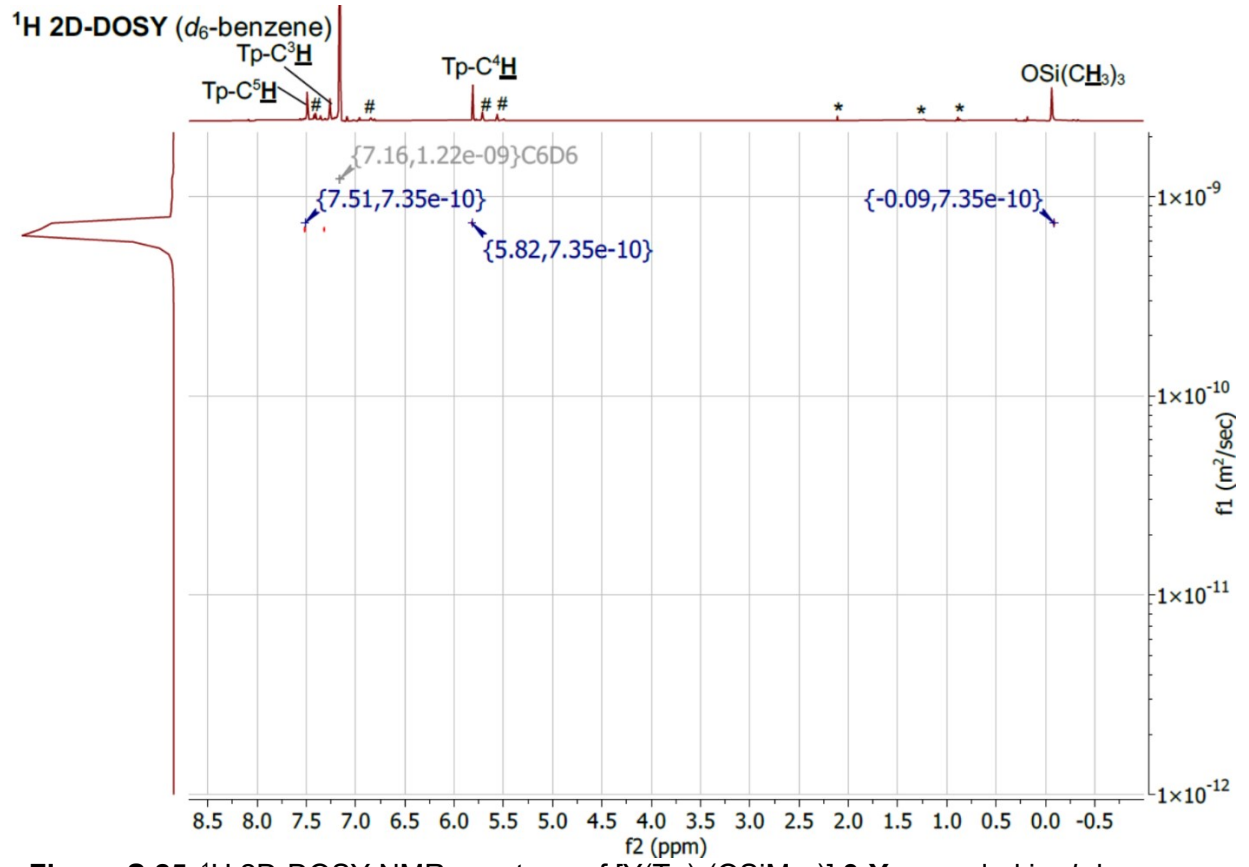

Figure S 25. ^{1}H 2D-DOSY NMR spectrum of [Y(Tp)$_2$(OSiMe$_3$)] **3-Y**, recorded in d_6-benzene. Residual hexane and toluene are denoted with * and minor byproducts are denoted with #. The horizontal scale shows ^{1}H chemical shifts (ppm) and the vertical dimension the diffusion scale (m^2s^{-1}) with diffusion cross-peaks for **3-Y** centred at 7.35×10^{-10} m^2s^{-1}.

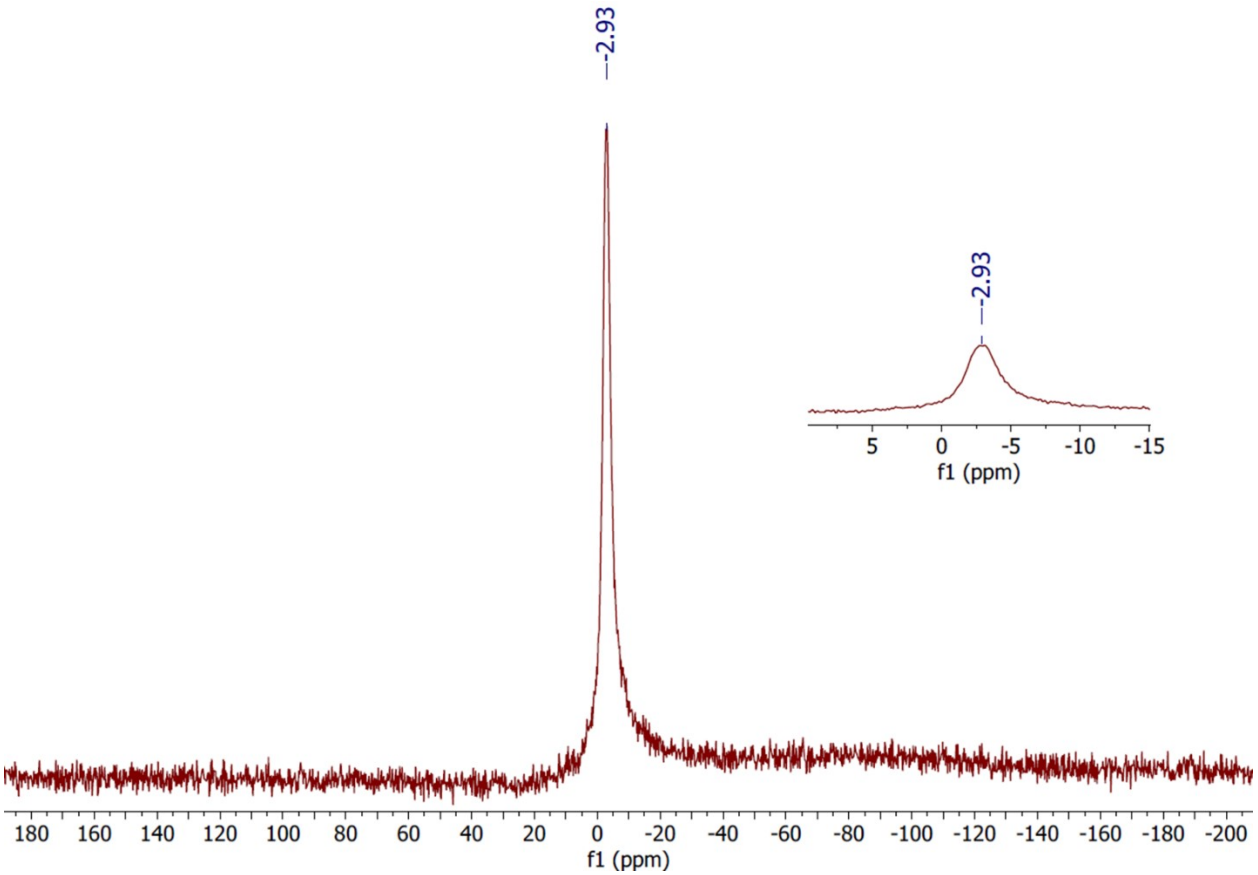

Figure S 26. ^{11}B NMR spectrum of [Y(Tp)$_2$(OSiMe$_3$)] **3-Y**, recorded in d_6-benzene.

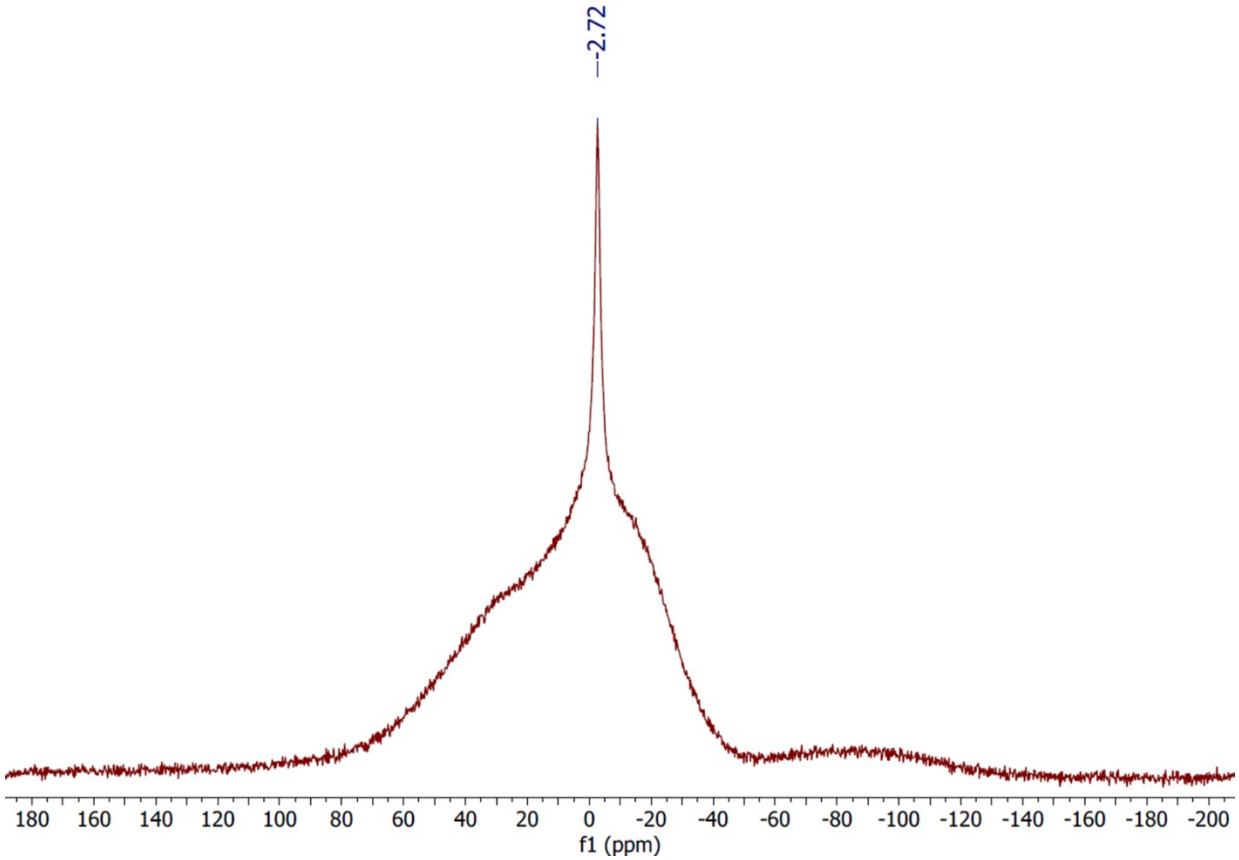

Figure S 27. ^{11}B NMR spectrum of [Y(Tp)$_2$(OSiMe$_3$)] **3-Y**, recorded in d_6-benzene.

A1.5 $[Sm(Tp)_2(OSiMe_3)]$ 3-Sm

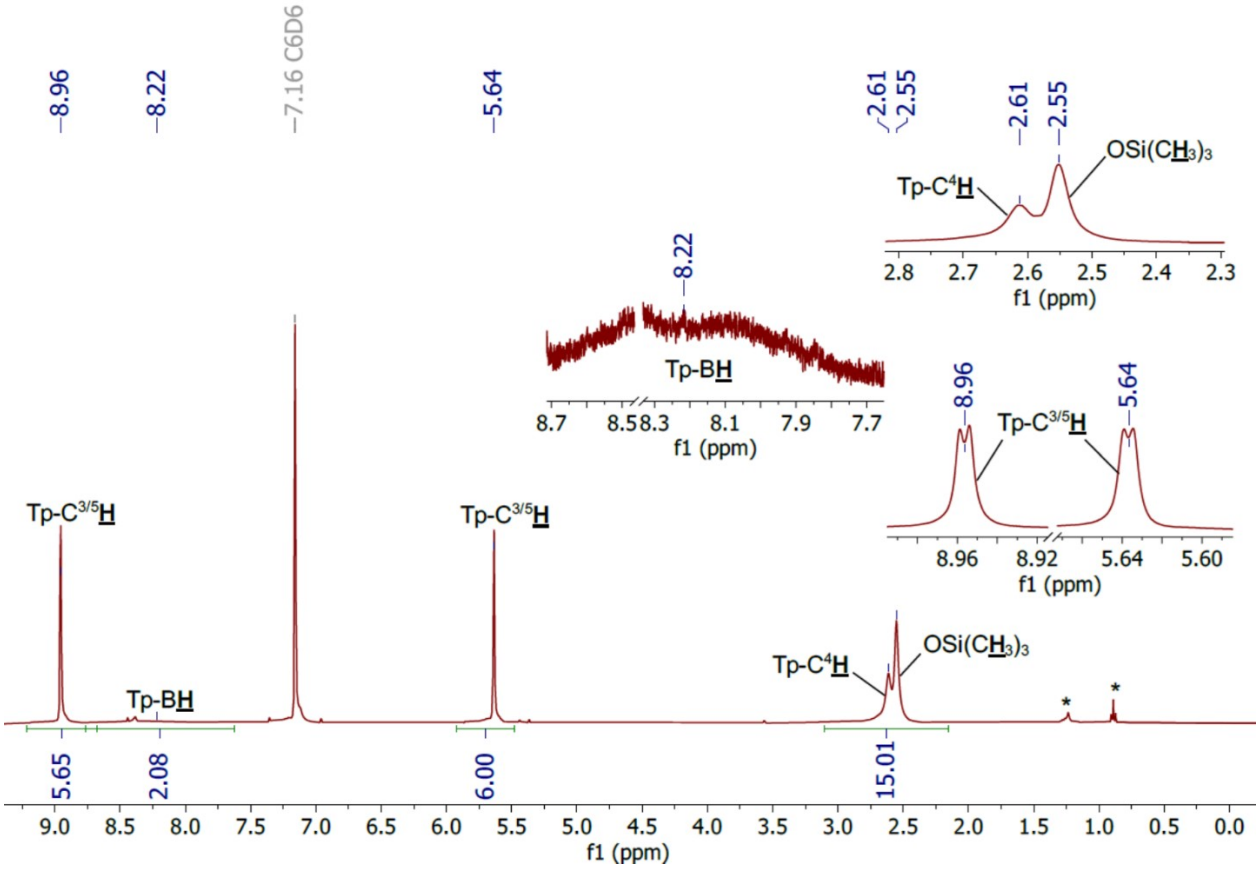

Figure S 28. ^{1}H NMR spectrum of $[Sm(Tp)_2(OSiMe_3)]$ **3-Sm**, recorded in d_6-benzene. Residual hexane is denoted with *.

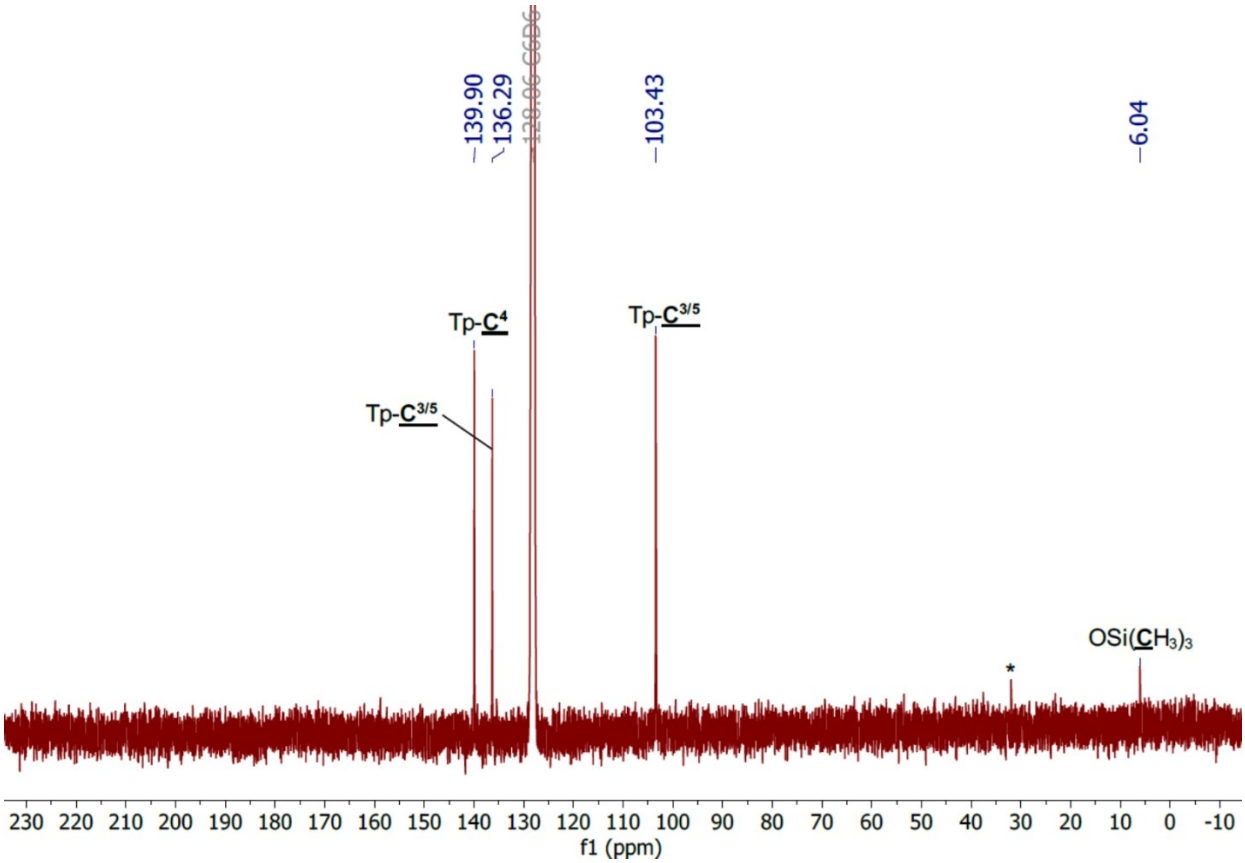

Figure S 29. $^{13}C\{^{1}H\}$ NMR spectrum of $[Sm(Tp)_2(OSiMe_3)]$ **3-Sm**, recorded in d_6-benzene. Residual hexane is denoted with *.

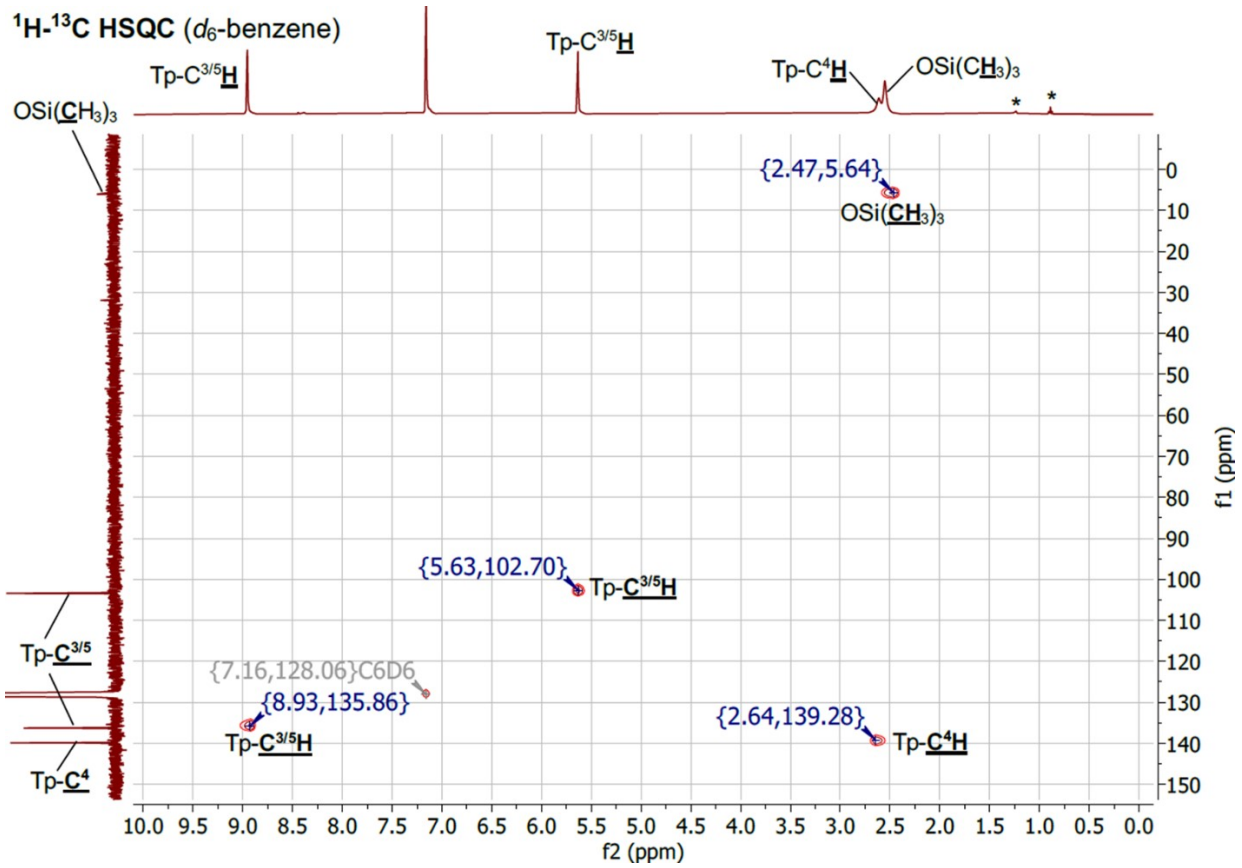

Figure S 30. ^{1}H-^{13}C HSQC NMR spectrum of [Sm(Tp)$_2$(OSiMe$_3$)] **3-Sm**, recorded in d_6-benzene. Residual hexane is denoted with *.

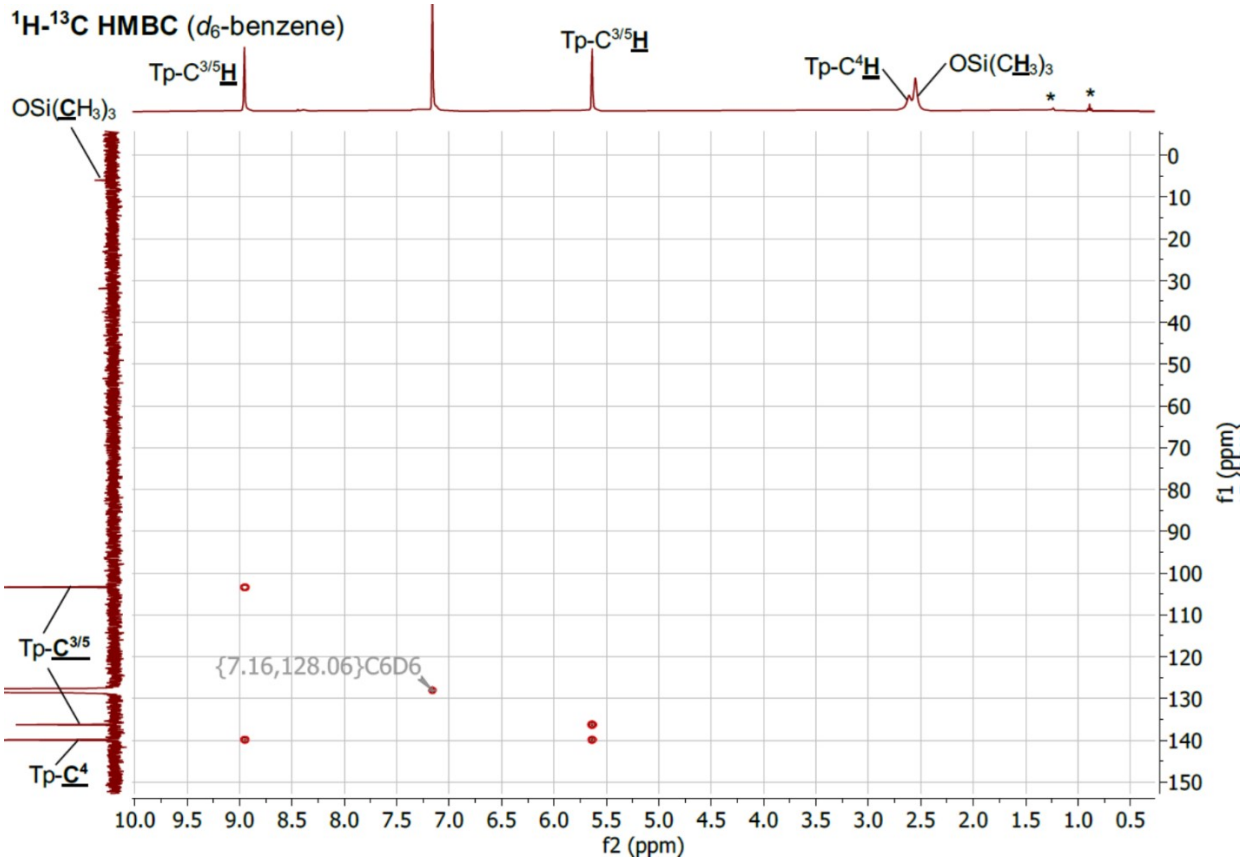

Figure S 31. ^{1}H-^{13}C HMBC NMR spectrum of [Sm(Tp)$_2$(OSiMe$_3$)] **3-Sm**, recorded in d_6-benzene. Residual hexane is denoted with *.

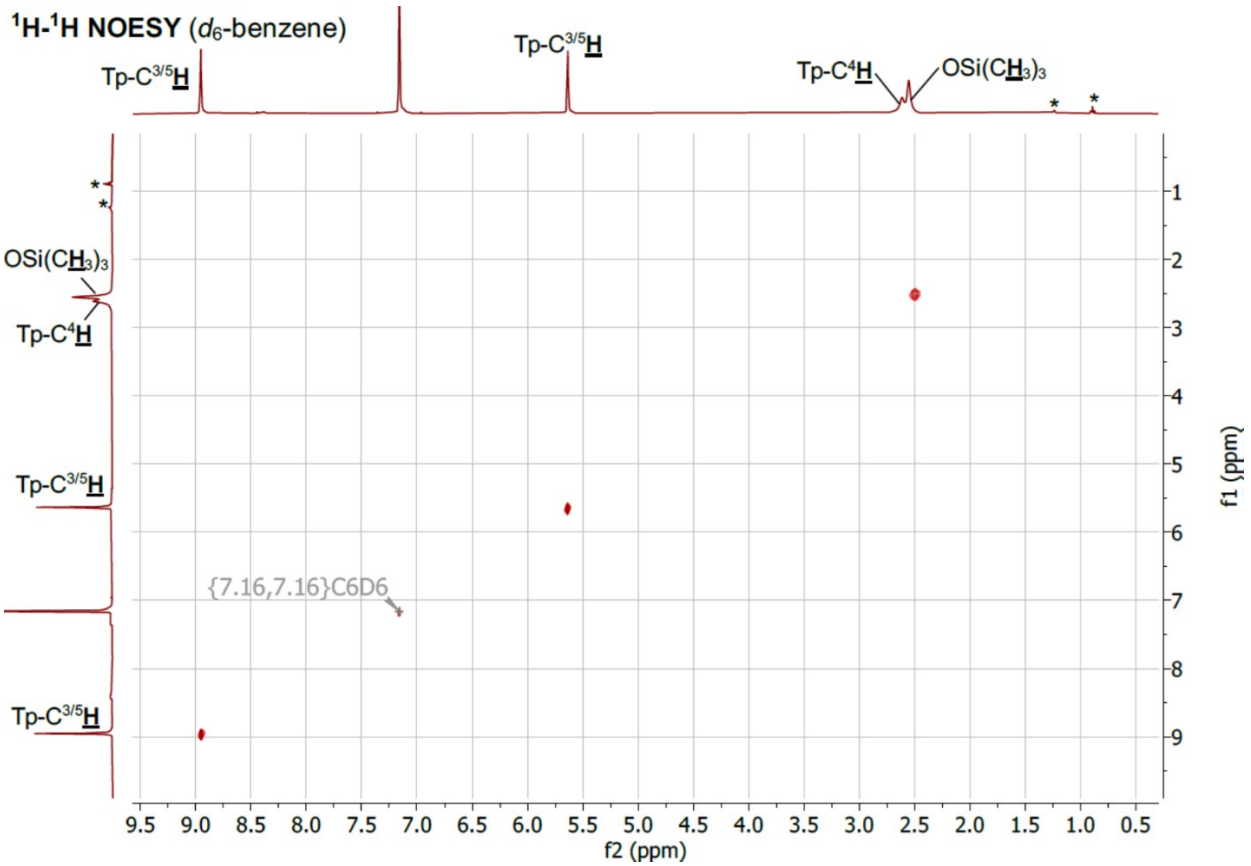

Figure S 32. ^{1}H-^{1}H NOESY NMR spectrum of [Sm(Tp)$_2$(OSiMe$_3$)] **3-Sm**, recorded in d_6-benzene. Residual hexane is denoted with *.

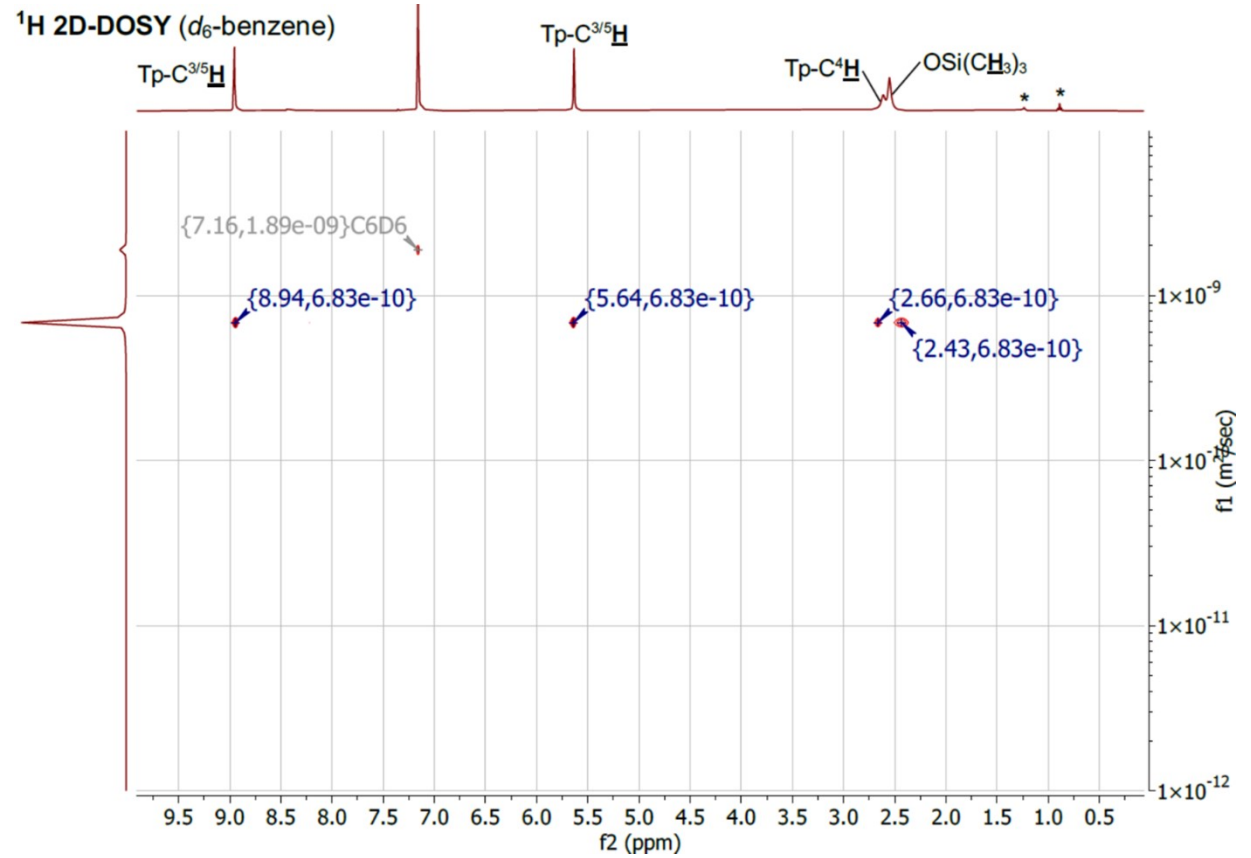

Figure S 33. ^{1}H 2D-DOSY NMR spectrum of [Sm(Tp)$_2$(OSiMe$_3$)] **3-Sm**, recorded in d_6-benzene. Residual hexane is denoted with *. The horizontal scale shows ^{1}H chemical shifts (ppm) and the vertical dimension the diffusion scale (m^2s^{-1}) with diffusion cross-peaks for **3-Sm** centred at 6.83 × 10^{-10} m^2s^{-1}.

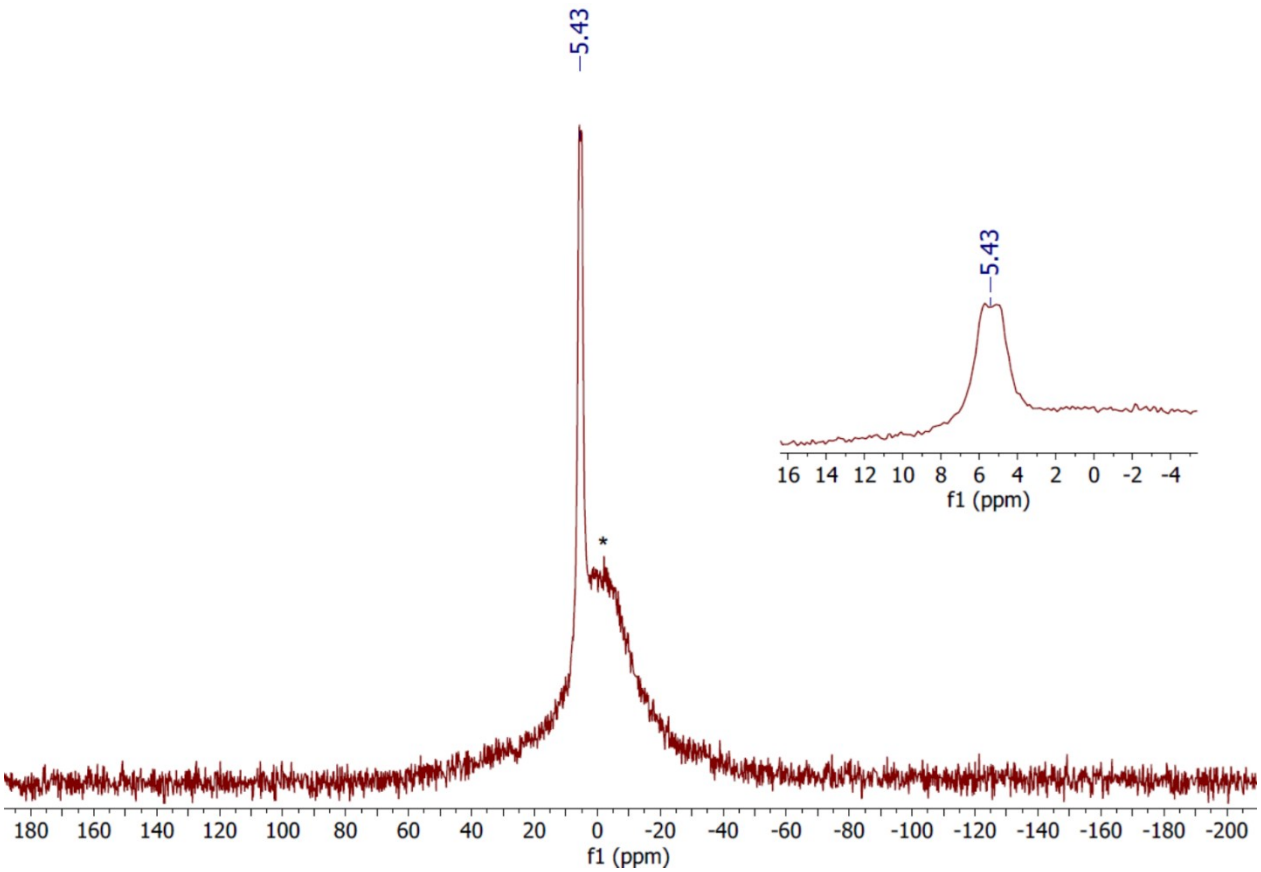

Figure S 34. ^{11}B NMR spectrum of [Sm(Tp)$_2$(OSiMe$_3$)] **3-Sm**, recorded in d_6-benzene.

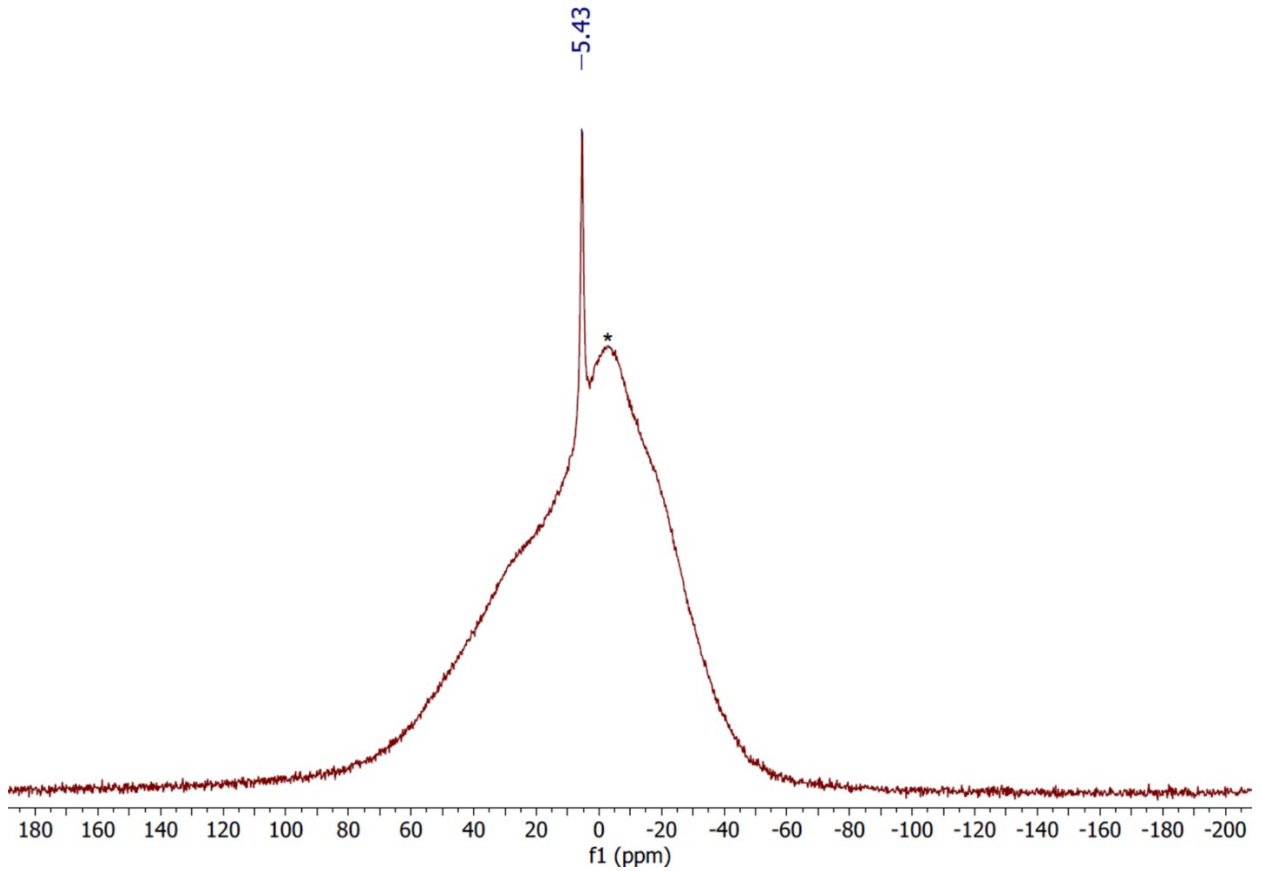

Figure S 35. ^{11}B NMR spectrum of [Sm(Tp)$_2$(OSiMe$_3$)] **3-Sm**, recorded in d_6-benzene.

A1.6 $[Sm_5(Tp)_6(\mu_2\text{-}OH)_6(\mu_3\text{-}OH)_2(\mu_4\text{-}OH)]$ 4-Sm

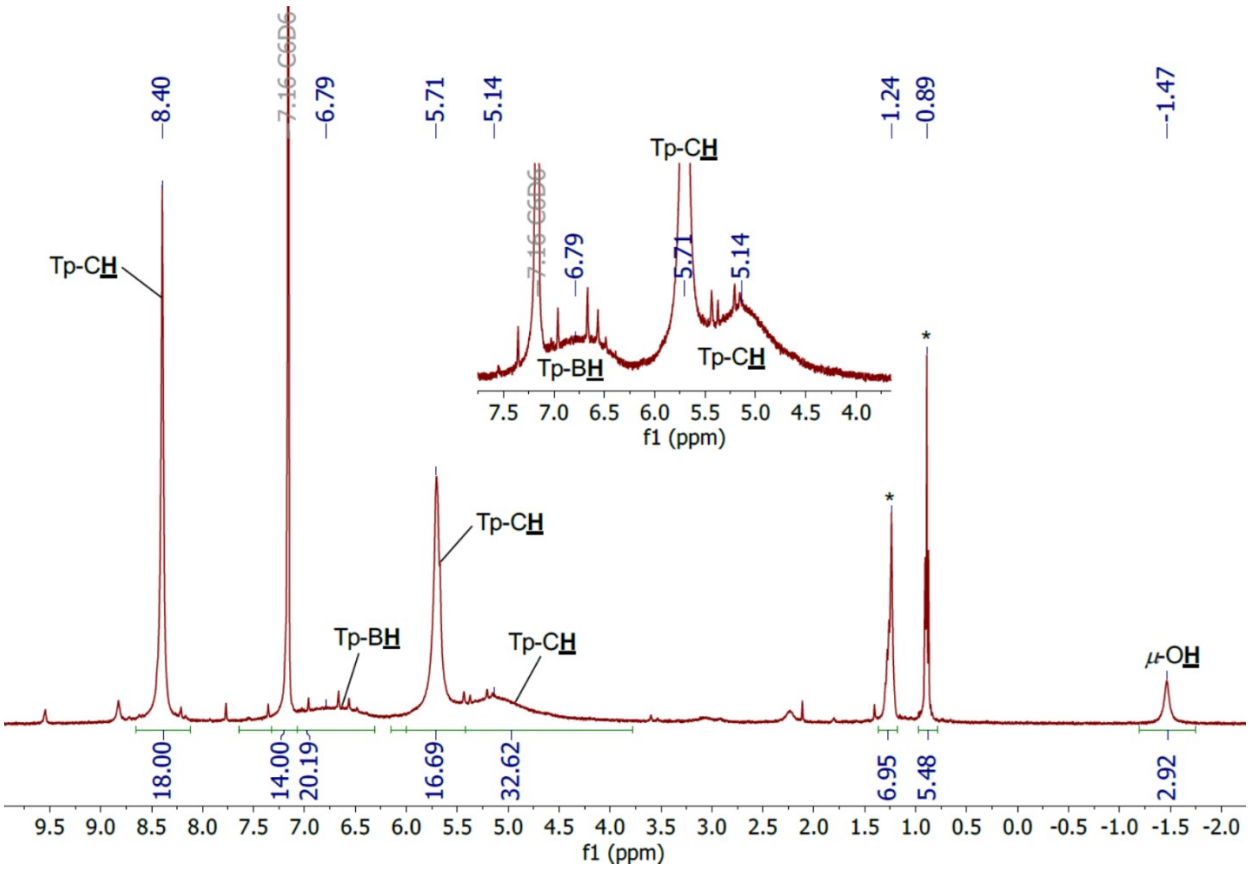

Figure S 36. ^{1}H NMR spectrum of $[Sm_5(Tp)_6(\mu_2\text{-}OH)_6(\mu_3\text{-}OH)_2(\mu_4\text{-}OH)]$ **4-Sm**, recorded in d_6-benzene. Lattice hexane of crystallisation is denoted with *.

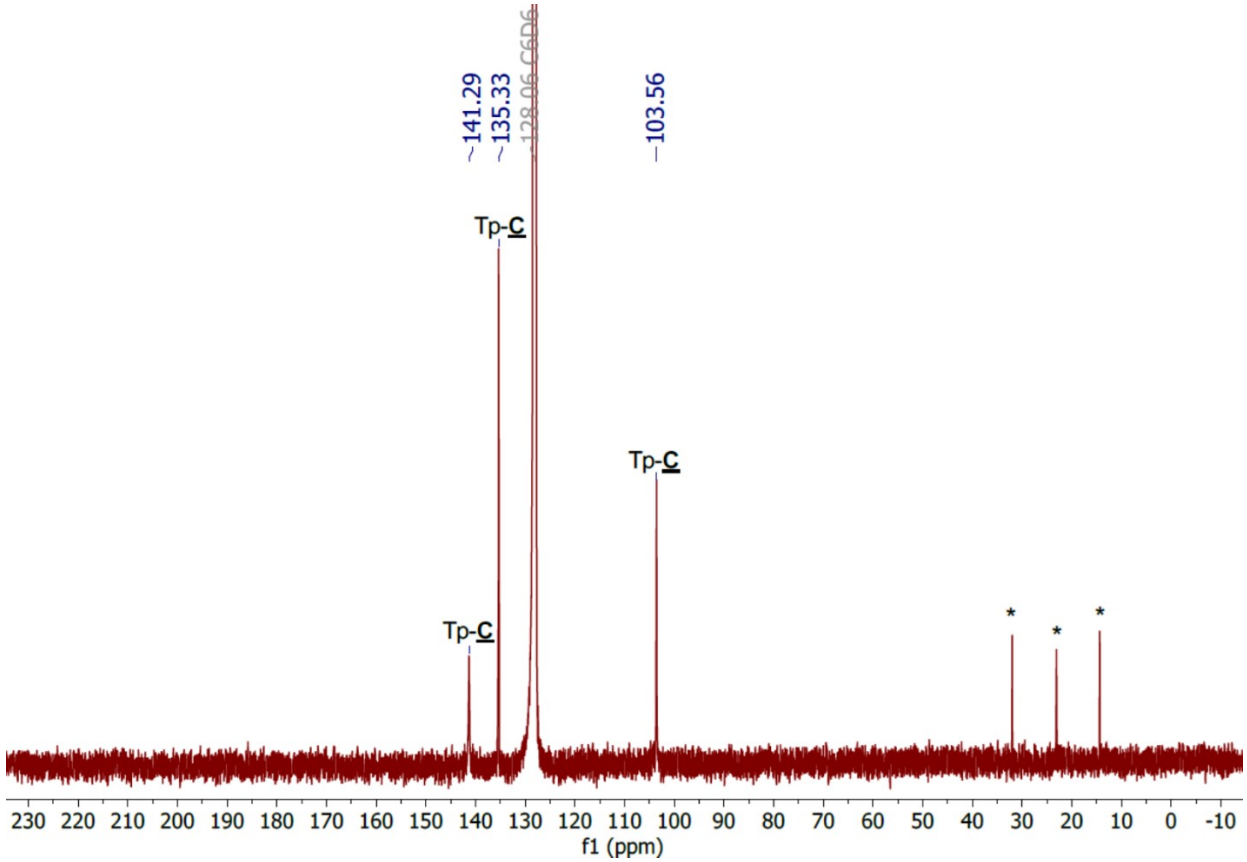

Figure S 37. $^{13}C\{^{1}H\}$ NMR spectrum of $[Sm_5(Tp)_6(\mu_2\text{-}OH)_6(\mu_3\text{-}OH)_2(\mu_4\text{-}OH)]$ **4-Sm**, recorded in d_6-benzene. Lattice hexane of crystallisation is denoted with *.

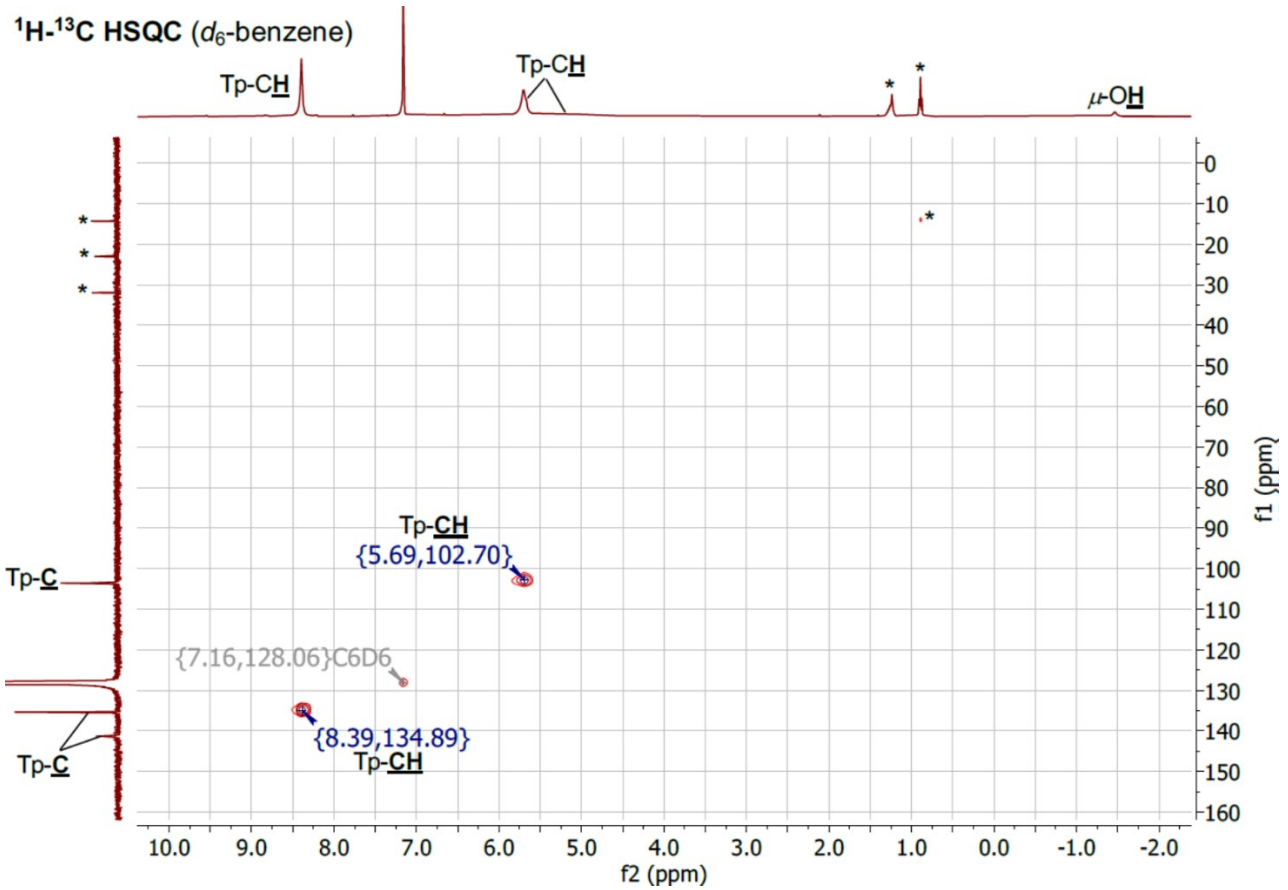

Figure S 38. ^{1}H-^{13}C HSQC NMR spectrum of [$Sm_5(Tp)_6(\mu_2\text{-}OH)_6(\mu_3\text{-}OH)_2(\mu_4\text{-}OH)$] **4-Sm**, recorded in d_6-benzene. Lattice hexane of crystallisation is denoted with *.

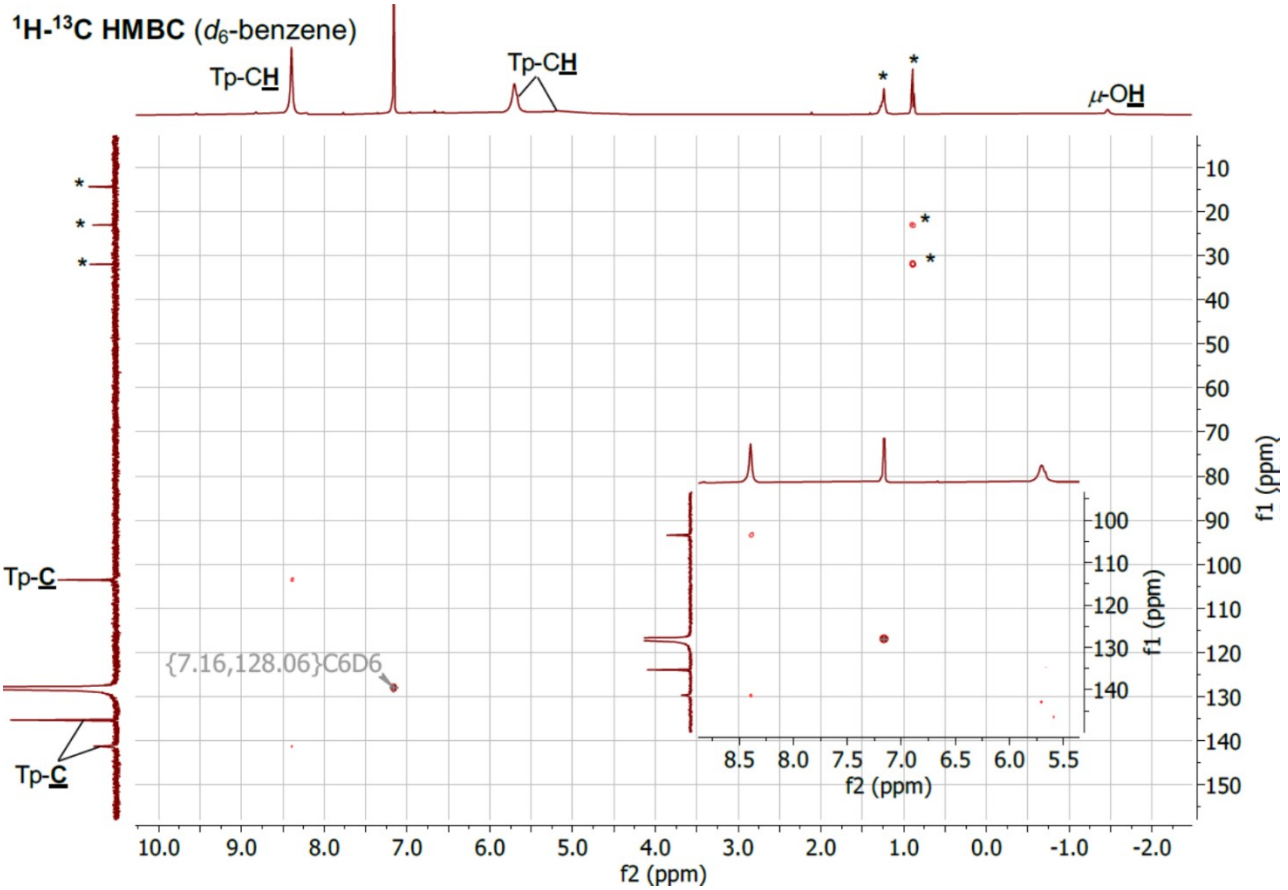

Figure S 39. ^{1}H-^{13}C HMBC NMR spectrum of [$Sm_5(Tp)_6(\mu_2\text{-}OH)_6(\mu_3\text{-}OH)_2(\mu_4\text{-}OH)$] **4-Sm**, recorded in d_6-benzene. Lattice hexane of crystallisation is denoted with *.

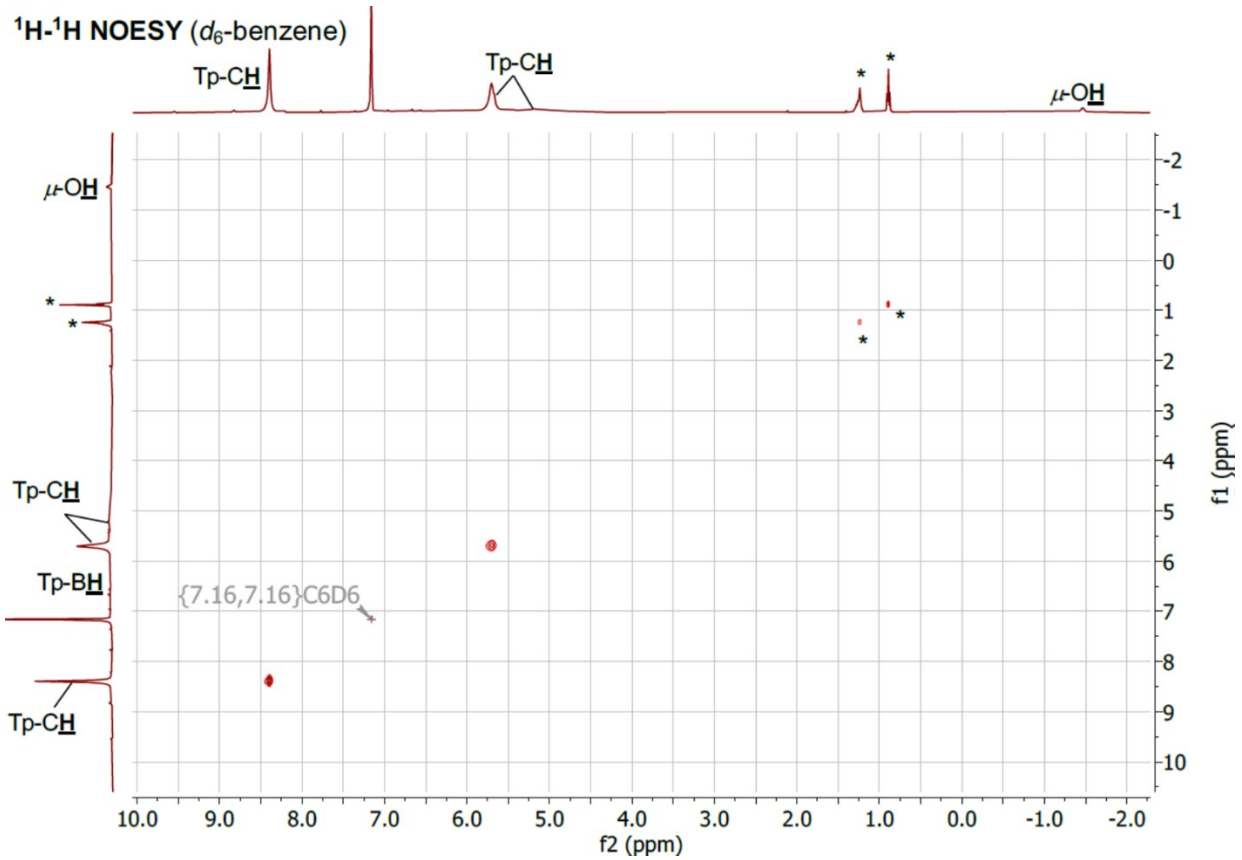

Figure S 40. ^{1}H-^{1}H NOESY NMR spectrum of [$Sm_5(Tp)_6(\mu_2\text{-}OH)_6(\mu_3\text{-}OH)_2(\mu_4\text{-}OH)$] **4-Sm**, recorded in d_6-benzene. Lattice hexane of crystallisation is denoted with *.

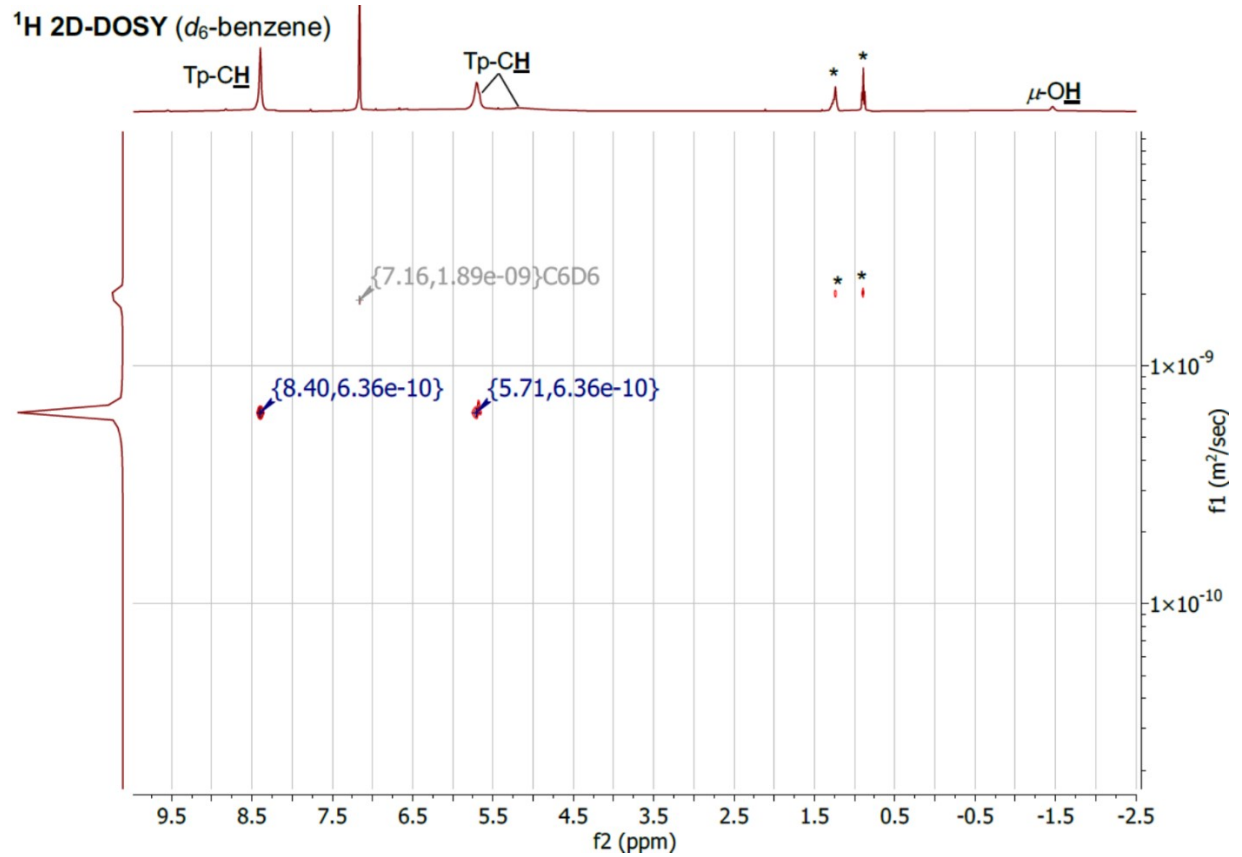

Figure S 41. ^{1}H 2D-DOSY NMR spectrum of [$Sm_5(Tp)_6(\mu_2\text{-}OH)_6(\mu_3\text{-}OH)_2(\mu_4\text{-}OH)$] **4-Sm**, recorded in d_6-benzene. The horizontal scale shows ^{1}H chemical shifts (ppm) and the vertical dimension the diffusion scale (m^2s^{-1}) with diffusion cross-peaks for **4-Sm** centred at 6.36 x 10^{-10} m^2s^{-1}. Lattice hexane of crystallisation and the corresponding diffusion cross-peak for hexane are denoted with *.

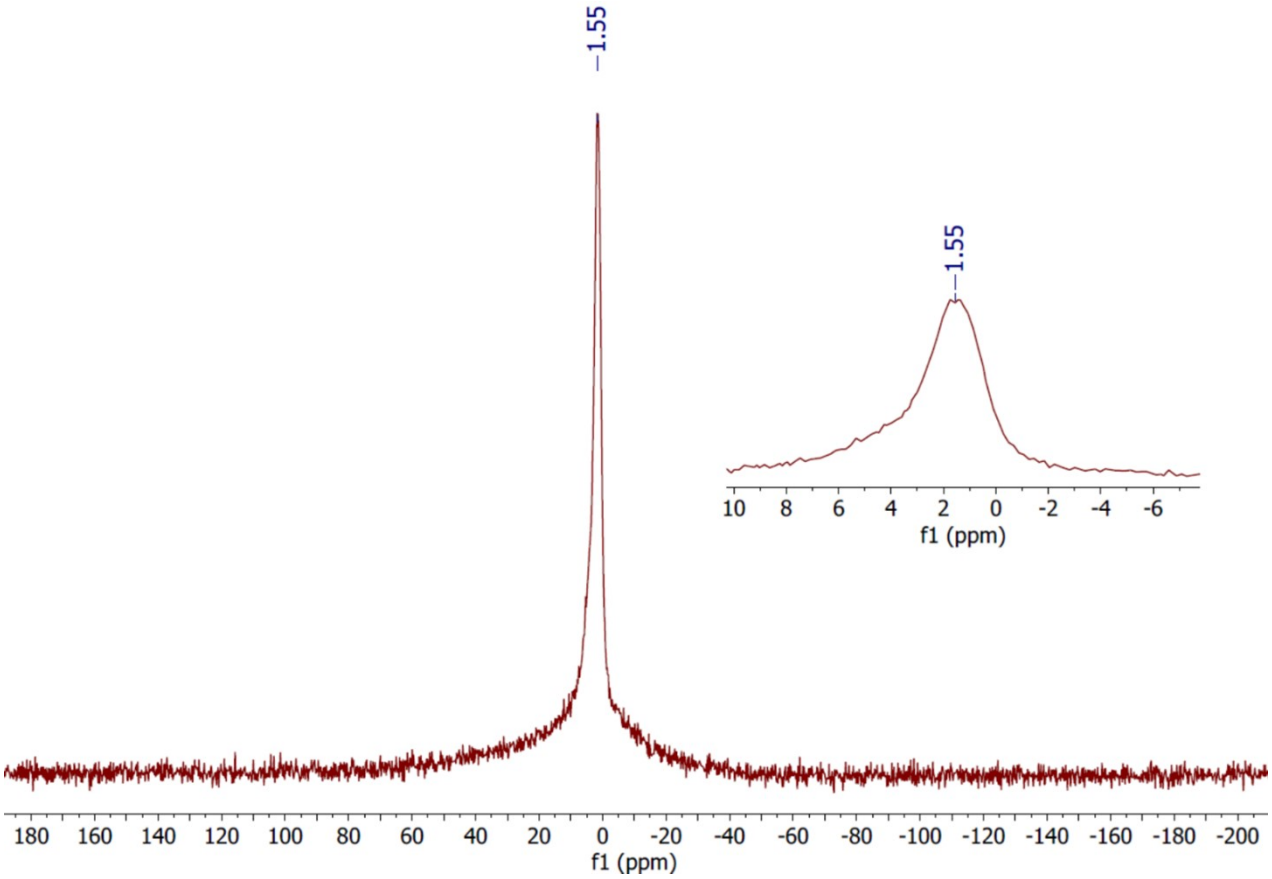

Figure S 42. ^{11}B NMR spectrum of [$Sm_5(Tp)_6(\mu_2\text{-}OH)_6(\mu_3\text{-}OH)_2(\mu_4\text{-}OH)$] **4-Sm**, recorded in d_6-benzene.

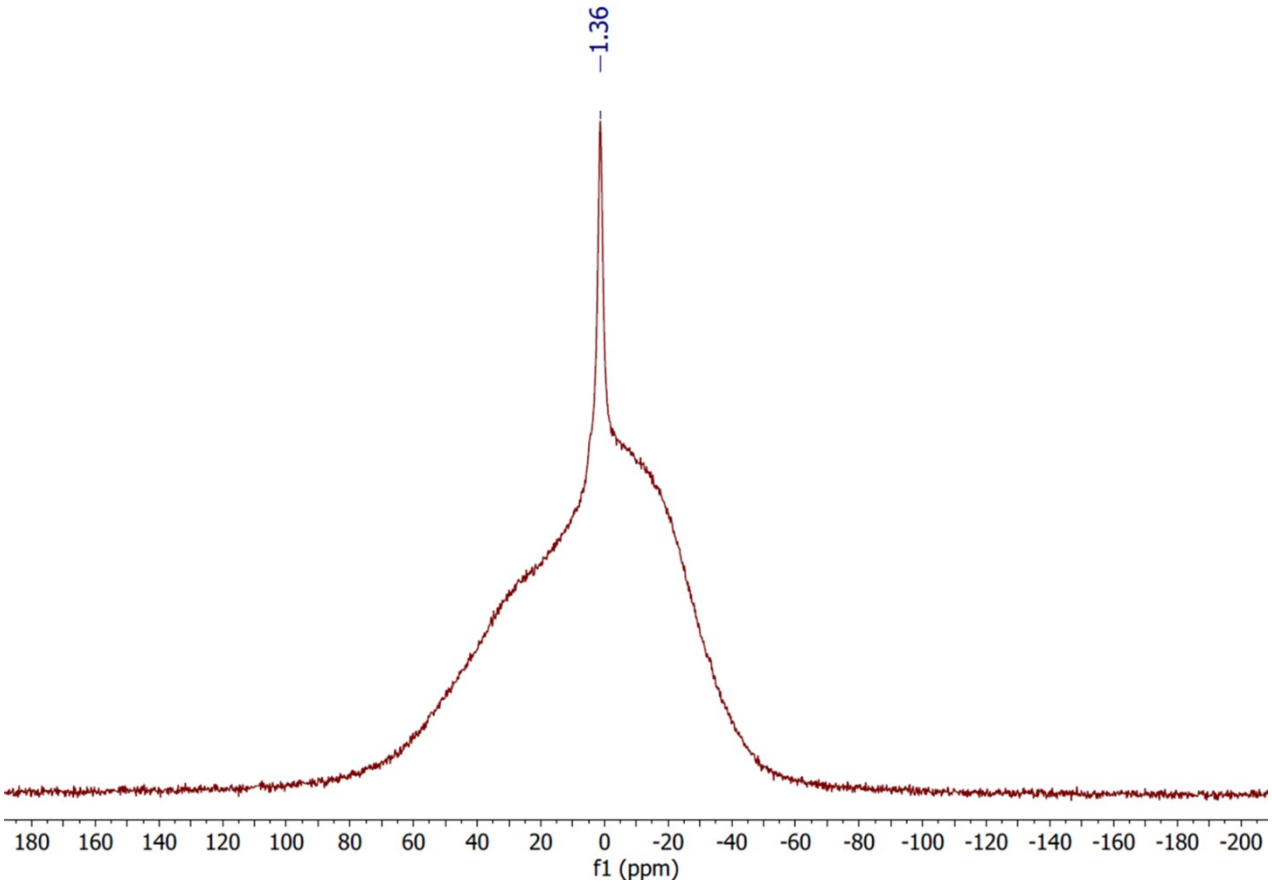

Figure S 43. ^{11}B{^{1}H} NMR spectrum of [$Sm_5(Tp)_6(\mu_2\text{-}OH)_6(\mu_3\text{-}OH)_2(\mu_4\text{-}OH)$] **4-Sm**, recorded in d_6-benzene.

A2 NMR data for NMR-scale reactions with carbon dioxide (CO_2)

A2.1 NMR-scale reaction between [Sm(Tp)$_2$(DME)] 1-Sm(DME) and CO_2 in d_8-THF to yield [{Sm(Tp)$_2$}$_2$(μ-η^2:η^2-O_2CCO_2)] 2-Sm

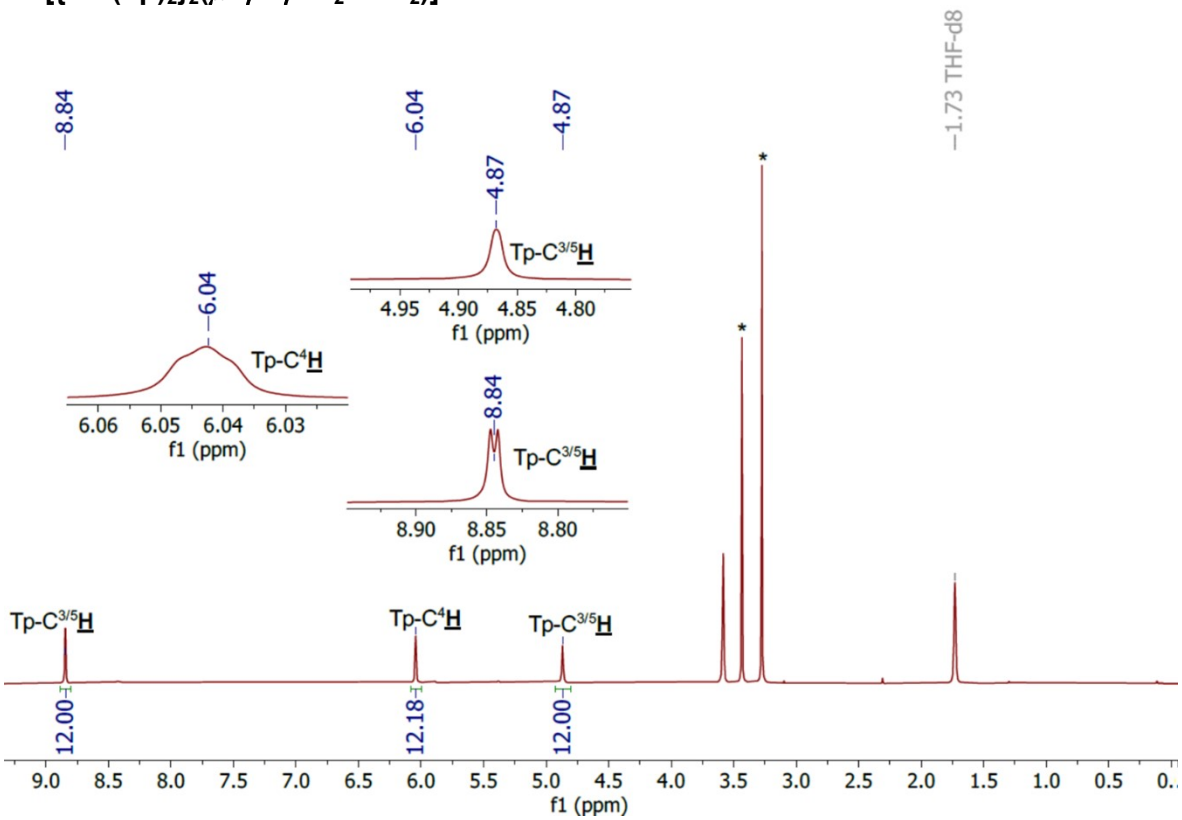

Figure S 44. ^{1}H NMR spectrum of [{Sm(Tp)$_2$}$_2$(μ-η^2:η^2-O_2CCO_2)] **2-Sm**, from the reaction of [Sm(Tp)$_2$(DME)] **1-Sm(DME)** with CO_2 in d_8-THF. Free DME is denoted with *.

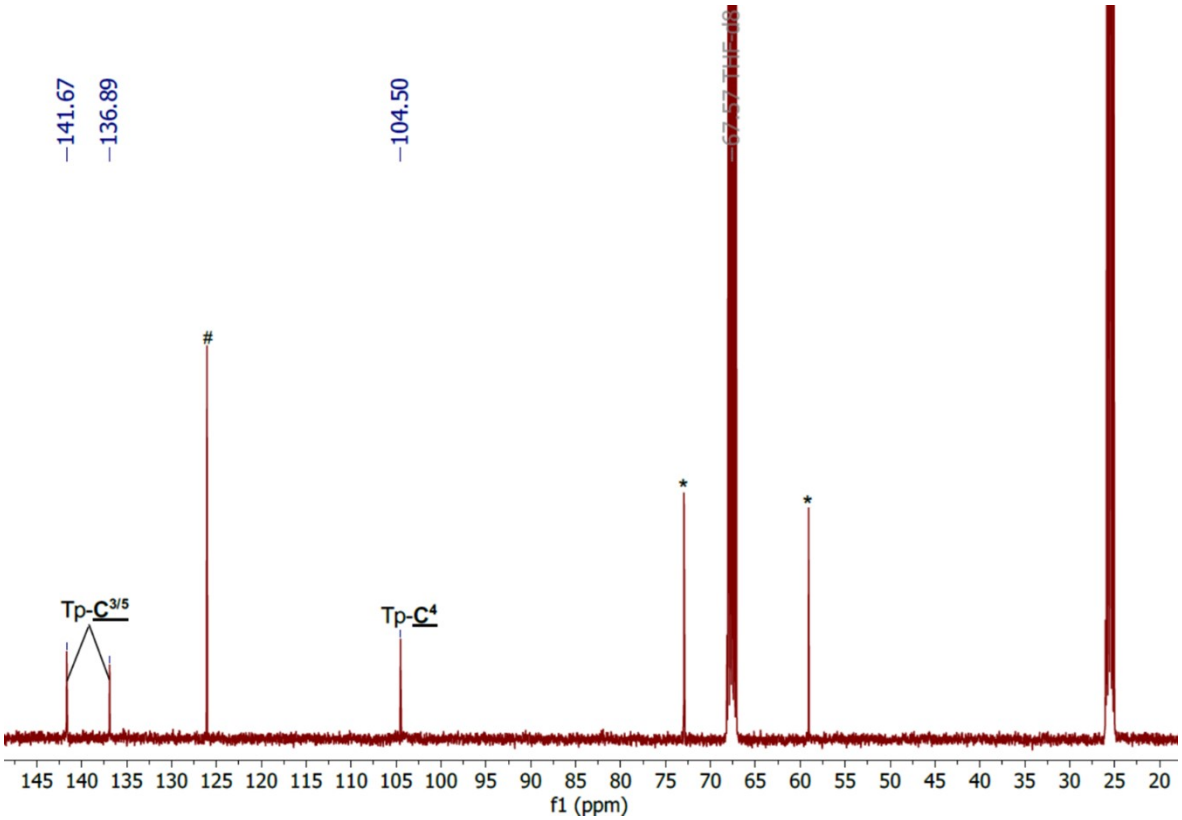

Figure S 45. ^{13}C{^{1}H} NMR spectrum of [{Sm(Tp)$_2$}$_2$(μ-η^2:η^2-O_2CCO_2)] **2-Sm**, from the reaction of [Sm(Tp)$_2$(DME)] **1-Sm(DME)** with CO_2 in d_8-THF. Free DME is denoted with * and excess CO_2 is denoted with #.

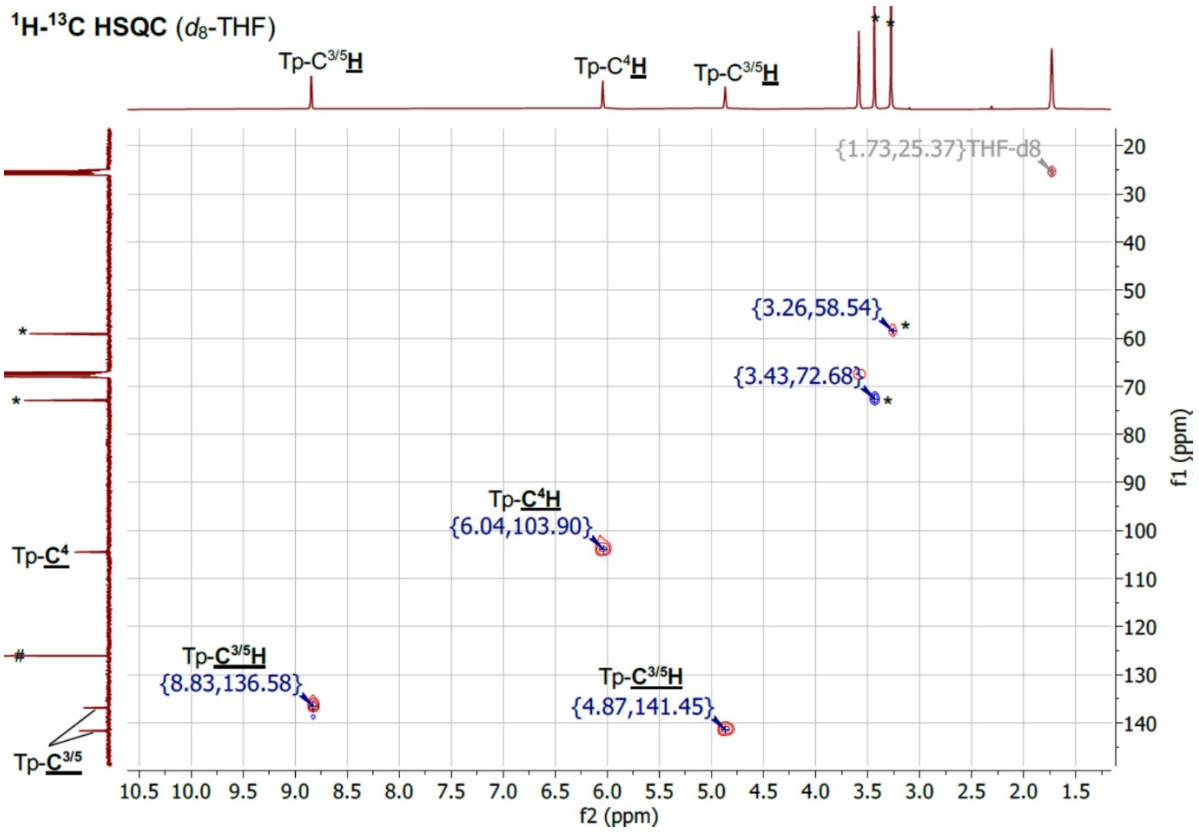

Figure S 46. ^{1}H-^{13}C HSQC NMR spectrum of [{Sm(Tp)$_2$}$_2$(μ-η^2:η^2-O$_2$CCO$_2$)] **2-Sm**, from the reaction of [Sm(Tp)$_2$(DME)] **1-Sm(DME)** with CO_2 in d_8-THF. Free DME is denoted with * and excess CO_2 is denoted with #.

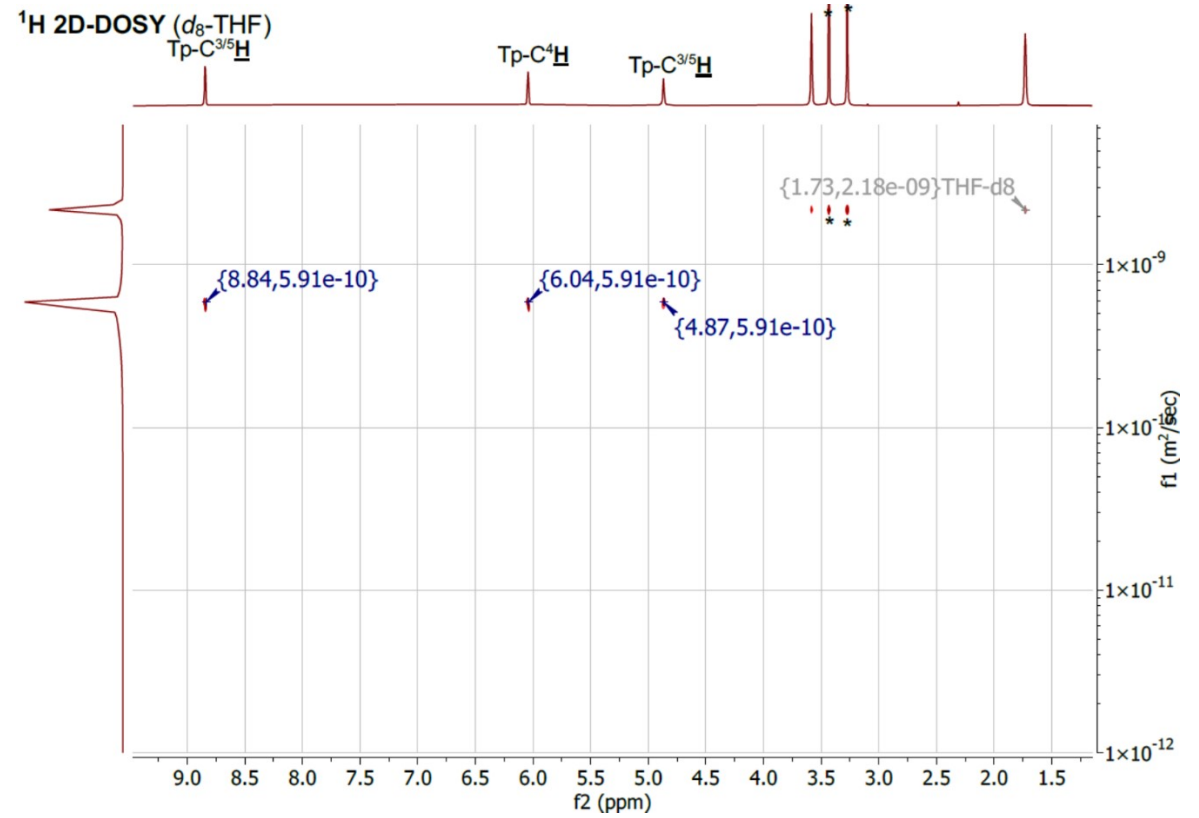

Figure S 47. ^{1}H 2D-DOSY NMR spectrum of [{Sm(Tp)$_2$}$_2$(μ-η^2:η^2-O$_2$CCO$_2$)] **2-Sm**, from the reaction of [Sm(Tp)$_2$(DME)] **1-Sm(DME)** with CO_2 in d_8-THF. The horizontal scale shows ^{1}H chemical shifts (ppm) and the vertical dimension the diffusion scale (m^2s^{-1}) with diffusion cross-peaks for **2-Sm** centred at 5.91 × 10^{-10} m^2s^{-1}. Free DME and the corresponding diffusion cross-peak for free DME are denoted with *.

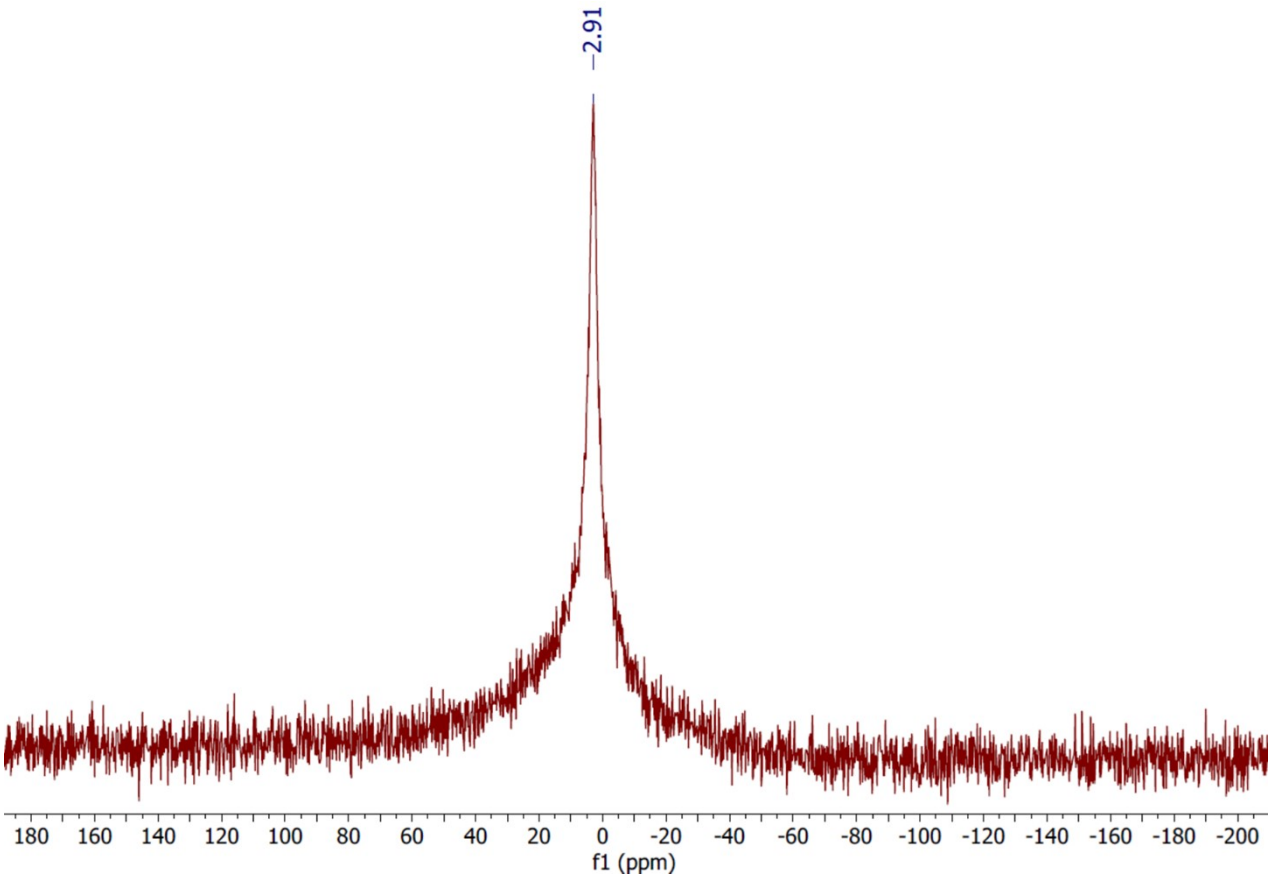

Figure S 48. ^{11}B NMR spectrum of [{Sm(Tp)$_2$}$_2$(μ-η^2:η^2-O$_2$CCO$_2$)] **2-Sm**, from the reaction of [Sm(Tp)$_2$(DME)] **1-Sm(DME)** with CO_2 in d_8-THF.

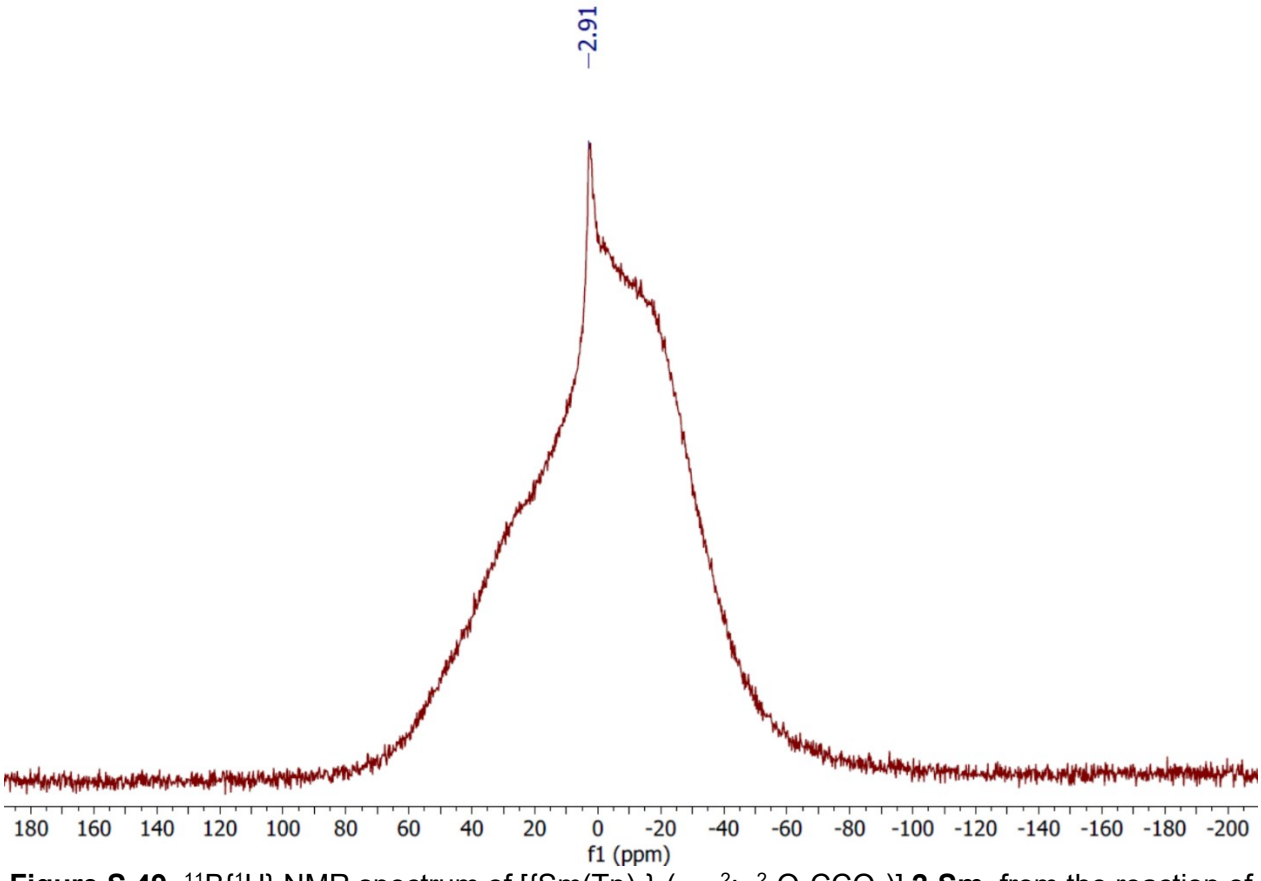

Figure S 49. ^{11}B{^{1}H} NMR spectrum of [{Sm(Tp)$_2$}$_2$(μ-η^2:η^2-O$_2$CCO$_2$)] **2-Sm**, from the reaction of [Sm(Tp)$_2$(DME)] **1-Sm(DME)** with CO_2 in d_8-THF.

A2.2 NMR-scale reaction between [Y(Tp)$_2$(N")] and CO_2 in d_6-benzene

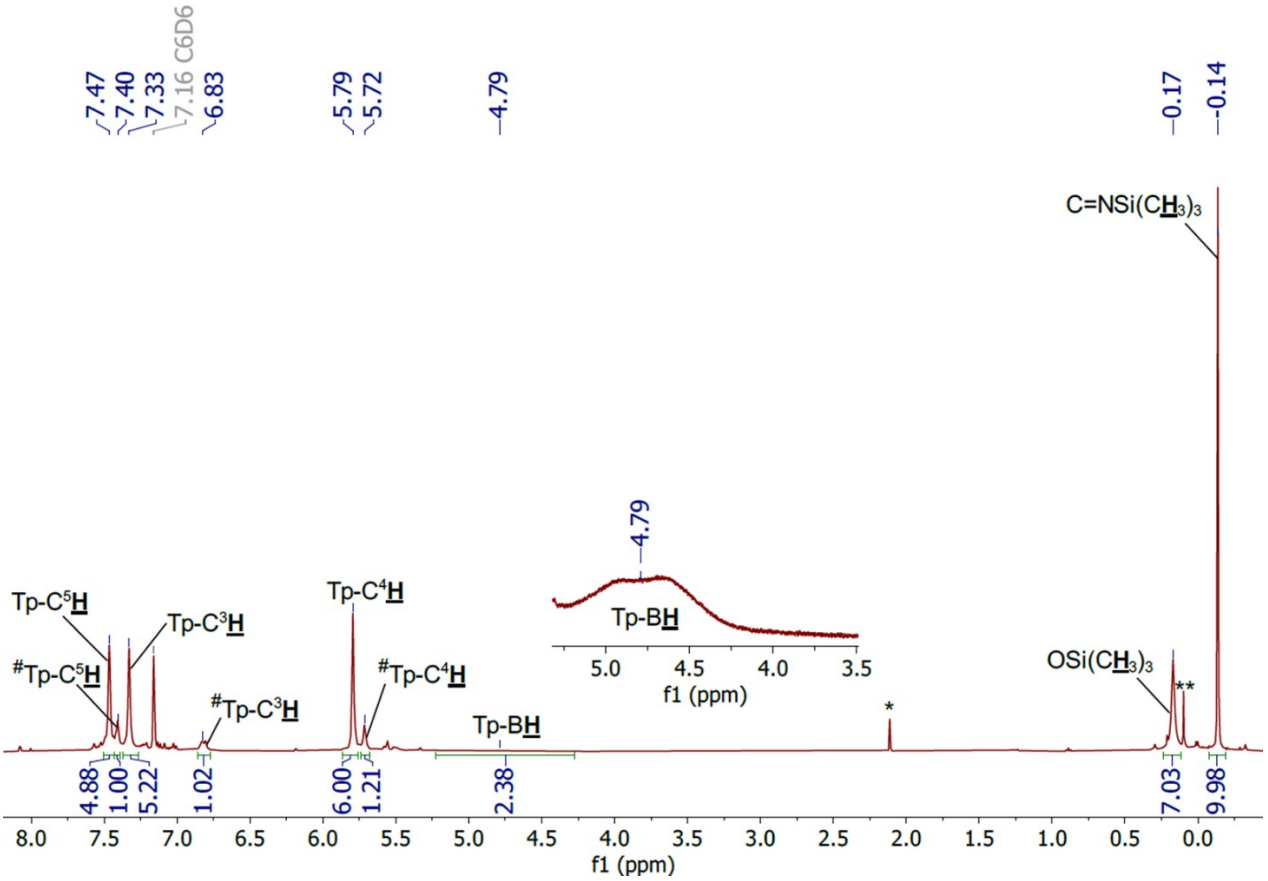

Figure S 50. ^{1}H NMR spectrum of the reaction of [Y(Tp)$_2$(N")] with CO_2 in d_6-benzene, showing [Y(Tp)$_2$(κ^2-O,O(SiMe$_3$)C=NSiMe$_3$)] as the major intermediate and a minor unidentified [Y(Tp)$_2$(X)] intermediate (denoted with #). Residual toluene is denoted with * and minor HN" is denoted with **.

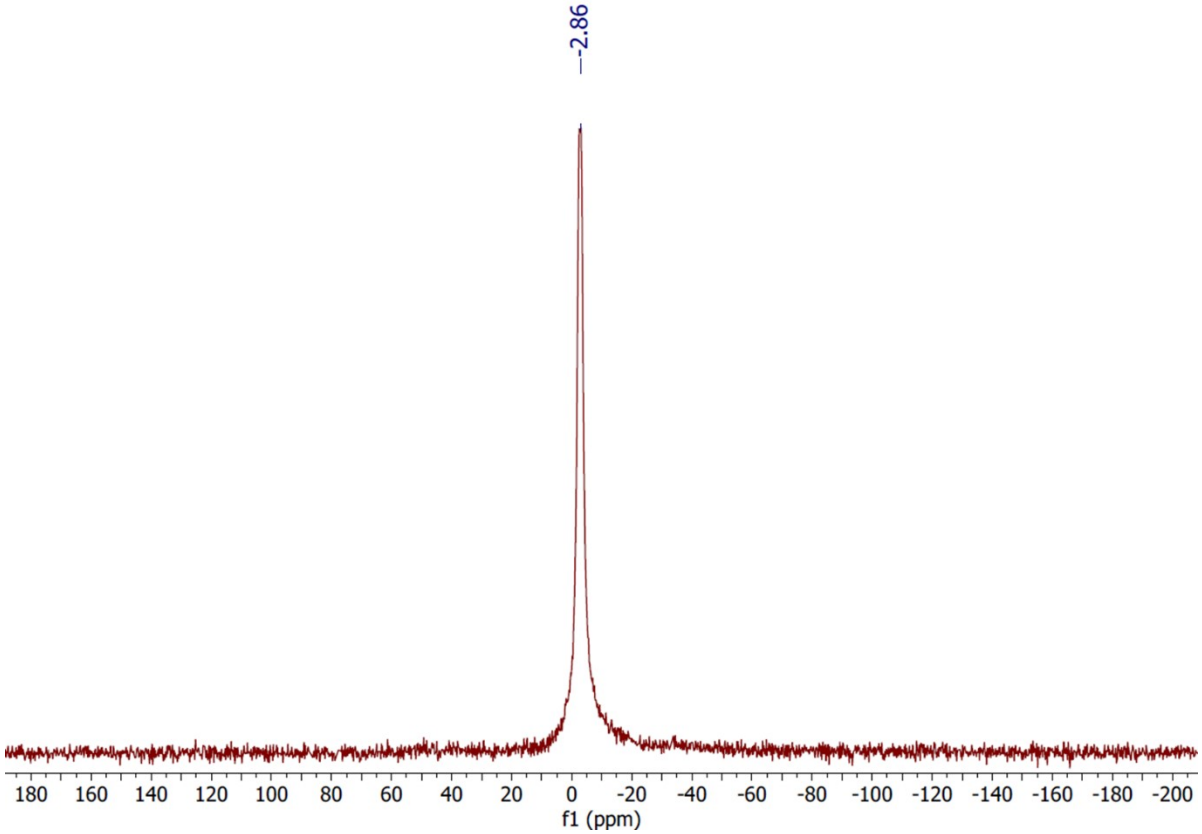

Figure S 51. ^{11}B NMR spectrum of the reaction of [Y(Tp)$_2$(N")] with CO_2 in d_6-benzene, showing the major intermediate [Y(Tp)$_2$(κ^2-O,O(SiMe$_3$)C=NSiMe$_3$)].

A2.3 NMR-scale reaction between [Sm(Tp)$_2$(N'')] and CO_2 in d_6-benzene

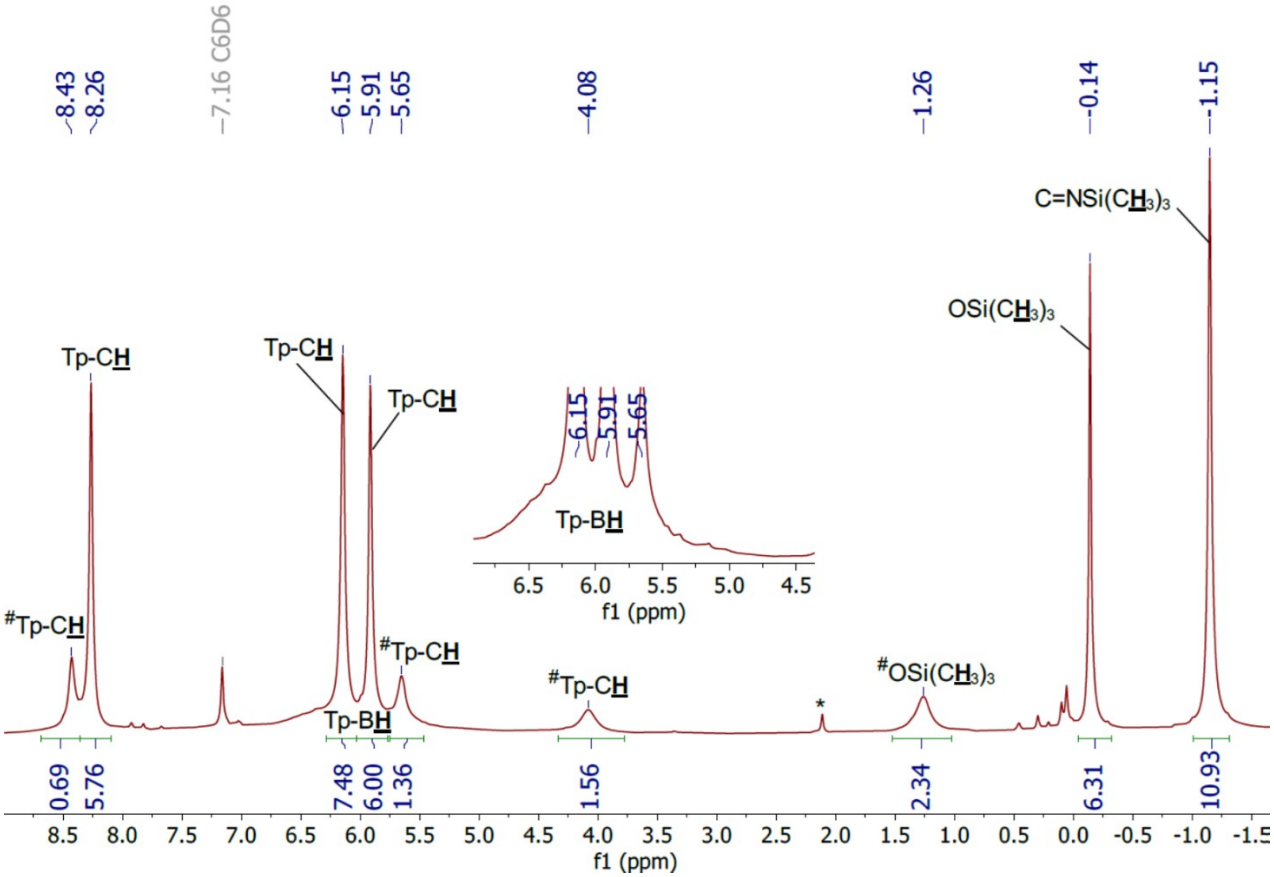

Figure S 52. ^{1}H NMR spectrum of the reaction of [Sm(Tp)$_2$(N'')] with CO_2 in d_6-benzene, showing [Sm(Tp)$_2$(κ^2-O,O(SiMe$_3$)C=NSiMe$_3$)] as the major intermediate and a minor unidentified [Sm(Tp)$_2$(X)] intermediate (denoted with #). Residual toluene is denoted with *.

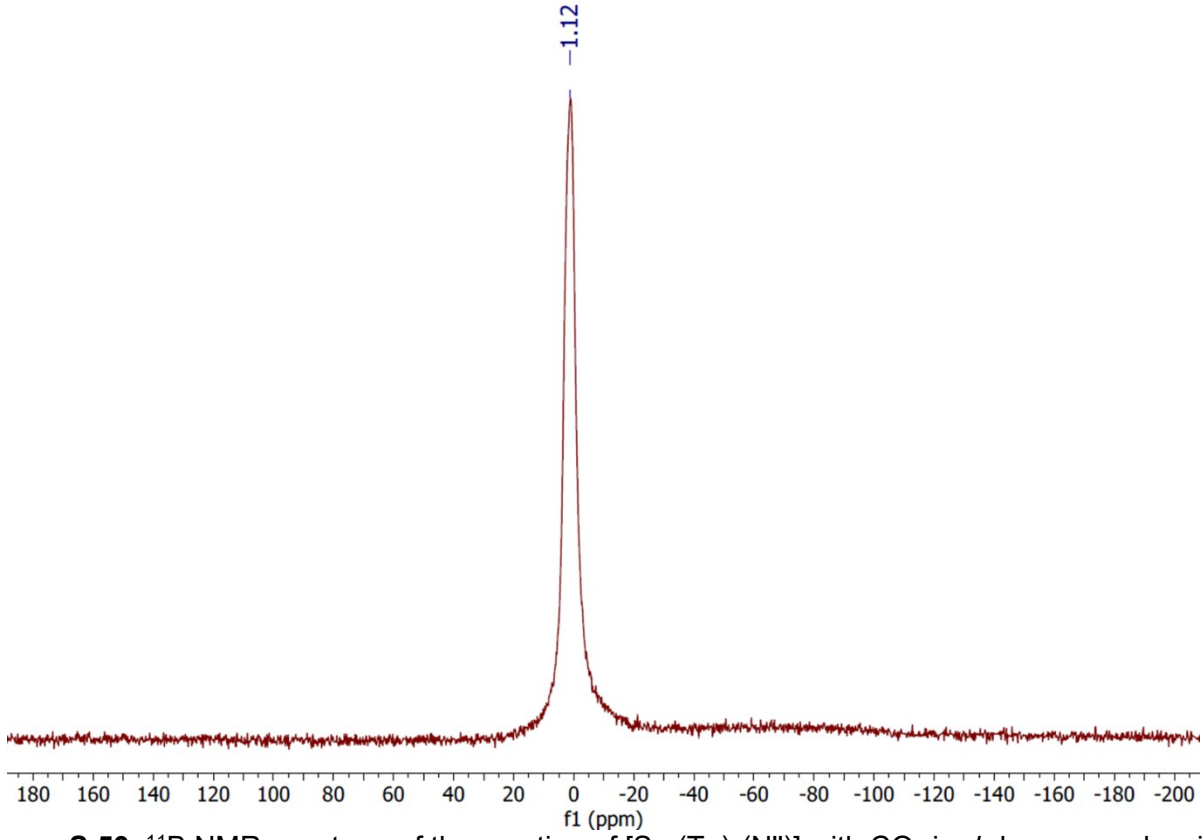

Figure S 53. ^{11}B NMR spectrum of the reaction of [Sm(Tp)$_2$(N'')] with CO_2 in d_6-benzene, showing the major intermediate [Sm(Tp)$_2$(κ^2-O,O(SiMe$_3$)C=NSiMe$_3$)].

A3 NMR data for the small-scale reaction of $[Dy(Tp)_2(OTf)]$ with KC_8 in toluene

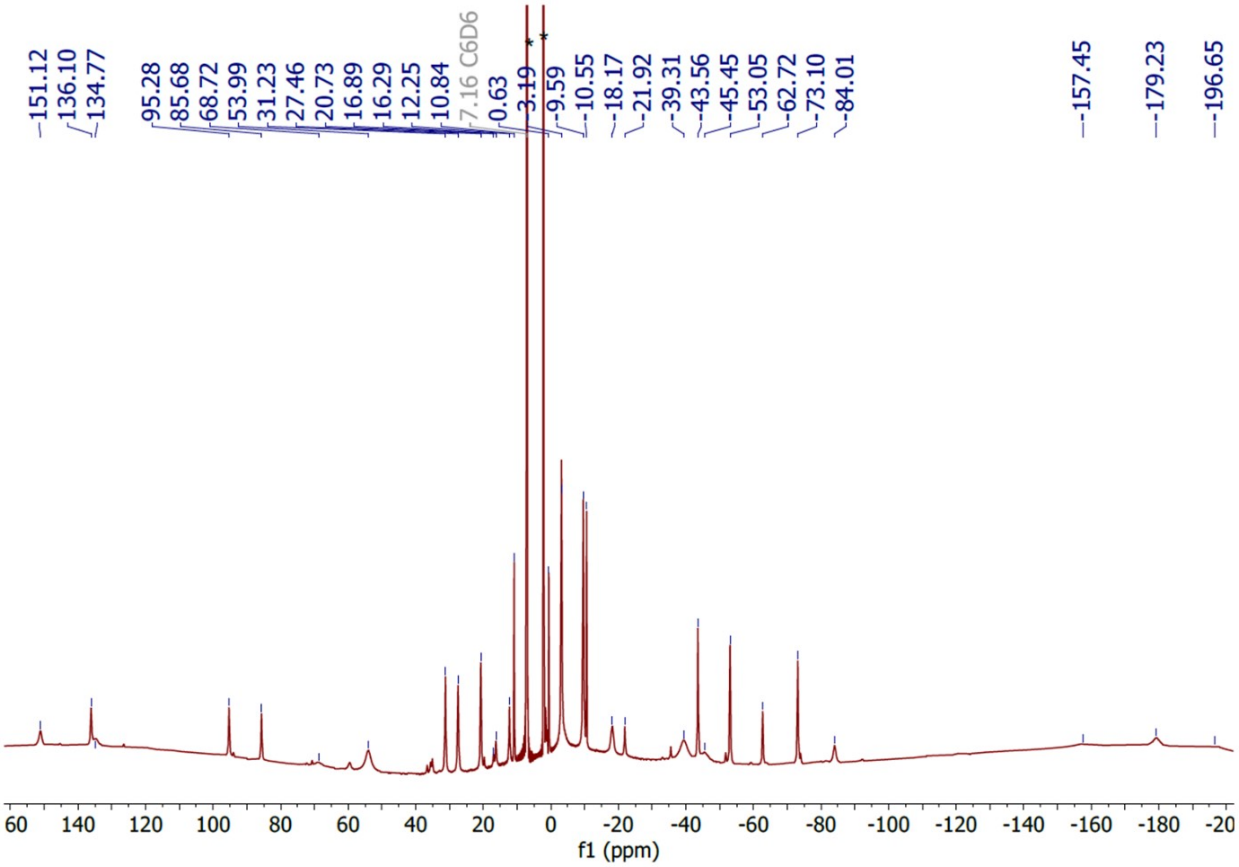

Figure S 54. ^{1}H NMR spectrum of the reaction of $[Dy(Tp)_2(OTf)]$ with 1.9 equivalents KC_8 in toluene, recorded in d_6-benzene, showing $[Dy(Tp)_3]$ as the major product.[2] Residual toluene is denoted with *.

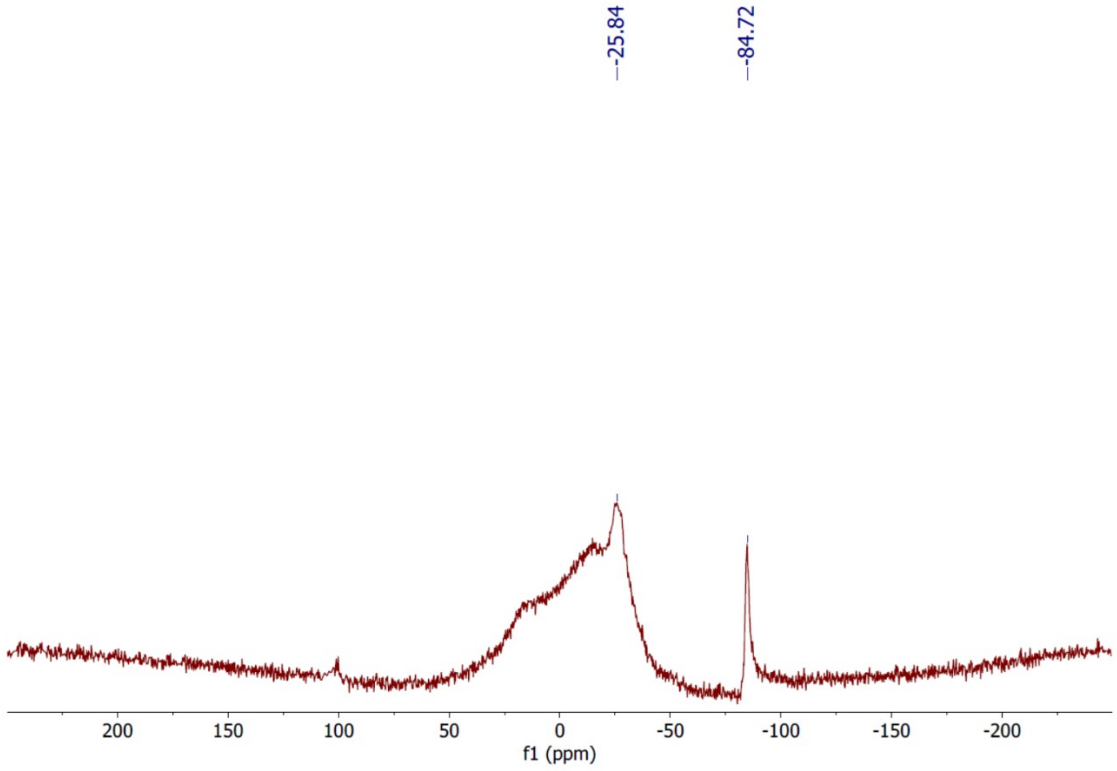

Figure S 55. ^{11}B NMR spectrum of the reaction of $[Dy(Tp)_2(OTf)]$ with 1.9 equivalents KC_8 in toluene, recorded in d_6-benzene, showing $[Dy(Tp)_3]$ as the major product.[2]

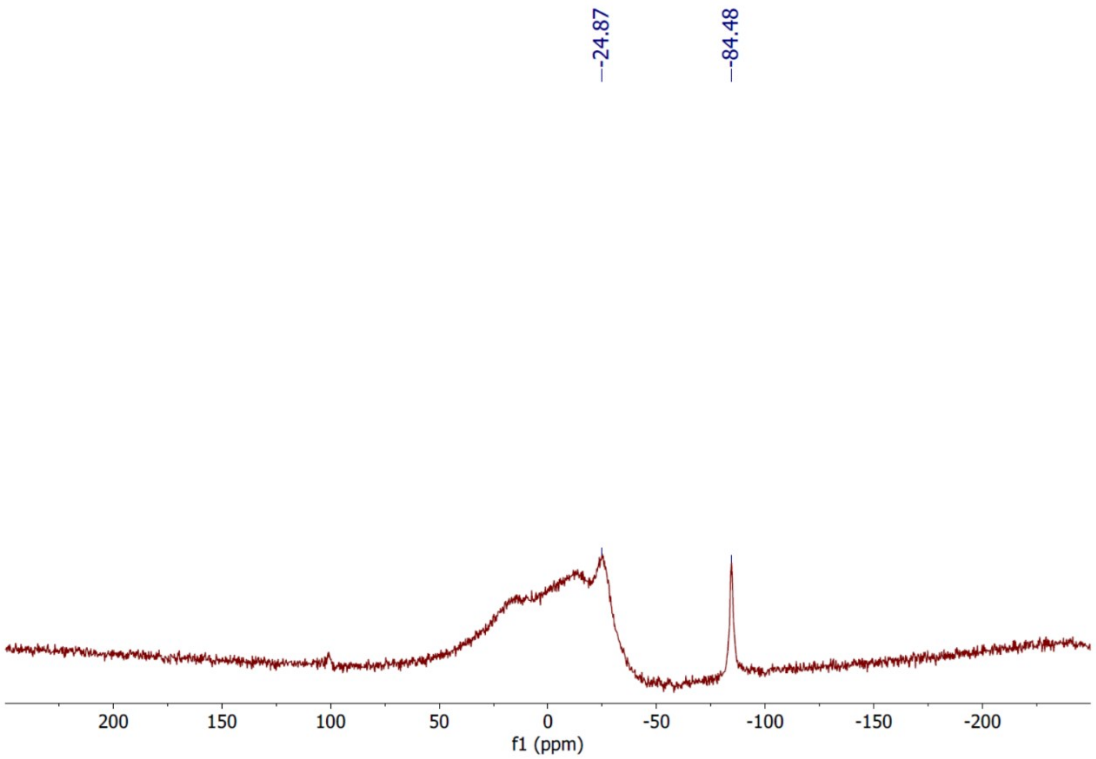

Figure S 56. $^{11}B\{^{1}H\}$ NMR spectrum of the reaction of $[Dy(Tp)_2(OTf)]$ with 1.9 equivalents KC_8 in toluene, recorded in d_6-benzene, showing $[Dy(Tp)_3]$ as the major product.[2]

A4 Infrared (IR) data

A4.1 [{Sm(Tp)$_2$}$_n$] 1-Sm and [Sm(Tp)$_2$(DME)] 1-Sm(DME)

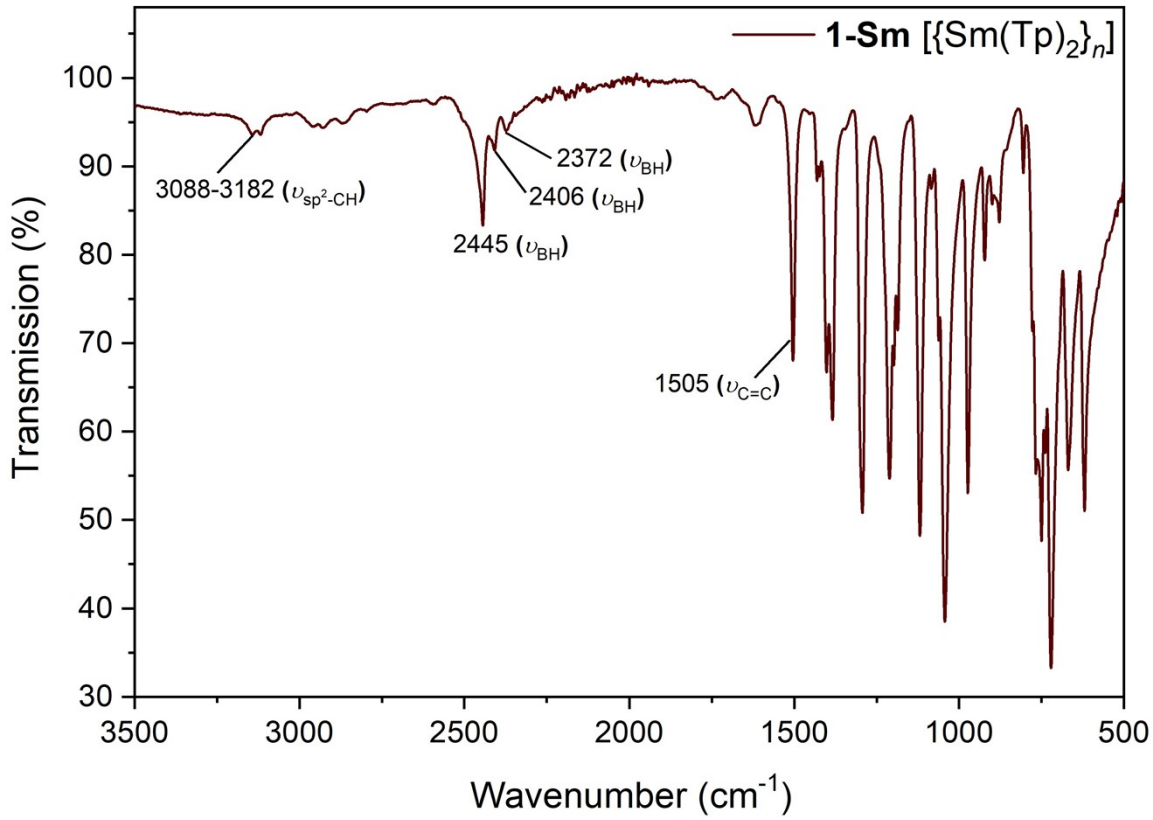

Figure S 57. ATR-IR spectrum of [{Sm(Tp)$_2$}$_n$] **1-Sm**.

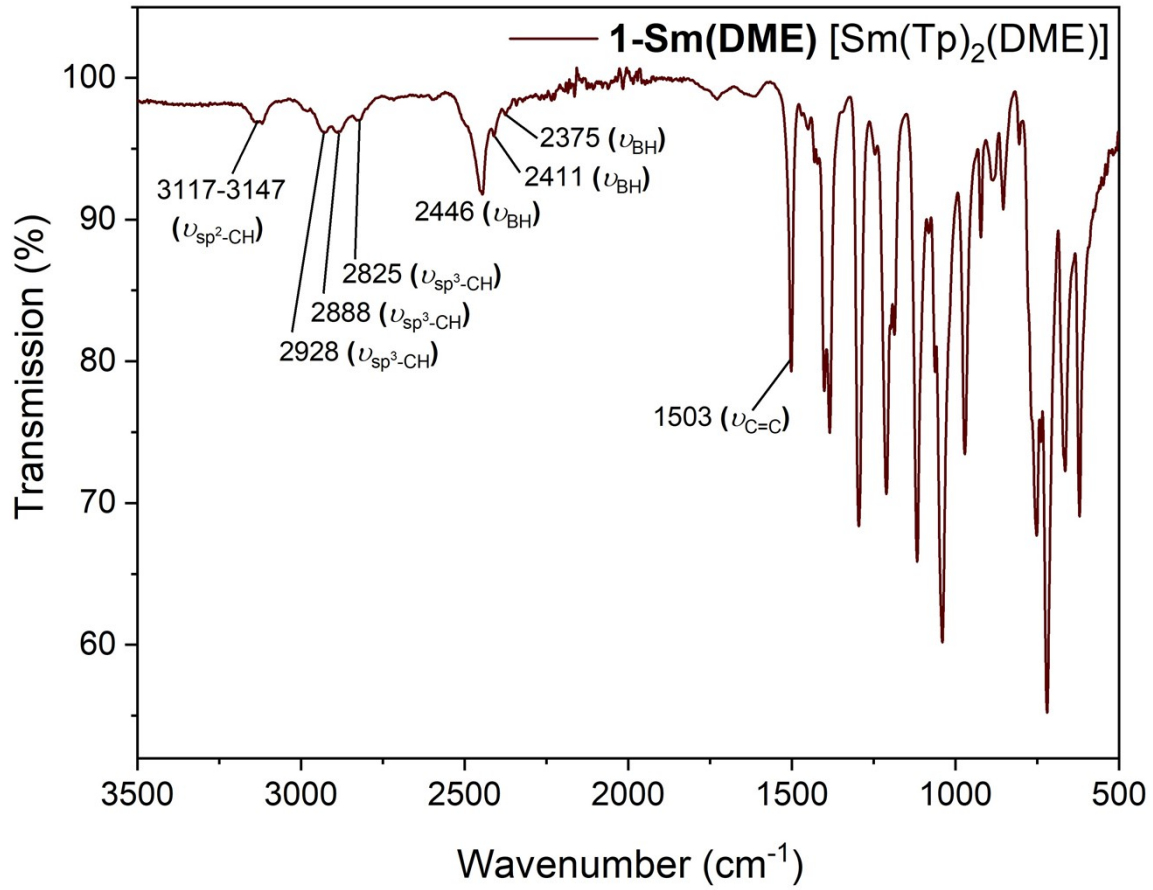

Figure S 58. ATR-IR spectrum of [Sm(Tp)$_2$(DME)] **1-Sm(DME)**.

A4.2 [{Sm(Tp)$_2$}$_2$(μ-η^2:η^2-O$_2$CCO$_2$)] 2-Sm

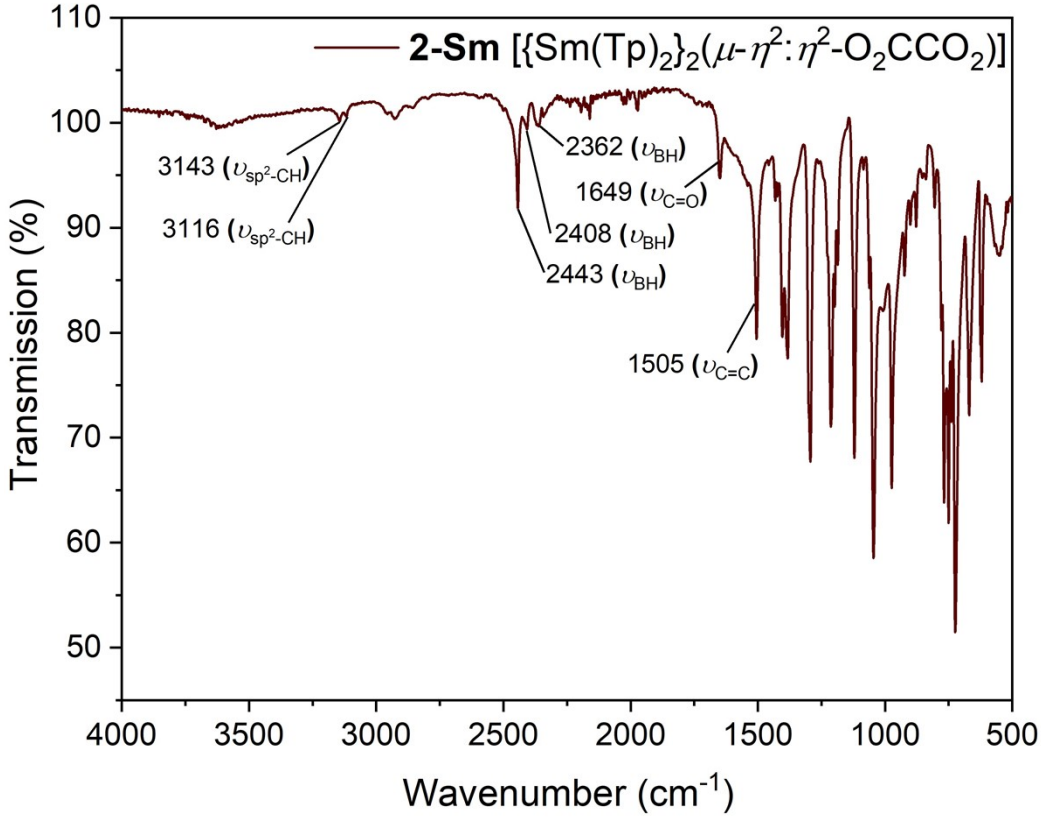

Figure S 59. ATR-IR spectrum of [{Sm(Tp)$_2$}$_2$(μ-η^2:η^2-O$_2$CCO$_2$)] **2-Sm**.

A4.3 [Ln(Tp)$_2$(OSiMe$_3$)] 3-Ln (Ln = Y, Sm)

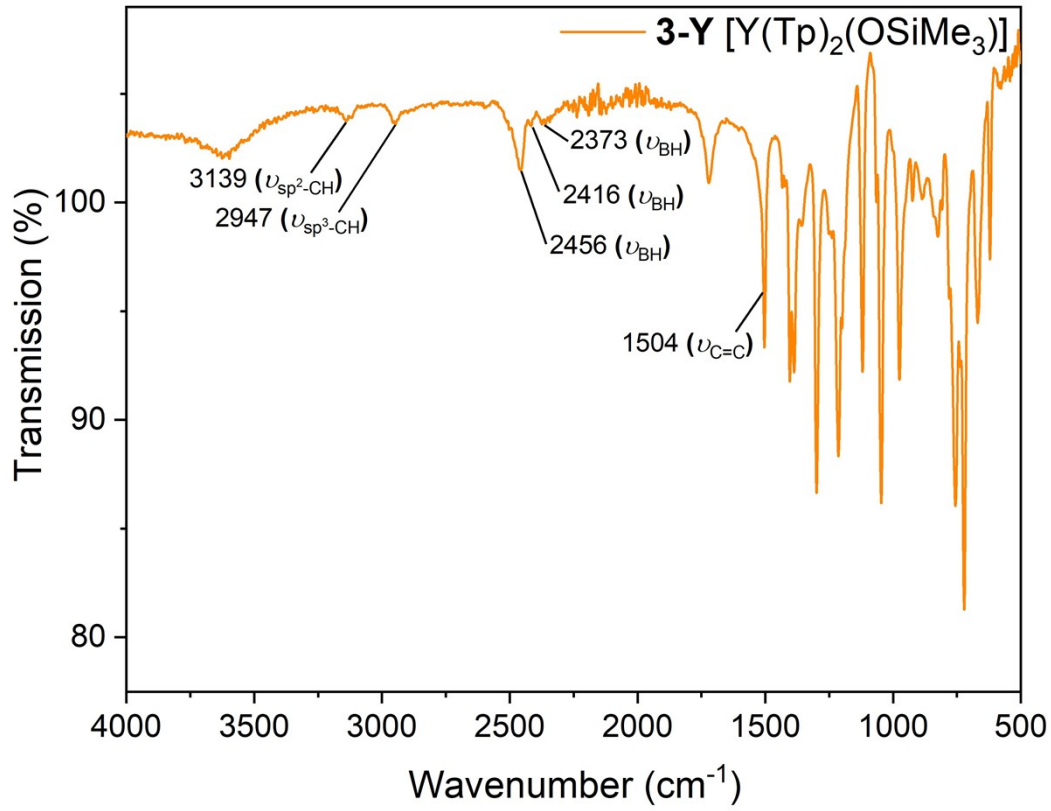

Figure S 60. ATR-IR spectrum of [Y(Tp)$_2$(OSiMe$_3$)] **3-Y**.

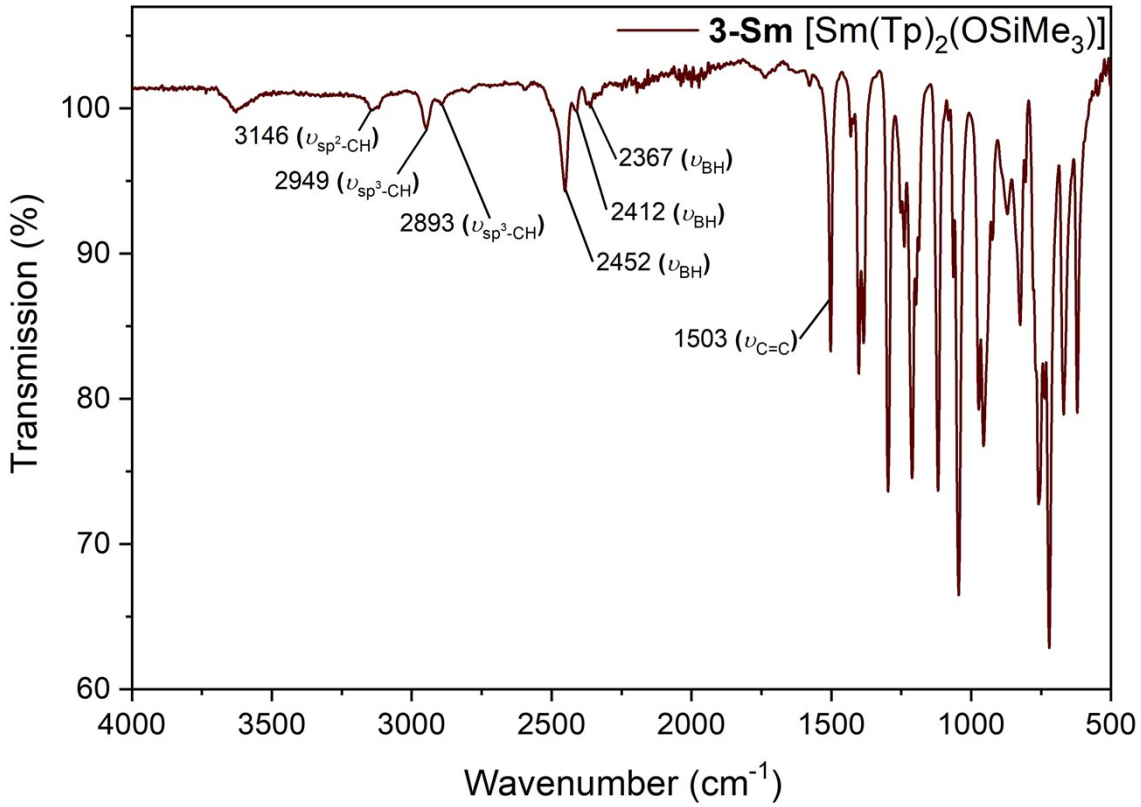

Figure S 61. ATR-IR spectrum of [Sm(Tp)$_2$(OSiMe$_3$)] **3-Sm**.

A4.4 [Sm$_5$(Tp)$_6$(μ_2-OH)$_6$(μ_3-OH)$_2$(μ_4-OH)] 4-Sm

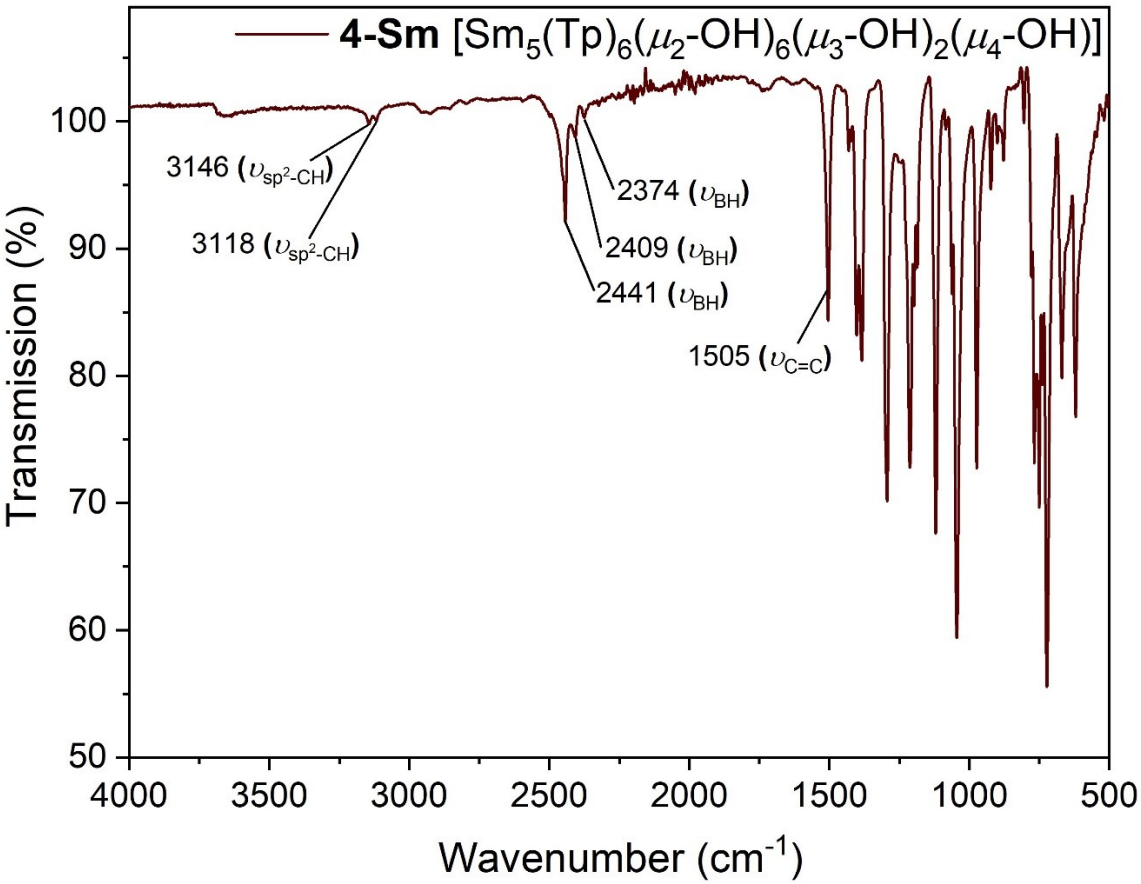

Figure S 62. ATR-IR spectrum of [Sm$_5$(Tp)$_6$(μ_2-OH)$_6$(μ_3-OH)$_2$(μ_4-OH)] **4-Sm**.

B. Single-crystal X-Ray diffraction (SCXRD) data

CIFs for all structures reported here have been deposited with the CCDC and are available free of charge. The CCDC numbers and selected crystallographic details for all structures are given in **Table 2**. Views of crystal structures are shown below, with selected atom labels; hydrogen atoms are omitted for clarity, carbon atoms of Tp (and pyrazolyl), THF, and DME displayed in wireframe and displacement ellipsoids for all other atoms are drawn at 50% probability level. Selected metrics are given in **Table 1**. Specific details for individual structures are provided in the figure captions.

Computing details: (a) Data collection and data reduction for all structures except **2-Sm** and **4-Sm**: *APEX3* Ver. 2016.9-0;[3] (b) Cell refinement for all structures except **2-Sm** and **4-Sm**: *SAINT* V8.37A;[3] (c) Data collection, data reduction, and cell refinement for **2-Sm** and **4-Sm**: *CrysAlis PRO* 1.171.42.90a (Rigaku OD, 2023); (d) Program(s) used to solve structure: *SHELXT*;[4] (e) Program(s) used to refine structure: *SHELXL* 2018/3;[4] (f) Molecular graphics: Olex2 1.5;[5] (g) Software used to prepare material for publication: Olex2 1.5,[5] Mercury.[6]

Table 1. Selected metrics for $[Sm(Tp)_2(THF)_2]$ **1-Sm(THF)**, $[Sm(Tp)_2(DME)]$ **1-Sm(DME)**, $[\{Sm(Tp)_2\}_2(\mu\text{-}\eta^2\text{:}\eta^2\text{-}O_2CCO_2)]$ **2-Sm**, and $[Ln(Tp)_2(OSiMe_3)]$ **3-Ln** (Ln = Y, Sm) complexes, analogous structural comparators Ln(II) $[Ln(Tp^R)_2]$ (Tp^R = substituted analogues of Tp), Ln(II) $[Ln(Tp)_2(LB)_x]$ (LB = Lewis base), Sm(III) $[\{Sm(L)_2\}_2(\mu\text{-}\eta^2\text{:}\eta^2\text{-}O_2CCO_2)]$, and Ln(III) $[Ln(L)_2(OSiMe_3)]$ complexes are included for reference.

$[Ln(Tp^R)_2]$ and $[Ln(Tp)_2(LB)_x]$ complexes	Bond metrics associated with the respective ligands				Reference
	Tp		***O*-donor Lewis bases (LB)**		
	Bond lengths (Å)	Bond angles (°)	Bond lengths (Å)	Bond angles (°)	
	Ln–N(Tp)	B(Tp)–Ln–B(Tp)	Ln–O(LB)	O(LB)–Ln–O(LB)	
$[Sm(Tp)_2(THF)_2]$ **1-Sm(THF)**	2.662(6)-2.744(7)	127.5	2.692(4)	91.0(2)	This work
$[Sm(Tp)_2(DME)]$ **1-Sm(DME)**	2.6805(16)-2.7180(16)	128.1	2.6696(14), 2.7044(14)	61.30(4)	
$[Sm(Tp^{Me2})_2]$ or $[Sm(Tp^*)_2]$	2.616(2)	180.0	-	-	7
$[Sm(Tp^{iPr2})_2]$	2.587(2)-2.680(2)	148.3	-	-	8
$[Sm(Tp^{Me2,4\text{-}Et})_2]$	2.609(3)-2.623(3)	180.0	-	-	7b
$[Eu(Tp)_2(THF)_2]$	2.6438(14)-2.7696(14)	128.0, 154.17	2.6361(13), 2.683(6)	89.8(3), 126.86(6)	9
$[Yb(Tp)_2(THF)]$	2.481(2)-2.595(2)	165.25	2.494(2)	-	
$[Yb(Tp)_2(DME)]$	2.496(3)-2.629(3)	127.6, 132.0	2.559(3)-2.614(3)	63.26(9)-63.66(10)	

[{Ln(L)(L/L′)}$_2$(μ-η^2:η^2-O_2CCO_2)] complexes	Bond metrics associated with the respective ligands						Reference
	Tp		**μ-η^2:η^2-O_2CCO_2**				
	Bond lengths (Å)	Bond angles (°)	Bond lengths (Å)	Bond angles (°)	Bond lengths (Å)		
	Ln–N(Tp)	B(Tp)–Ln–B(Tp)	Ln–O(C_2O_4)	O(C_2O_4)–Ln–O(C_2O_4)	C–C	C–O	
[{Sm(Tp)$_2$}$_2$(μ-η^2:η^2-O_2CCO_2)]	2.480(6)-2.592(7)	130.6, 131.2	2.423(6), 2.425(5)	66.4(3), 67.6(3)	1.529(13)	1.248(13), 1.254(12)	This work
[{Dy(Tp)$_2$}$_2$(μ-η^2:η^2-O_2CCO_2)]	2.424(3)-2.519(3)	128.6, 130.6	2.355(3), 2.367 (3)	69.00(12)	1.552(7)	1.251(5)-1.259(5)	[10]
[{Sm(C_5Me_5)$_2$}$_2$(μ-η^2:η^2-O_2CCO_2)]†	-	-	2.382(5)-2.390(6)	67.9(2)	1.542(9)	1.252(9)-1.255(9)	[11]
[{Sm(C_5Me_4{$SiMe_2$(CH_2CH=CH_2)}$_2$}$_2$(μ-η^2:η^2-O_2CCO_2)]	-	-	2.398(2)-2.400(2)	67.76(7)	1.560(6)	1.253(4)-1.257(4)	[12]
[{Sm(κ^2-Giso)$_2$}(μ-η^2:η^2-O_2CCO_2){Sm(κ^2-Giso)(κ^2-O_2CGiso)}]	-	-	2.321(10), 2.328(10), 2.348(9), 2.377(9)	68.9(3)-69.5(3)	1.585(16)	1.222(15), 1.255(16), 1.263(15), 1.273(15)	[13]

[Ln(L)$_n$($OSiMe_3$)$_{3-n}$(LB)$_x$] complexes	Bond metrics associated with the respective ligands					Reference
	Tp		***O/N*-donor Lewis bases (LB)**		**$OSiMe_3$**	
	Bond lengths (Å)	Bond angles (°)	Bond lengths (Å)	Bond angles (°)	Bond lengths (Å)	
	Ln–N(Tp)	B(Tp)–Ln–B(Tp)	Ln–O/N(LB)	O/N(LB)–Ln–O/N(LB)	Ln–O($OSiMe_3$)	
[Y(Tp)$_2$($OSiMe_3$)] **3-Y**	2.451(6)-2.567(8)	134.7	-	-	2.094(6)	This work
[Sm(Tp)$_2$($OSiMe_3$)] **3-Sm**	2.538(3)-2.589(3)	137.1	-	-	2.155(2)	
[Y{DADMB}($OSiMe_3$)(THF)$_2$]	-	-	2.358(3), 2.365(3)	169.8(1)	2.111(3)	[14]
[Y($OSiMe_3$)$_2$(pyridine)$_5$][BPh_4]	-	-	2.527(2)-2.568(2)	-	2.1350(16), 2.1499(15)	[15]
[Na(12-crown-4)$_2$][Sm(N")$_3$($OSiMe_3$)]	-	-	-	-	2.166(9)	[16]

[Ln($OSiR_3$)$_{3-n}$(LB)$_x$] complexes	Bond metrics associated with the respective ligands		Reference
	***O/N*-donor Lewis bases (LB)**	**$OSiMe_3$**	
	Bond lengths (Å)	Bond lengths (Å)	
	Ln–O/N(LB)	Ln–O($OSiR_3$)	
[Y($OSi(O^tBu)_3$)$_3$(Me_3tacn)]	2.5753(13)-2.5753(14)	2.1319(11)	[17]
[Y($OSi(O^tBu)_3$)$_3$(4,4′-Me_2bipy)]	2.475(5)-2.514(4)	2.069(4)-2.119(4)	[18]
[Y($OSiPh_3$)$_3$(THF)$_3$]	2.374(20)-2.462(21)	2.118(18)-2.138(18)	[19]
[Y($OSiPh_3$)$_3$(OP(^{n}Bu)$_3$)$_2$]	2.261(3)-2.266(3)	2.118(3)-2.129(3)	[19c]
[Sm($OSiPh_3$)$_3$(THF)$_3$]	2.513(2)-2.557(2)	2.152(2)-2.186(2)	[20]
[Sm($OSi(SiMe_3)_3$)$_3$(THF)$_2$]	2.428(8)-2.469(6)	2.156(2)-2.173(2)	[21]

Legend: Tp^{Me2} or Tp* = hydrotris(3,5-dimethyl-1-pyrazolyl)borate; Tp^{iPr2} = hydrotris(3,5-diisopropyl-1-pyrazolyl)borate; $Tp^{Me2,4-Et}$ = hydrotris(3,5-dimethyl-4-ethyl-1-pyrazolyl)borate; Giso = [(Ar)NC(NCy_2)N(Ar)] (Ar = 2,6-diisopropylphenyl, Cy = cyclohexyl); DADMB = 2,2′-*bis*-((*tert*-butyldimethylsilyl)amido)-6,6′-dimethylbiphenyl; Me_3tacn = 1,4,7-trimethyl-1,4,7-triazacyclononane

†Bond metrics for this structure has been provided here by measuring the metrics in Mercury.[6] Note: The bond metrics data of [{Sm(C_5Me_4{$SiMe_2$($CH_2CH=CH_2$)})$_2$}$_2$(μ-η^2:η^2-O_2CCO_2)] provided the first detailed structural information,[12] since the data for the analogous [{Sm(C_5Me_5)$_2$}$_2$(μ-η^2:η^2-O_2CCO_2)] were not of high enough quality.[11]

Table 2. Crystallographic data table for $[Sm(Tp)_2(THF)_2]$ **1-Sm(THF)**, $[Sm(Tp)_2(DME)]$ **1-Sm(DME)**, $[Y(Tp)_2(\kappa^2\text{-pz})]$ **Y-pz**, $[\{Sm(Tp)_2\}_2(\mu\text{-}\eta^2\text{:}\eta^2\text{-}O_2CCO_2)]$ **2-Sm**, $[Ln(Tp)_2(OSiMe_3)]$ **3-Ln** (Ln = Y, Sm), and $[Sm_5(Tp)_6(\mu_2\text{-}OH)_6(\mu_3\text{-}OH)_2(\mu_4\text{-}OH)]$ **4-Sm** complexes.

CCDC No.	**2347955**	**2347954**	**2347960**	**2347956**
Parameter	**1-Sm(THF)**	**1-Sm(DME)**	**Y-pz**	**2-Sm**
Formula	$C_{26}H_{36}B_2N_{12}O_2Sm$ •(C_4H_8O)	$C_{22}H_{30}B_2N_{12}O_2Sm$•(C_7H_8)	$C_{21}H_{23}B_2N_{14}Y$	$C_{38}H_{40}B_4N_{24}O_4Sm_2$• solvent*
*F*w	792.74	758.68	582.06	1240.88
Colour and shape	Lath, red	Shard, red	Plate, colourless	Block, colourless
Dimensions (mm)	0.15 × 0.06 × 0.02	0.16 × 0.14 × 0.04	0.17 × 0.07 × 0.02	0.16 × 0.12 × 0.10
Crystal System	Orthorhombic	Monoclinic	Monoclinic	Orthorhombic
Space group	*Cmc2₁*	*P2₁/c*	*P2₁/c*	*Fdd2*
a (Å)	14.5538(6)	13.9317(5)	13.007(3)	20.9732(6)
b (Å)	16.0627(7)	18.7012(7)	9.3117(17)	28.6287(8)
c (Å)	15.1034(7)	13.5115(5)	21.482(4)	21.4608(6)
α (°)	90	90	90	90
β (°)	90	101.987(1)	96.332(7)	90
γ (°)	90	90	90	90
V (Å^3)	3530.8(3)	3443.5(2)	2586.0(9)	12885.8(6)
Z	4	4	4	8
D_x (Mg m^{-3})	1.491	1.463	1.495	1.279
No. of reflections measured	60756	58561	19751**	54122
No. of independent reflections	4541	8530	4885	9847
No. of reflections with $I > 2\sigma(I)$	3379	7587	3296	7474
R_{int}	0.079	0.047	0.145	0.071
R_1 ($I > 2\sigma$)[a]	0.031	0.023	0.084	0.051
$wR_2(F^2)$[b]	0.076	0.058	0.212	0.149
GoF[c]	1.04	1.06	1.00	1.05
CCDC No.	**2347958**	**2347957**	**2347959**	
Parameter	**3-Y**	**3-Sm**	**4-Sm**	
Formula	$C_{21}H_{29}B_2N_{12}OSiY$	$C_{21}H_{29}B_2N_{12}OSiSm$	$C_{54}H_{69}B_6N_{36}O_9Sm_5$†	
*F*w	604.18	665.62	2183.06	
Colour and shape	Rod, colourless	Tablet, colourless	Plate, colourless	
Dimensions (mm)	0.20 × 0.02 × 0.02	0.15 × 0.09 × 0.02	0.06 × 0.04 × 0.02	
Crystal System	Hexagonal	Monoclinic	Monoclinic	
Space group	*P6₃/m*	*P2₁/c*	*P2₁/c*	
a (Å)	19.7600(13)	17.2101(9)	16.5313(5)	
b (Å)	19.7600(13)	7.7251(3)	39.6991(18)	
c (Å)	13.3004(12)	21.3419(10)	27.9152(10)	
α (°)	90	90	90	
β (°)	90	104.927(2)	105.905(3)	
γ (°)	120	90	90	
V (Å^3)	4497.5(7)	2741.7(2)	17618.8(12)	
Z	6	4	8	
D_x (Mg m^{-3})	1.338	1.613	1.646	
No. of reflections measured	6143	42242	87712	
No. of independent reflections	3216	6797	31093	
No. of reflections with $I > 2\sigma(I)$	2320	5528	16092	
R_{int}	0.076	0.075	0.237	
R_1 ($I > 2\sigma$)[a]	0.097	0.033	0.179	
$wR_2(F^2)$[b]	0.193	0.072	0.461	
GoF[c]	1.17	1.03	1.39	

[a]$R_1 = \Sigma(||F_0| - |F_c||) / \Sigma|F_0|$, $F_0 > 4\sigma(F_0)$. [b]$wR_2 = \{\Sigma[w(F_0^2 - F_c^2)^2 / \Sigma[w(F_0^2)^2]\}^{1/2}$. [c]$GOF = [\Sigma w (F_0^2 - F_c^2)^2 / (n_0 - n_p)]^{1/2}$.
†The hydrogen atoms of the hydroxides were not added to the bridging oxygen atoms in the structure, but have been accounted for in the molecular formula and all values derived from the formula.
*Solvent mask used to account for poorly defined THF lattice solvent molecules, 129 electrons per formula unit.
**Data processed as a multiple crystal with 3 components, completeness ~90%.

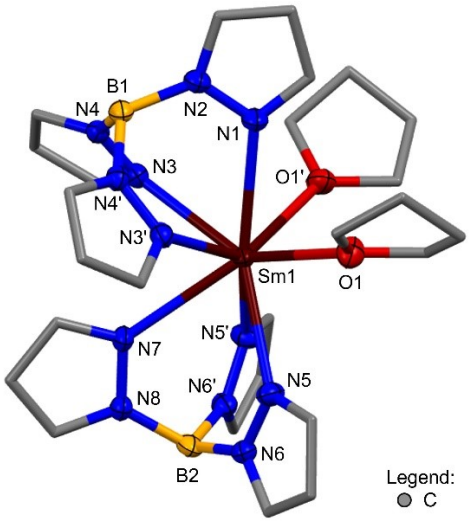

Figure S 63. Molecular structure of **1-Sm(THF)**. The molecule **1-Sm(THF)** crystallises with the Sm lying on a mirror plane containing two pyrazolyl arms of two Tp ligands (N1, N2 and N7, N8) on the mirror plane and two pyrazolyl arms of two Tp ligands (N3, N4 and N5, N6) on either side of the mirror plane and one THF (O1) on the same side of the mirror plane as the pyrazolyl arm (N5, N6); 'prime' atom labels denote symmetry equivalent (1-x, y, z).

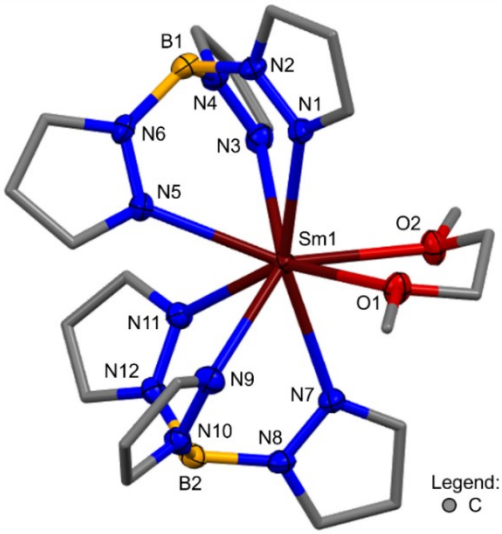

Figure S 64. Molecular structure of **1-Sm(DME)**.

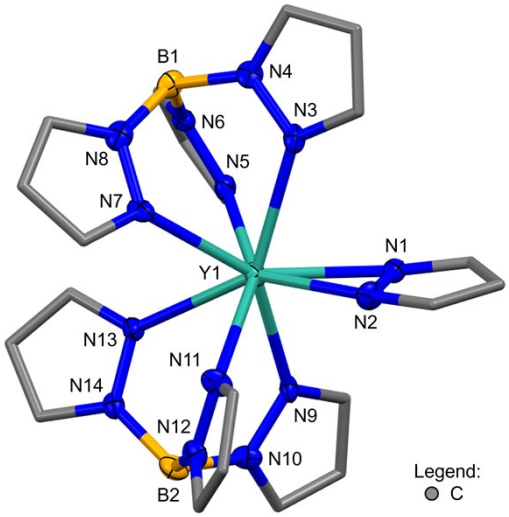

Figure S 65. Molecular structure of [Y(Tp)$_2$(κ^2-pz)] (pz = pyrazolyl). Selected bond distances: Y–N(pz) 2.307(11)-2.389(11) Å, Y–N(Tp) 2.424(12)-2.535(11) Å; selected bond angles: N1(pz)–Y–N2(pz) 33.7(4)°, B(Tp)–Y–B(Tp) 131.8°.

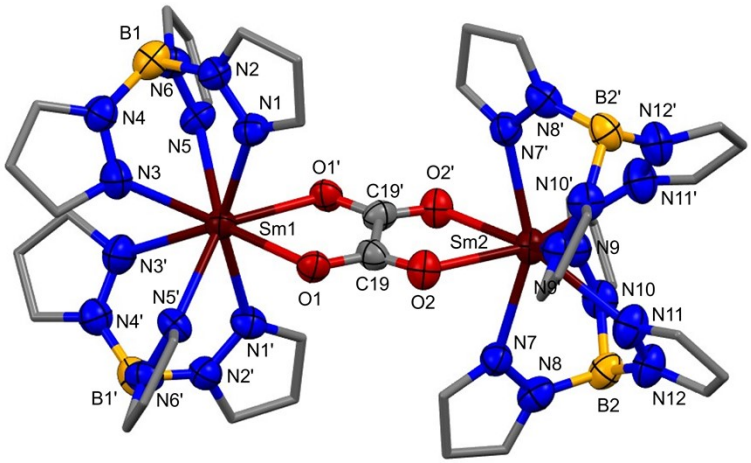

Figure S 66. Molecular structure of **2-Sm**. The molecule **2-Sm** crystallises across a 2-fold rotation axis (running through the two Sm atoms and mid-point of the oxalate C-C bond) with the asymmetric unit containing one Sm atom, half of the bridging oxalate; 'prime' atom labels denote symmetry equivalent (1-x, 1-y, z), lattice THF solvent molecules were accounted for through the use of a solvent mask.

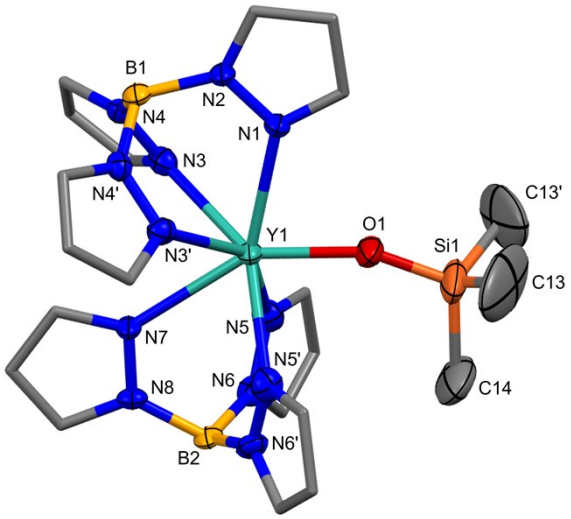

Figure S 67. Molecular structure of **3-Y**. The trimethyl silyloxide group adopts two possible orientations of the three methyl groups, only one of which is shown. The molecule **3-Y** crystallises across a mirror plane containing the Y, Tp boron atoms and one of the pyrazolyl rings of each Tp (N1, N2 and N7, N8) and the atoms of the trimethyl silyloxide (O1, Si1, C14) and two pyrazolyl arms of two Tp ligands (N3, N4 and N5, N6) and the atoms of the trimethyl silyloxide (C13) on either side of the mirror plane; 'prime' atom labels denote symmetry equivalent (x, y, 1.5-z).

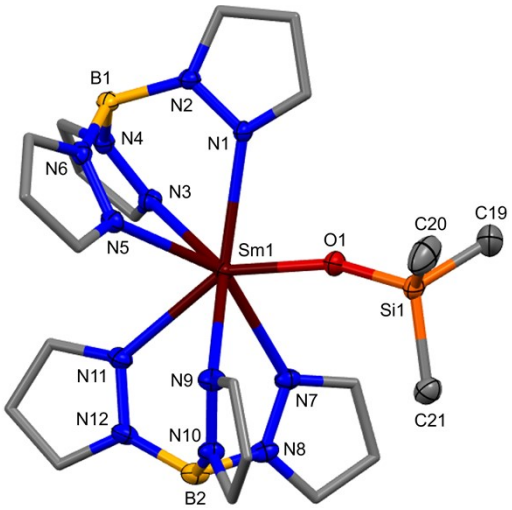

Figure S 68. Molecular structure of **3-Sm.**

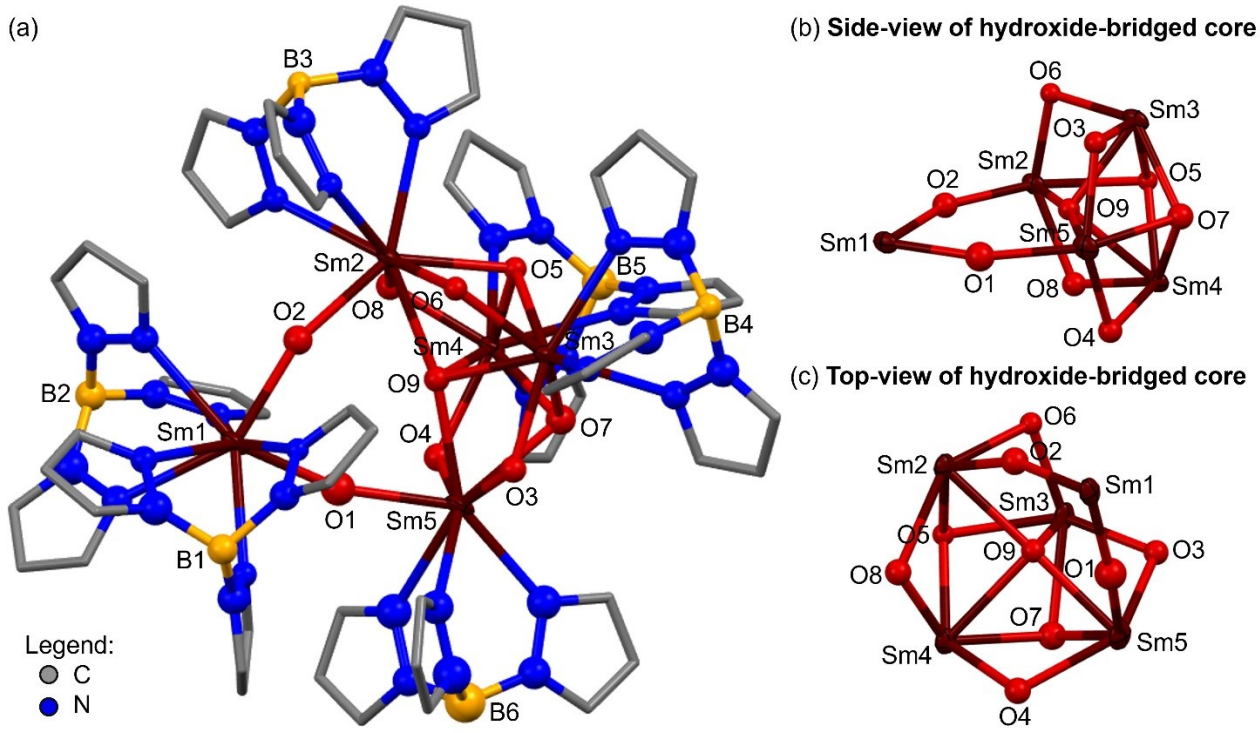

Figure S 69. Molecular structure of **4-Sm** (a), showing one of the two crystallographically independent molecules, the second omitted for clarity. Views of the hydroxide-bridged core in this structure (side-view (b) and top-view (c)), where Tp ligands are omitted for clarity and only the bridging core atoms are shown. The structure shows the different bridging modes of the hydroxides to the Sm atoms: six μ_2-OH (O1, O2, O3, O4, O6, O8), two μ_3-OH (O5, O7), and one μ_4-OH (O9). With the exception of the Sm atoms, all other atoms were refined with isotropic atomic displacement parameters. The sample suffered significant radiation affecting the data quality and only connectivity is reported for this structure.

C. References

1. T. Chowdhury, C. Wilson, C. Maichle-Mössmer, R. Anwander and J. H. Farnaby, *European Journal of Inorganic Chemistry*, 2024, **27**, e202300731.

2. C. Apostolidis, J. Rebizant, B. Kanellakopulos, R. Von Ammon, E. Dornberger, J. Müller, B. Powietzka and B. Nuber, *Polyhedron*, 1997, **16**, 1057-1068.
3. Bruker AXS Inc.: Madison, WI, 2016.
4. G. M. Sheldrick, *Acta Crystallographica Section C*, 2015, **71**, 3-8.
5. O. V. Dolomanov, L. J. Bourhis, R. J. Gildea, J. A. K. Howard and H. Puschmann, *Journal of Applied Crystallography*, 2009, **42**, 339-341.
6. C. F. Macrae, I. Sovago, S. J. Cottrell, P. T. A. Galek, P. McCabe, E. Pidcock, M. Platings, G. P. Shields, J. S. Stevens, M. Towler and P. A. Wood, *Journal of Applied Crystallography*, 2020, **53**, 226-235.
7. (a) J. Takats, X. W. Zhang, V. W. Day and T. A. Eberspacher, *Organometallics*, 1993, **12**, 4286-4288; (b) A. C. Hillier, Zhang, G. H. Maunder, S. Y. Liu, T. A. Eberspacher, M. V. Metz, R. McDonald, Â. Domingos, N. Marques, V. W. Day, A. Sella and J. Takats, *Inorganic Chemistry*, 2001, **40**, 5106-5116.
8. A. Momin, L. Carter, Y. Yang, R. McDonald, S. Essafi, F. Nief, I. Del Rosal, A. Sella, L. Maron and J. Takats, *Inorganic Chemistry*, 2014, **53**, 12066-12075.
9. T. Chowdhury, M. J. Evans, M. P. Coles, A. G. Bailey, W. J. Peveler, C. Wilson and J. H. Farnaby, *Chemical Communications*, 2023, **59**, 2134-2137.
10. G.-F. Xu, Q.-L. Wang, P. Gamez, Y. Ma, R. Clérac, J. Tang, S.-P. Yan, P. Cheng and D.-Z. Liao, *Chemical Communications*, 2010, **46**, 1506-1508.
11. W. J. Evans, C. A. Seibel and J. W. Ziller, *Inorganic Chemistry*, 1998, **37**, 770-776.
12. W. J. Evans, J. M. Perotti, J. C. Brady and J. W. Ziller, *Journal of the American Chemical Society*, 2003, **125**, 5204-5212.
13. L. Castro, D. P. Mills, C. Jones and L. Maron, *European Journal of Inorganic Chemistry*, 2016, **2016**, 792-796.
14. T. I. Gountchev and T. D. Tilley, *Organometallics*, 1999, **18**, 2896-2905.
15. Y. Ma, Y.-Q. Zhai, Y.-S. Ding, T. Han and Y.-Z. Zheng, *Chemical Communications*, 2020, **56**, 3979-3982.
16. M. Karl, G. Seybert, W. Massa, K. Harms, S. Agarwal, R. Maleika, W. Stelter, A. Greiner, W. H. B. Neumüller and K. Dehnicke, *Zeitschrift für anorganische und allgemeine Chemie*, 1999, **625**, 1301-1309.
17. A. Mortis, C. Maichle-Mössmer and R. Anwander, *Dalton Transactions*, 2022, **51**, 1070-1085.
18. G. Lapadula, A. Bourdolle, F. Allouche, M. P. Conley, I. del Rosal, L. Maron, W. W. Lukens, Y. Guyot, C. Andraud, S. Brasselet, C. Copéret, O. Maury and R. A. Andersen, *Chemistry of Materials*, 2014, **26**, 1062-1073.
19. (a) M. J. McGeary, P. S. Coan, K. Folting, W. E. Streib and K. G. Caulton, *Inorganic Chemistry*, 1989, **28**, 3283-3284; (b) P. S. Gradeff, K. Yunlu, T. J. Deming, J. M. Olofson, R. J. Doedens and W. J. Evans, *Inorganic Chemistry*, 1990, **29**, 420-424; (c) M. J. McGeary, P.

S. Coan, K. Folting, W. E. Streib and K. G. Caulton, *Inorganic Chemistry*, 1991, **30**, 1723-1735.

20. Z. Xie, K. Chui, Q. Yang, T. C. W. Mak and J. Sun, *Organometallics*, 1998, **17**, 3937-3944.
21. T. J. Boyle, F. Guerrero, R. E. Cramer, P. C. Reuel, D. M. Boye and H. L. Brooks, *Inorganic Chemistry*, 2022, **61**, 5048-5059.